In presenting this thesis in partial fulfillment of the requirements for an advanced degree at Idaho State University, I agree that the Library shall make it freely available for inspection. I further state that permission to download and/or print my thesis for scholarly purposes may be granted by the Dean of the Graduate School, Dean of my academic division, or by the University Librarian. It is understood that any copying or publication of this thesis for financial gain shall not be allowed without my written permission

Signature________________________________

Date____________________________________

# An investigation into the Poison Creek thrust:

## A Sevier thrust with Proterozoic implications


by

Connor Hansen


A thesis

submitted in partial fulfillment

of the requirements for the degree of

Master of Science in the Department of Geosciences

Idaho State University

Summer 2015

**Committee Approval**

To the Graduate Faculty:

The members of the committee appointed to examine the thesis of Connor Hansen find it satisfactory and recommend that it be accepted.

David Pearson
Major Advisor

Paul Karl Link
Committee Member

Tracy Payne
Graduate Faculty Representative

# Acknowledgements

I would like to thank my advisor, Dr. David Pearson, for the tremendous guidance he provided, his consistent patience, the keen insight he offered, and his unwavering enthusiasm during the course of this study. I would also like to thank my committee member, Paul Karl Link, for sharing his wealth of knowledge and humor, and for his fiery motivational speeches. Lastly, I'd like to thank my third committee member, Tracy Payne, for graciously providing her assistance to this project. I greatly appreciate everything all of you have done for me. With all of the heartiness and earnestness I can muster, I extend my sincerest gratitude.

In addition to my committee, I would like to thank Reed Lewis and the other members of the Idaho Geologic Survey, including Dave “Bad Uncle Dave” Stewart, Russell Burmester, and Loudon Stanford, for their advice and assistance throughout the course of this study. Thanks to Cody Stock for keeping my sanity for a little while longer during the course of field mapping, providing mental support and friendship during my time spent in Idaho, and for just being an all-around stand up “dude”.

I would like to thank Bob Baker for welcoming me on to his property and being a gracious host.

Thank you to the people and facilities of University of Arizona where much of the analyses were conducted, specifically, the University of Arizona Laserchron Center and Arizona Radiogenic Helium Dating Laboratory. I would like to thank Midland Valley for generously providing the Move software

I would also like to express my gratitude to the entire Idaho State University's Geoscience department. Everyone, top to bottom, has been wonderful during my time here. In particular, I would like to thank Melissa Neiers, Kate Zajanc, and Diana Boyak, your support has been invaluable to me.

Furthermore, I'd like to thank my housemates, officemates, and friends with whom I spent time these past two years. Specifically, I would like to thank Jess, Lisa, and Miranda for not going too crazy after sharing a roof with me; Brock, Natalie, John, Tess, Chuck, and again Jess for keeping my offices studious (even if I didn't want them that way); the good natured attendees of the weekly “Thrusty Thursday” for abiding, imbibing, guiding, and simply not hiding at home; Stella, Kashi, Wander, and last, but not least, Bella for your unwavering goofiness and companionship.

I would also like to thank and acknowledge Jane Kelson and Jen Bradham, my high school geology instructor and my Physical Geology teaching assistant from my freshman year at UCSB, respectively. Without them, I would be stuck with a B.A. in business finance.

Lastly, I would like to thank my family, especially my parents, Russ and Laura, for their undying support and unconditional love. Without your love and support I surely would not have made it this far.

This research was supported by the U. S. Geological Survey, National Cooperative Geologic Mapping Program, under USGS award number G14AC00162 and Idaho State University. The views and conclusions contained in this document are those of the authors and should not be interpreted as necessarily representing the official policies, either expressed or implied, of the U. S. Government.

# Table of Contents

**List of Figures:**

## Abstract

This study is focused south of Salmon, Idaho at the northern margin of the Wyoming salient in the east-central Idaho thrust belt. I present new field mapping of the Poison Creek thrust fault, the western most Sevier-correlated thrust, in addition to thermochronometry of the Poison Creek thrust hanging-wall and detrital zircon analysis of the Ordovician Kinnikinic Quartzite. Within the study area, the Kinnikinic Quartzite sits with angular unconformity upon Mesoproterozoic Lemhi subbasin strata, a relationship that is an expression of the Lemhi Arch, a regional northwest-trending Neoproterozoic to early Paleozoic paleo-topographic high. Detrital zircon results from the Kinnikinic Quartzite show distinct age populations that differ from those in known Paleoproterozoic, Mesoproterozoic Belt Supergroup-equivalent, or early Paleozoic rocks in the area. The Poison Creek thrust fault and the imbricate Goldbug thrust fault placed Mesoproterozoic Lemhi subbasin strata atop the Ordovician Kinnikinic and Saturday Mountain formations. The reconstructed structural configuration of Mesoproterozoic strata across the Poison Creek thrusts requires normal faulting of likely Neoproterozoic to early Paleozoic age. Southeastward-shallowing lateral ramps in both the Poison Creek thrust and Goldbug thrusts are coincident with several imbricate thrust sheets in the footwall of the main thrust. These lateral ramps and imbricate thrust sheets coincide spatially with the Salmon River extensional fault system, a likely Neoproterozoic feature that displays evidence of reactivation at least three times during the Phanerozoic. These observations suggest that the geometry of the Poison Creek thrust fault was strongly influenced by pre-Mesozoic structural features. (U-Th)/He zircon cooling ages of the Poison Creek thrust hanging-wall constrain the timing of faulting to 68-57 Ma, which is contemporaneous with slip along the Absaroka thrust in southeastern Idaho.

# Chapter I: Introduction

The Sevier orogeny of the North American Cordillera resulted from ocean-continent convergence (DeCelles, 2004). The timing of initial orogenesis coincided with an increase in the absolute velocity of the North American plate over the trench and subducting Farallon plate (Coney and Evenchick, 1994). Deformation resulting from this orogeny mostly occurred within Paleozoic passive margin sediments, suggesting a pre-orogenic, Paleozoic continental margin control on the geometry of the fold-thrust belt (Fig. 1) (Crosby, 1969; Lund, 2008).

DeCelles (2004) expanded Armstrong's (1968) definition of the "Sevier orogenic belt" and suggested the Sevier as the portion of the Cordilleran fold-thrust belt from Alaska to southeastern California flanked on the east by the foreland basin and on the west by "hinterland" metamorphic rocks. Cordilleran orogenesis initiated in what is now western Nevada at ~155 Ma and propagated to the east, eventually forming the Laramide orogen in Late Cretaceous and early Tertiary time. Laramide structures generally post-date Sevier faults and are characterized by mostly northwest-striking, basement-involved structures located to the east of the Sevier fold-thrust belt.

South of the Snake River Plain, within the Wyoming salient, the geometry, style, and age of the Sevier fold-thrust belt are well-constrained (Armstrong and Oriel, 1965; Armstrong, 1968; Wiltschko and Dorr, 1983; Burtner et al., 1994; DeCelles, 2004). The Wyoming salient represents a Paleozoic embayment; deformation of the Paleozoic sediments has exaggerated the eastward convexity (Crosby, 1969; Weil and Yonkee, 2012). In this region, Sevier deformation is characterized as thin-skinned, meaning that thrusts root into a stratigraphically-controlled décollement at <15 km depth and do not

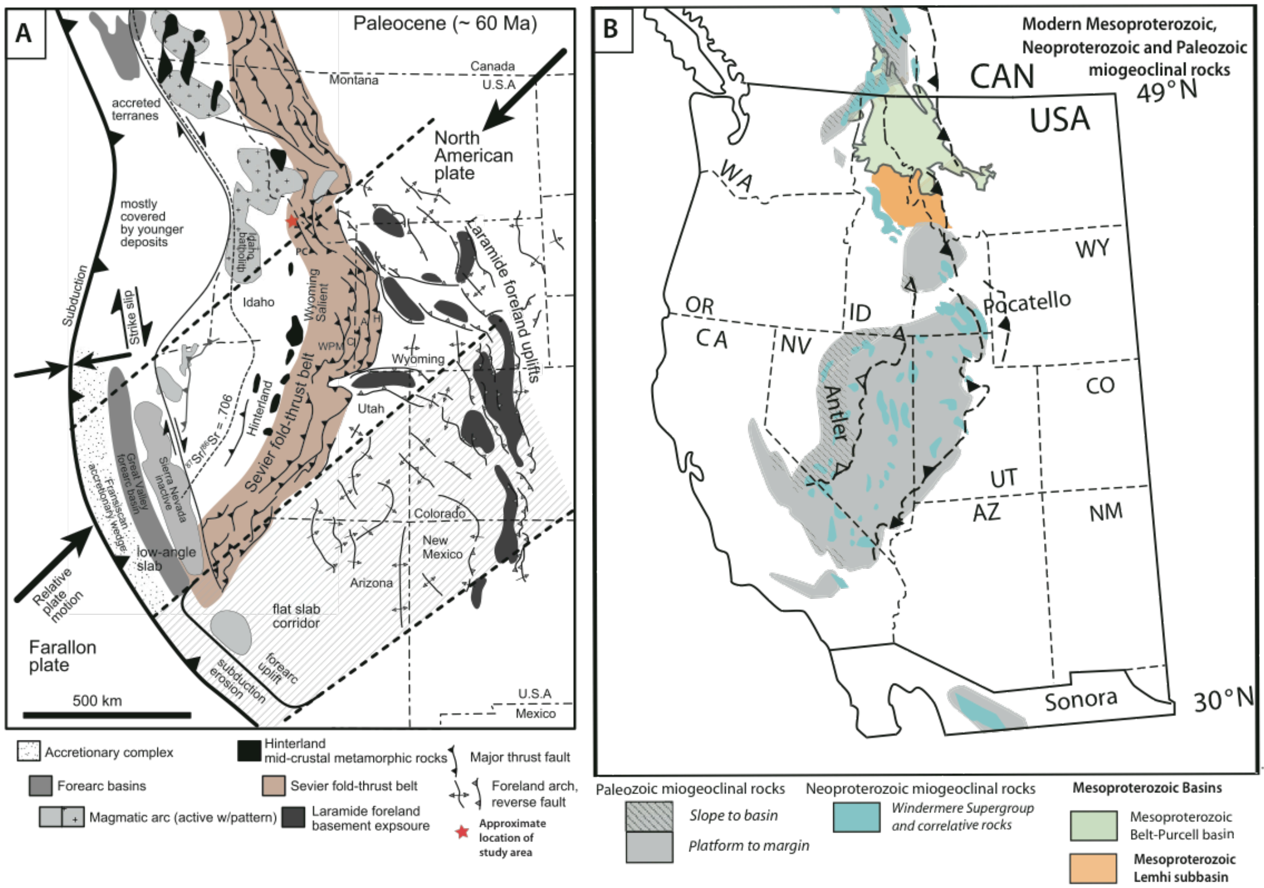

*Figure 1. A. Tectonic map of the North American Cordillera showing major features present during Paleocene time (modified from Weil and Yonkee, 2012). The major thrust faults of the Sevier belt within the Wyoming Salient are annotated as WPM - Willard-Paris Meade; C - Crawford; A - Absaroka and H - Hogsback. The Poison Creek thrust is labeled as PC. The red star denotes the location of the map area of this study as well as the general location of the southwest Montana reentrant. To the east of the Sevier fold-thrust belt is the Laramide province, which is interpreted to have resulted from shallow slab subduction. B. Distribution of Mesoproterozoic, Neoproterozoic, and Paleozoic sedimentary deposits in relation to the frontal thrusts of the Sevier fold-thrust belt (Modified from Lund et al., 2010 with Lemhi subbasin from Lewis et al., 2010)*

involve basement rocks. In the Wyoming salient, the basal décollement occurs in Cambrian-aged shales and deepens into Neoproterozoic strata to the west (Royse et al., 1975). Within the salient, faults and folds generally verge toward the east (Armstrong and Oriel, 1965).

Through the use of dating of syntectonic sediments and thermochronometry, the initiation of deformation has been constrained to Late Jurassic-Early Cretaceous time (Wiltschko and Dorr, 1983; Yonkee et al., 1989; Burtner et al., 1994; DeCelles, 1994). The timing of thrust faulting generally decreases from west to east in the Wyoming salient (DeCelles and Mitra, 1995). This pattern of thrusting is consistent with critical taper theory, a model of thrusting whereby increased friction on the basal décollement of a thrust wedge (i.e. fold-thrust belt) promotes formation of a new frontal thrust below the wedge (Davis et al., 1983). This new thrust propagates into the undeformed foreland of the fold thrust belt, thus reducing the "taper," which is the angle between the décollement and the surface slope of the thrust wedge (Davis et al., 1983).

In contrast to the well-studied central portion of the Wyoming salient, at the northern end of the Wyoming salient in east-central Idaho and southwest Montana the Sevier fold-thrust belt remains poorly understood. This region of the Sevier fold-thrust belt is referred to as the southwest Montana reentrant. Here the thrust belt is closer to the magmatic arc to the west (Crosby, 1969). In this area, the thrust belt incorporates both Archean and Proterozoic rocks but is generally described as thin-skinned because it is not considered to reactivate basement structures and the thrusts are interpreted to root into a <15 km deep décollement (Skipp, 1988). Previous work suggests a possible correlation between this reentrant and a basement arch (inconsistently defined as the Lemhi or

Salmon River Arch) (Armstrong, 1975). Within the study area, most workers call the feature the Lemhi Arch and conclude that it was a paleotopographic high that precluded the deposition of early Paleozoic sediments (Sloss, 1954; Scholten, 1957; Ruppel, 1986; Todt, 2014).

In the Beaverhead Range, the westernmost thrust fault previously recognized as part of the Sevier fold-thrust belt is the Hawley Creek thrust (Skipp, 1988), which correlates along-strike to the northwest to the Poison Creek thrust of the Lemhi Range (Janecke et al., 2000; Evans and Green, 2003). In the northern Lemhi Range, the Poison Creek thrust placed Apple Creek Formation of Mesoproterozoic Lemhi subbasin strata over Ordovician and Silurian-aged passive margin sediments (Tysdal, 2002). Thus, the fault clearly has a thrust sense of displacement. However, previous work focused on the Poison Creek thrust used Mesoproterozoic stratigraphy that has since been reorganized. The Apple Creek Formation is now considered to be above the Lemhi Group rather than low in the Lemhi Group stratigraphy (Burmester et al., 2013). Evans and Green (2003) recognized Swauger Formation, which overlies the Lemhi Group (Burmester et al., 2013), beneath Paleozoic sediments in the footwall of the Poison Creek thrust. Prior to the revision of the Mesoproterozoic stratigraphy, the overall relationship of Mesoproterozoic rocks across the fault was a thrust offset, but is now consistent with a normal offset. To resolve these discrepancies and constrain the geometry and kinematics of the thrust and other structures in the area, this study conducted detailed field mapping of the Poison Creek thrust in the vicinity of the Degan Mountain, Goldbug Ridge, and Poison Peak quadrangles at 1:24,000 scale. In addition, detrital zircon analysis was utilized to evaluate whether early Paleozoic quartzite units in the study area were duplicated vs. in different stratigraphic positions.

Prior to this study, the age of displacement on the Poison Creek thrust was only constrained as post-Triassic due to the presence of a locally pervasive cleavage in its hanging-wall (Tysdal, 2002). To constrain the timing of thrust sheet exhumation, this study used zircon (U-Th)/He thermochronometry on rocks collected from the Poison Creek hanging-wall.

This study not only targets the timing of thrusting on the Poison Creek thrust via isotopic dating of exhumation of the hanging-wall, it also utilizes detrital zircon analysis as a tool to test stratigraphic and structural hypotheses. It includes new field observations of the Mesoproterozoic-Paleozoic contact in the northern Lemhi Range. Additionally, geometric controls on Mesozoic-aged shortening structures by pre-existing structures are discussed. Lastly, the reactivation of pre-existing structures is evaluated as a means to explain kinematic indicators and stratigraphic relationships in the field area.

## **Chapter II**: **Geologic setting**

*Lemhi subbasin*

During the ~1.5 Ga incomplete breakup of the supercontinent Nuna, the western margin of Laurentia consisted of an intracratonal rift basin, which included the Belt-Purcell basin and the neighboring Lemhi subbasin (Harrison, 1972; Ruppel, 1975; Winston, 1986; Lydon, 2007). Temporal, detrital, and lithostratigraphic correlations suggest that deposition of over 15 km of Lemhi subbasin sediments (Burmester et al., 2013) were deposited between 1445 and 1400 Ma, which is coeval with Missoula Group deposition (Winston et al., 1999; Evans et al., 2000; Stewart et al., 2010; Aleinikoff et al., 2012).

The Lemhi subbasin stratigraphy is divided into the Lemhi Group and overlying strata (Fig. 2; Burmester et al., 2013). Two formations of the Lemhi Group had been previously mapped in the study area (Fig. 3; Evans and Green, 2003): the older 3.1 km thick Big Creek Formation and younger 1.8 km thick Gunsight Formation. The Big Creek Formation is a light-gray, coarse-grained siltite to quartzite, whereas the Gunsight Formation is a fine-grained feldspathic quartzite (Evans and Green, 2003; Burmester et al., 2013). The Gunsight Formation has a gradational upper contact with the Swauger Formation (Evans and Green, 2003). The Swauger Formation and the strata that overlie it are not considered part of the Lemhi Group (Fig. 2; Burmester et al., 2013). The Swauger Formation is generally a pure coarse- to medium- grained quartzite that bears rare distinct chert and purple quartzite lithic fragments (Burmester et al., 2013).

The youngest Lemhi subbasin stratigraphic unit mapped in the field area is the Apple Creek Formation (Evans and Green, 2003), which is divided into several informal members (Burmester et al., 2013). The oldest unit of the Apple Creek Formation is the

Jahnke Lake member, which consists of a fine-grained feldspathic quartzite with abundant hematite-rich laminae (Burmester et al., 2013). The next youngest member of the Apple Creek Formation found in the area is a quartz-rich green-gray to dark gray siltite, named the coarse siltite member. Stratigraphically above the coarse siltite member is the banded siltite member, which is a dark gray to black, very fine-grained quartzite, argillite, and siltite.

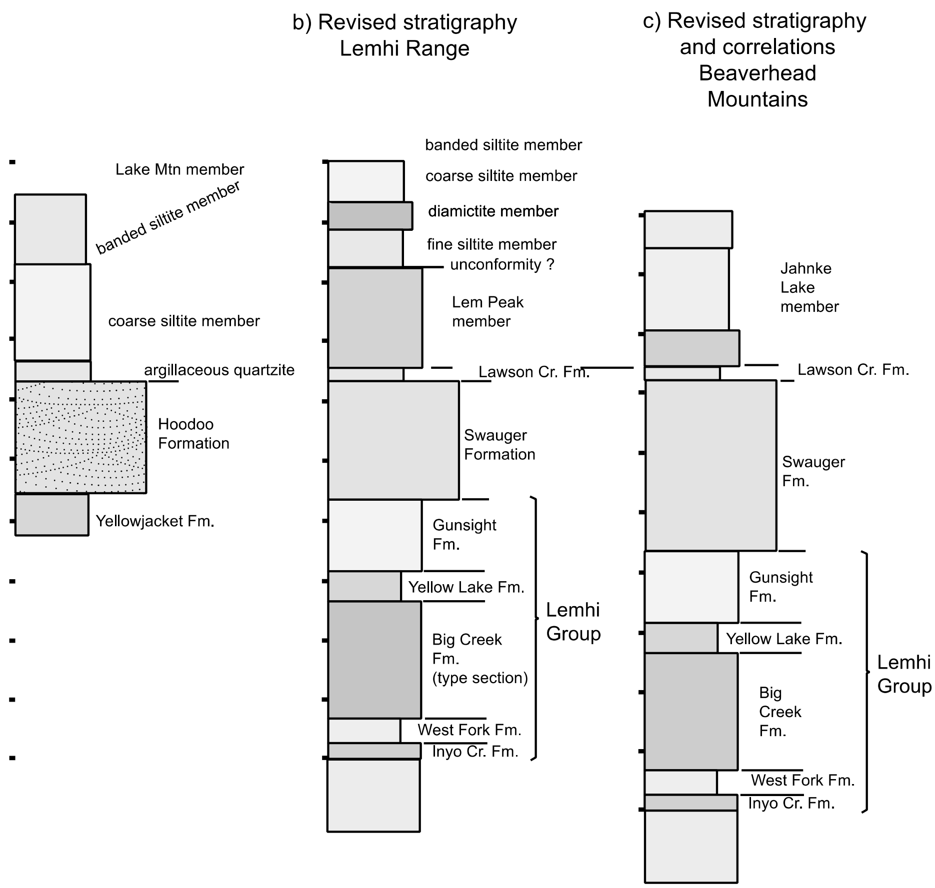


*Figure 2. Newly revised stratigraphy of the Lemhi subbasin for the Salmon River Mountains, Lemhi Range, and the Beaverhead Range (Modified from Burmester et al, in press).*

Previous mapping in the study area had interpreted problematic distributions of the Mesoproterozoic strata and bounding faults (Fig. 3). The revised stratigraphy of the Lemhi subbasin conflicts with relative fault offsets and map relationships in the area. The previous mapping in the area showed the Big Creek Formation as present in both the hanging-walls and footwalls of normal faults in ways that are inconsistent with both the old and new stratigraphy (Fig. 3; Evans and Green, 2003). Earlier work by Evans and Green (2003) also determined that the Gunsight Formation makes up a thrust sheet located in the Poison Creek thrust footwall in the northwestern portion of the field area. Additionally, low angle normal faults and thrust faults were mapped entirely within units, with many faults apparently not required by map patterns (Evans and Green, 2003). Additionally, the Jahnke Lake member was not recognized as a member of the Apple Creek Formation when the area was last mapped in the early 2000s (Burmester et al., 2013). Lastly, the hanging-wall of the Poison Creek thrust is composed of the Apple Creek Formation (Evans and Green, 2003), which was moved above the Lemhi Group during stratigraphic reorganization (Burmester et al., 2013).

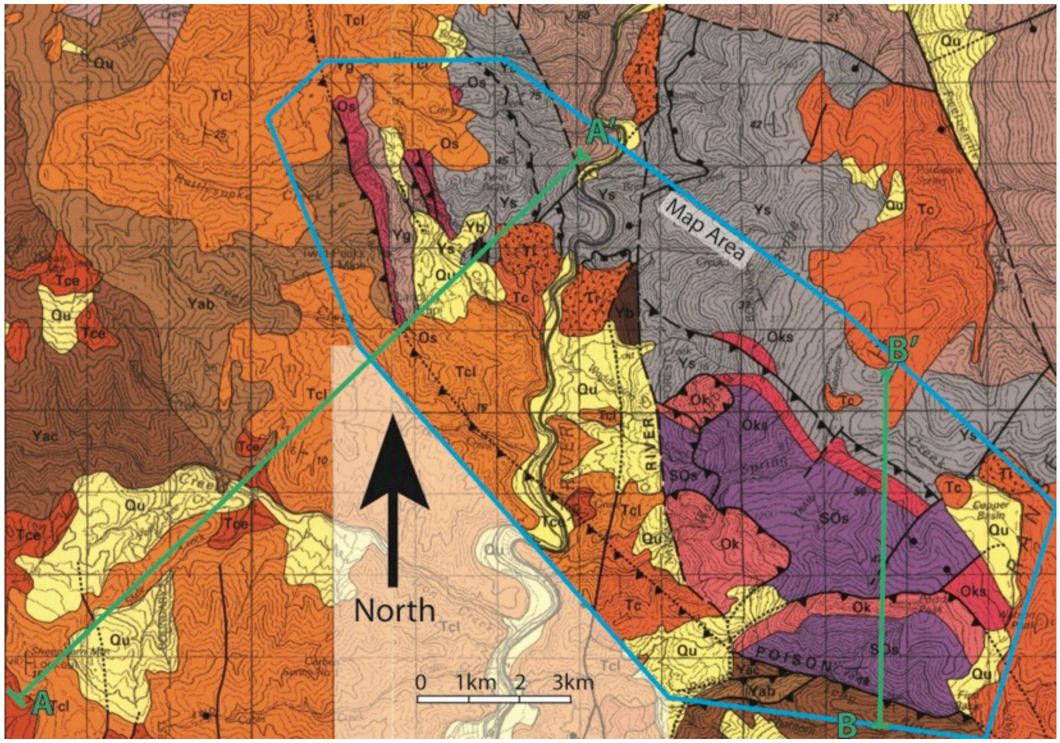


*Figure 3. The most recent mapping done prior to this study shows a complex system of contractional and extensional faults within the area. Abbreviations: Yb- Mesoproterozoic Big Creek Formation; Yg – Mesoproterozoic Gunsight Formation; Ys- Mesoproterozoic Swauger Formation; Yac – coarse siltite member of the Mesoproterozoic Apple Creek Formation; Yab- banded siltite member of the Mesoproterozoic Apple Creek Formation; Os- lower Ordovician Summerhouse Formation; Ok- Ordovician Kinnikinic Formation; Oks- Undifferentiated Summerhouse and Kinnikinic Formations; SOs- Ordovician-Silurian Saturday Mountain Formation (from Evans and Green, 2003). Outline of Plate 1 is shown as a blue polygon. The turquoise lines denote cross-sections A-A' and B-B' of Plate 1.*

*Paleozoic Laurentian passive margin*

Following the late Proterozoic continental breakup of Rodinia, the western margin of Laurentia remained a passive margin throughout much of Paleozoic time (Stewart, 1972). In the mapping area, undifferentiated lower Ordovician Summerhouse Formation, Ordovician Kinnikinic Quartzite, and the Ordovician-Silurian Saturday Mountain Formation are the only Paleozoic strata recognized (Fig. 3). No Neoproterozoic or Cambrian rocks have been observed in this area of the Lemhi Range (Evans and Green, 2003), in contrast to thin sections exposed in the neighboring Beaverhead Range and the southern Lemhi Range (Link and Skipp, 1992).

The Summerhouse Formation and Kinnikinic Quartzite are both similar quartzites, based upon similarities in thickness, purity, color, and grain size (James and Oaks, 1977; Ruppel, 1980; Evans and Green, 2003). However, detrital zircon studies have shown zircon age populations that differ between the two formations (Link, unpublished).

Above the Kinnikinic Quartzite, across a sharp contact, is the Saturday Mountain Formation, which thins toward the southeast within the Lemhi Range (Ruppel and Lopez, 1988; Evans and Green, 2003). In the central Lemhi Range Evans and Green (2003) describe the 370 m thick Saturday Mountain Formation as cream to medium blue-gray, very fine- to medium-grained limestone, with local outcrops of dolomitic wackestone and rare limy mudstone. Generally, the formation is massive, but is locally laminated (Evans and Green, 2003).

Previous mapping in the study area identified a thick carbonate (~1 km) as the Saturday Mountain Formation on top of undifferentiated Ordovician Kinnikinic Quartzite and early Ordovician Summerhouse Formation (Evans and Green, 2003). Identifying the undifferentiated quartzite as Kinnikinic Quartzite would confirm the carbonate as Saturday Mountain Formation. Alternatively, identifying the quartzite as the Summerhouse Formation would suggest the carbonate is the lower Ordovician Ella Dolomite, which is exposed stratigraphically beneath the Kinnikinic Quartzite ~75 km southwest of the study area (Hobbs, 1985).

Previous mapping in the study area at 1:100,000-scale, compiled by Evans and Green (2003), only locally differentiated different Paleozoic units, had unjustified intraformational faulting with minimal offset, had faults losing displacement along-strike or ending rather than being offset along younger faults, had mapped thrusts with unrealistic map traces, and contained noncommittal geologic interpretations such as faults that are everywhere parallel to stratigraphic contacts.

*Lemhi Arch*

Between Proterozoic and Carboniferous time, >2.5 km of carbonate and clastic sediment were deposited directly to the northwest of the current location of the Snake River Plain (Ruppel, 1986). However, in east-central Idaho to the northwest, as little as 200 m were deposited in some localities during the same period of time, unconformably upon Mesoproterozoic rocks (Ross, 1947; Sloss, 1954; Scholten, 1957; Ruppel, 1986). This thin region of Neoproterozoic and Paleozoic stratigraphy defines the Lemhi Arch. Proposed mechanisms for Paleozoic exposure of the Lemhi Arch include: 1) a rotated fault block associated with Rodinian rifting (Lund et al., 2010); 2) a horst active during continental rifting (Lund, 2008); 3) uplift relating to regional-scale folding caused by a proposed late Proterozoic orogenic event (Ruppel, 1986); 4) thermal uplift related to late Cambrian pluton emplacement (Lund et al., 2010); and 5) dynamic uplift resulting from a mantle drip (Link and Janecke, 2009). Recent detrital zircon results link erosion of Cambrian plutons within the Lemhi Arch to concurrent deposition in southeastern Idaho establishing the presence of the high during late Cambrian time (Todt, 2014).

In the area of the Lemhi Arch, the total thickness of Paleozoic sediments is thin relative to neighboring portions of the Paleozoic passive margin (Sloss, 1954; Ruppel, 1986). Paleozoic sediment was the primary wedge deformed by the Mesozoic Sevier orogeny (Fig. 1) (Crosby, 1969; DeCelles, 2004). Royse et al. (1975) recognized that the detachment of most Sevier thrust faults within the Wyoming salient is located in

Cambrian shale. Within the Lemhi Arch of east-central Idaho, however, Neoproterozoic and Cambrian aged sediments are absent (Sloss, 1954; Ruppel, 1986). This along-strike transition to thinner sediments within the area of the Lemhi Arch coincides with the northern boundary of the Wyoming salient, suggesting that thrust belt geometry may have a pre-orogenic, stratigraphic control (Pearson and Becker, 2015).

*Sevier fold-thrust belt*

During Late Jurassic to Early Cretaceous time, the Sevier retroarc fold-thrust belt began to form, eventually accommodating at least 240 km of horizontal shortening in central Nevada and central Utah, >160 km in the area of the Wyoming Salient (DeCelles, 2004), and >50 km across the Beaverhead and Lemhi Ranges of central Idaho (Skipp, 1988). Sevier thrust faults are generally shallowly (<45°) west-dipping (DeCelles, 2004). During the growth of the Sevier fold-thrust belt, thrusting generally propagated toward the undeformed foreland, which has been interpreted to result from a critically tapered orogenic wedge (DeCelles and Mitra, 1995). However, occasional out of sequence faulting has been interpreted as a way of maintaining a critically tapered orogenic wedge (DeCelles and Mitra, 1995).

In the area of east-central Idaho, the Sevier fold-thrust belt bends back away from the direction of transport in a convex toward the west shape, forming a recess between the Helena and Wyoming salients (Crosby, 1969). Mapped thrust faults to the southwest of the Poison Creek thrust, including the Pioneer and Copper Basin thrusts in the White Knob Mountains (Skipp and Hait, 1977), are presumed to be Mesozoic in age (e.g., Skipp and Hait, 1977; Rodgers and Janecke, 1992), but have not been characterized in an Idaho-Montana thrust belt-scale framework. Skipp's (1988) >50 km of shortening in the southwestern Montana-central Idaho segment of the Sevier fold-thrust belt is considered a minimum estimation because it does not include shortening accommodated by thrust faults found farther to the west (DeCelles, 2004). Thus, major uncertainties in the magnitude and timing of shortening remain due to a lack of detailed mapping (1:24,000), thermochronometry, and structural analysis of major thrust faults in east-central Idaho.

*Challis volcanism and extension*

In Eocene time, the thickened lithosphere from Sevier orogenesis began to collapse, resulting in exposure of a metamorphic belt in the Sevier hinterland (Coney and Harms, 1984). Volcanic activity swept southwestward during this time, possibly due to slab steepening at the end of the Laramide orogeny (Humphreys, 1995). During this sweep, mafic lavas and lithic-rich tuffs associated with Challis Group volcanism covered a large portion of the region that is now east-central Idaho (Fisher et. al., 1983; Evans and Green, 2003; Meyers, 2014). Concurrently with Challis volcanism, NW-SE extension was accommodated by northeast striking normal faults in the Trans-Challis fault system (Bennett, 1986). The Challis volcanic deposits have been linked to multiple calderas and vents in the region surrounding the northern Lemhi Range (McIntyre et al., 1982; Ruppel et al., 1993; Janecke and Snee, 1993). Many of the Challis volcanic deposits found in the field area, including the Tuff of Ellis Creek and associated mafic lavas, were likely sourced from the Twin Peaks Caldera located approximately 40 km to the southwest of the field area (Fisher et. al., 1983; Link and Janecke, 1999).

*Basin and Range extension*

Following Eocene gravitational collapse of the thickened crust via metamorphic core complex formation, the Cordillera experienced Basin and Range extension since ~20

Ma (e.g., Proffett, 1977). This extension is still active today and exemplified by active seismicity and GPS data gathered from east-central Idaho (Payne et al., 2008).

The eastern half of the Basin and Range province is typified by half graben bounded by west-dipping normal faults. These features continue on the north side of the Snake River Plain where faults strike in a distinctly more southeasterly direction. In east-central Idaho, half graben constitute the Lemhi, Pahsimeroi, and Lost River valleys, from northeast to southwest (Link and Janecke, 1999). The range-bounding faults that form these valleys and associated mountain ranges continue northwestward until they are no longer mapped west of the Salmon River lineament.

The Salmon River lineament is a south-striking system of normal faults (Salmon River fault system) that spans over 175 km from Salmon to the southeastern end of the Sawtooth Valley. Stratigraphic evidence suggests that faults defining the lineament were active at multiple points in time with the earliest age of activity during the Ordovician Period (Hobbs, 1985). Tysdal (2002) postulated the faults functioned as “tear faults” during Mesozoic shortening. During or after Challis volcanism, the Salmon River fault system down-dropped volcanic deposits to the west (Evans and Green, 2003). Most recently, the Salmon River lineament appears to segment the location of active Basin and Range extension. The stark contrast of topographic expression of the Basin and Range extension across the lineament from the east may reflect a transfer of extension southward to the Sawtooth Valley; further research is needed to test this possibility.

## **Chapter III**: **Methods**

*Mapping*

Reconnaissance mapping and sample collection trips in the fall of 2013 were followed by field mapping over the summer of 2014 by Connor Hansen conducted with the aid of ISU faculty Drs. David Pearson and Paul Link, ISU undergraduate student Cody Stock, and the Idaho Geological Survey. Mapping was conducted using standard geologic field methods, and satellite imagery. Specific attention was given to documenting the geometries and kinematics of the structures in the area. In assessing the mapping, emphasis was placed on reevaluating structures using the modified Lemhi subbasin stratigraphy. The resulting map was digitized using ArcGIS 10.2.2 (Plate 1).

*Detrital zircon separation for thermochronometry and U-Pb analysis*

During the course of this study, two samples were analyzed for U-Pb analysis and two samples were analyzed for (U-Th)/He thermochronometry. Three of these four samples were processed at Idaho State University's mineral separation lab. The separation process involved crushing the sample with a Braun Chipmunk jaw crusher. Crushed sample was then powdered using a Braun Pulverizer disc mill and sieved to remove particles greater than 425 microns. The material smaller than 425 microns was then separated using a Holman-Wilfley Ltd water table. After the heavy separates were dried, they were run through a Frantz isodynamic magnetic separator. From the remaining non-magnetic separate, zircons were separated by density using methylene-iodide. For U-Pb analysis, remaining non-zircons were removed by hand under an Olympus SZX16 microscope before the zircons were mounted in epoxy. Prior to analysis for (U-Th)/He thermochronometry at the Arizona Radiogenic Helium Dating Laboratory at the University of Arizona, Dr. Pearson picked, measured, and packed zircons at Idaho State University.

*(U-Th)/He zircon thermochronometry*

Zircon (U-Th)/He thermochronometry was performed on two samples collected from the hanging-wall of the Poison Creek thrust. Sample CMH13-02 was collected from mylonitic rocks south of Poison Peak at 2172 m elevation. Six zircons from this sample were analyzed. A set of five zircons from the Deep Creek Pluton, sampled at an elevation of ~1499 m, was also analyzed (sample 1LBK12 of Todt, 2014).

For the zircon (U-Th)/He thermochronometer, the temperature below which radiogenic He can no longer diffuse from the grain is ~180 °C (Reiners et al., 2004). Below this temperature, $^4$He produced from subsequent alpha decays are then trapped in the grain and can be measured (Reiners et al., 2004). Assuming an ~180° closure temperature and a typical geothermal gradient of ~20-25 °C/km (Allen and Allen, 2005), the date records the time since a rock passed though a depth of 6-7 km. Following analysis at the Arizona Radiogenic Helium Dating Laboratory at the University of Arizona, weighted means were calculated for each sample (Table 1; Taylor, 1982).

*U-Pb detrital zircon analysis*

Two samples of Paleozoic quartzite were collected during the summer of 2014 for detrital zircon analysis. The intent of the analyses was to confirm the unit identification. Recognition of two distinct quartzites would support an interpretation of an intact section containing the Summerhouse Formation, Ella Dolomite, Kinnikinic Quartzite, and Saturday Mountain Formation. In contrast, recognition of a single quartzite in two places would suggest duplication of stratigraphy by thrust faulting. Given that middle Paleozoic strata in the region of interest have detrital zircon populations distinct from those of the early Paleozoic strata (Link, unpublished), the analysis is a powerful tool beyond lithology to differentiate among early and middle Paleozoic rocks.

Samples were mounted at ISU and imaged using cathodolumenescence. 100 detrital zircons from each sample were measured for U, Pb, and Th isotopes using the MC-LA-ICP-MS at the University of Arizona. Age and uncertainty for each analyzed zircon were then calculated from ratios of $^{235}U$ to $^{207}Pb$, $^{238}U$ to $^{206}Pb$, and $^{232}Th$ to $^{208}Pb$ using the NUagecalc Excel macros (Gehrels, pers. commun.) and the Isoplot plug-in (Ludwig, 2003) for Excel (Table 2). To determine the potential statistical similarity of the samples' provenances, a two-sample Kolmogorov-Smirnov test was run using an Excel macro obtained from the University of Arizona Laserchron lab (Guynn and Gehrels, 2010). Through the test, a P-value is produced (Table 3). At 95% confidence a P-value greater than 0.05 suggests the two samples have the same detrital sources (Guynn and Gehrels, 2010).

*Microstructure/oriented thin sections*

Samples collected for the purpose of making oriented thin sections were cut into oriented billets at Idaho State University and sent to Spectrum Petrographics or Wagner Petrographics. These thin sections were used for kinematic analysis of structures in the field area and to better characterize deformational textures. Photomicrographs were taken of the thin sections using a Leica DFC 290 camera attached to a Nikon Eclipse C400 POL microscope (Figs. 5 and 8; Appendix 2).

*Cross-section construction and restorations*

Cross-sections were constructed using the finished geologic map (Plate 1) with supplementary data from outside the map area coming from maps from the east-central Idaho and southwestern Montana region (Evans and Green, 2003; Lewis et al., 2015), and published literature (Lonn et al., 2013a; Lonn et al., 2013b; Schmidt et al., 2013). Originally drafted by hand, the cross-sections were digitized in Adobe Illustrator with no vertical exaggeration (Plate 1). The software Move 2014.2 was used to test validity of a cross-section by restoring the section to its undeformed state (Fig. 13). The algorithms fault-parallel flow and tri-shear were used to restore motion along faults. In doing so, subsurface interpretations of geometry were tested for plausibility by restoring the stratigraphy to a horizontal, undeformed state.

## **Chapter IV**: **Results**

*Mesoproterozoic-Paleozoic contact*

North of Twin Peaks Ranch (Plate 1), Kinnikinic Quartzite in the immediate footwall of the Goldbug thrust dips 65-80° toward the southwest (260-230°), in contrast to the underlying Swauger Formation, which dips 45-65° toward the west-northwest (270-305°). Although there is locally minor fault breccia along this contact, there is no major fault here. Across the Salmon River to the southeast, the Kinnikinic Quartzite overlies the Swauger Formation. Here, the Kinnikinic Quartzite dips 55-64° toward the southwest whereas Swauger Formation dips only ~44°. No major shear strain was observed near this contact.

*Thrusts and related folds*

In the mapping area, the Poison Creek thrust is the most prominent structural feature, forming a ~20 to 40 m thick mylonitic zone and continuing throughout the mapping area. In the northwestern portion of the map area, mylonites are contained to a more discrete section ~20 m thick where grains have an observed aspect ratio of 1:50-100. Above the mylonitic zone, deformational fabrics are less intense (Fig. 4A). To the southeast, the mylonitic zone is thicker (closer to 40 m) and the strain is equally profound (Fig. 4B). Kinematic indicators (S-C fabrics) are clear in outcrop in both the northwest and southeast.

During the course of the mapping, a second notable thrust beyond the Poison Creek thrust was recognized. This thrust, which will be referred to as the Goldbug thrust, roughly parallels the Poison Creek thrust and is located to the northeast of it. Both thrusts cut deeper into the underlying stratigraphy in the footwall along-strike toward the northwest: the Poison Creek thrust cuts down through the Saturday Mountain Formation and the Goldbug thrust cuts down into the Swauger Formation in the northwestern portion of the map area. On the east side of the Salmon River, the Poison Creek thrust places the coarse siltite member of the Apple Creek Formation on top of the Saturday


*Figure 4A. Northwestward view of the Poison Creek thrust shear zone in the northwestern portion of the field area. S-C fabrics (highlighted in red) show a top to the right motion, consistent with a thrust sense of displacement.*


*Figure 4B. Southeastward view of the Poison Creek thrust shear zone in the southeastern portion of the field area. S-C fabrics (highlighted in red) show a top to the left (northeast) sense of slip.*

Mountain Formation. On the west side of the river, the banded siltite member of the Apple Creek Formation forms the hanging-wall of the Poison Creek thrust. The coarse siltite member is stratigraphically below the banded siltite member, meaning that the Poison Creek thrust has stratigraphically higher rocks in the hanging-wall exposed along-strike toward the northwest. This is in contrast to the observed deepening in the same direction represented in the footwall. In the northwestern portion of the mapping area, both the Goldbug and Poison Creek thrusts dip toward the west (250°-270° dip-direction). This changes toward a south-southwest dip-direction (200-230° dip-direction) to the southeast, all the while dipping in the range of 40-55°.

In both the northwestern and southeastern portions of the map, hanging-wall and footwall stratigraphy is roughly parallel to the thrust faults, which suggests flat on flat geometries. In the northwestern portion of the study area, the Goldbug thrust hanging-wall is characterized by a frontal anticline.

Along the Poison Creek thrust in the northwestern portion of the map area, S-C fabrics show a thrust sense of motion (Fig. 4A). Here, the footwall of the Poison Creek thrust consists of the Kinnikinic Quartzite overlying the Swauger Formation (previously mapped as the Gunsight Formation), which also dips southwestward. Near the top of the Rattlesnake Creek drainage (Plate 1), Challis mafic lava deposits and a Quaternary landslide obscure most of the pre-Cenozoic aged rocks. Southwest of here, fine-grained, greenish quartzite containing purple quartz pebbles and chert clasts is interpreted to be Swauger Formation in the hanging-wall of the Goldbug thrust. Laterally along the front of the Goldbug thrust’s hanging-wall, the grain size in the Swauger Formation remains consistently fine. Locally, the green hue is replaced by fine hematite-rich bedding. The local green hue is likely the result of reduced iron from pyrite grains that can be found in trace amounts. Although the lithology is consistent with the Swauger Formation, grain size and hue differ from the Swauger Formation in the footwall of the Goldbug thrust.

Near the middle of the map area, five south to southwest dipping imbricate thrust sheets compose Goldbug Ridge (Plate 1). These sheets are composed of Kinnikinic Quartzite at the base of each sheet, with overlying Saturday Mountain Formation. At the southern end of Goldbug Ridge, the Goldbug thrust juxtaposes the Kinnikinic Quartzite against the Saturday Mountain Formation.

To the southeast of the imbricated thrust sheets in the footwall of the Goldbug thrust, are two paired, southwest-verging anticlines and synclines with northwest-trending axial traces involving a thick section of Saturday Mountain Formation. This section lies in the hanging-wall of a northeast-striking normal fault that truncates the Kinnikinic Quartzite.

*Extension*

Along the eastern edge of the map area, near Watson Peak, Challis volcanic deposits are down-dropped by an approximately north-striking, east-dipping normal fault. Exposure of the fault is limited. However, outcrops of the Kinnikinic Quartzite found near the fault contain prominent fracture sets (dipping steeply toward 340-350° or near vertical dipping toward 80-90°). The most prominent fracture sets are consistent with east-west extension. Carbonate exposed near the proposed fault exhibits slickensided surfaces. These are interpreted as Riedel prime shears (R' shears) associated with a structure dipping near 60° toward the east-southeast, accommodating an oblique-normal offset. Additionally, microcrystalline silicified rocks (like the one in Fig. 5) can only be found in the drainage as float, suggesting a source within the drainage. Alteration suggests a greater permeability of the rocks, which could be achieved via fracturing related to normal faulting.

*Figure 5. A silicified piece of float from the base of the Copper Basin. The rock is microcrystalline and contains 2-3 mm scale vugs and oxidized orange to red horizons.*

Approximately four km northwest of the above fault, a northeast-striking normal fault juxtaposes the overlying Saturday Mountain Formation against the Kinnikinic Quartzite and dropped the Goldbug and Poison Creek thrusts down to the southeast. Removing the offset on the northeast-striking normal fault restores the series of four folds in the Saturday Mountain Formation to be above the imbricated thrust sheets of Goldbug Ridge. Challis volcanic deposits are present in both the hanging-wall and footwall of this fault.

In addition to the northeast-striking and the north-striking normal faults in the map area, the south-striking Salmon River fault system lowered a block of the Jahnke

Lake member of the Apple Creek Formation against the Swauger Formation. This block was previously identified as the Big Creek Formation. Lithologically, the two units are similar, although the Big Creek Formation is more thickly bedded, contains less quartz and has more planar layering than the observed rocks that make up the fault block. The basis for the reinterpretation is based on the stratigraphic position of the Big Creek Formation being located low in the Lemhi subbasin stratigraphy and the need for an anomalous reverse fault creating an excess of 5 km of throw to bring the Big Creek Formation to the current position. The new interpretation of these rocks as Jahnke Lake member is consistent with extension being accommodated on the Salmon River fault system. A second fault in the Salmon River fault system placed Challis volcanic deposits against the Jahnke Lake Formation on the block's west side.

*Challis-related deposits*

In the central portion of the map area to the east of the Salmon River fault system, Challis mafic lava flows in the hanging-wall of the Salmon River fault system contain foliations interpreted as flow laminations that gently dip (10°-20°) toward the east-southeast. These deposits are >100 m thick. The Tuff of Ellis Creek crops out in the northwestern portion of the map area, where it is found at the base of undifferentiated Challis volcanic deposits and is oriented similarly to the flow laminations observed in the mafic lavas of the immediate area. Satellite imagery of the Iron Creek drainage to the southwest of the field area (~1 km) shows what is interpreted to be thick (>30 m) white to light gray volcanic deposits similar to the Tuff of Ellis Creek, a thick (up to 300 m) wide-spread rhyodacite ash-flow tuff commonly found at the base of the volcanic stratigraphy in the area (Ekren, 1988; Evans and Green, 2003). This interpretation is validated by previous mapping of the Iron Creek drainage, which shows the Tuff of Ellis Creek below mafic lava flows in this location (Evans and Green, 2003). Assuming Challis-aged or younger faults are absent between this Tuff of Ellis Creek outcrop and the Iron Creek drainage, the inferred deposit under the mafic lavas in Iron Creek is probably the continuation of the observed outcrop. To the east of the Salmon River, undifferentiated Challis deposits are characterized by an increase of exposed tuff deposits toward the east.

To the north of Poison Peak in southeastern portion of the map area, ignimbrite deposits locally cover Paleozoic and Proterozoic rocks. Identical ignimbrite deposits occur at similar elevations on either side of the northeast-striking normal fault that truncates the northern Kinnikinic Quartzite deposits. Both contain lithic fragments ranging from a millimeter in diameter to tens of centimeters, fiamme that average one to two centimeters in width, and abundant biotite (~5%). These ignimbrites are interpreted to be the Tuffs of Camas Creek-Black Mountain as described by Ekren (1988). The presence of very similar Challis ignimbrite deposits at similar elevations on the footwall and hanging-wall is suggestive of fault offset and footwall erosion predating the deposition of the ignimbrites, presumably in Eocene time.

In the hanging-wall of the north-striking normal fault at the extreme eastern edge of the field area near Watson Peak, layering and flow laminations of Challis deposits dip ~20° to the east. Here, the stratigraphically lowest units are lithic rich ash-flow tuff deposits (interpreted to be the Tuff of Ellis Creek), which are overlain by compositionally intermediate lava flows ranging from latite and dacite to andesite. Above these deposits are aphanitic vesicular basalt flows occasionally interbedded with pumice rich tuffs and volcaniclastic sandstones.

At the eastern edge of the map area near Copper Basin, the southeastern margin of an intrusive granodiorite consists of an altered rhyolitic tuff. The northwestern boundary of this pluton consists of altered Swauger Formation. Southwest of here in the hanging-wall of the northeast-striking normal fault, multiple outcrops of Saturday Mountain Formation are altered to a reddish orange color. These outcrops have an increased hardness (>6.5 on the Mohs scale of hardness) relative to unaltered Saturday Mountain Formation and do not react to HCl, suggesting replacement of carbonate by silica. Within the Saturday Mountain Formation, a ~20 m thick altered microcrystalline silica-rich (Fig. 9) section parallels bedding. Similarly altered Saturday Mountain Formation can be found in the prospecting pits ("Prospects" in Plate 1) in the saddle to the northwest of the Poison Peak ridgeline.

*U-Pb analysis on zircons*

The two samples collected for detrital zircon analysis produced similar results (Table 2), with zircon age populations defining peaks at 1840 Ma and 1940 Ma (Fig. 6). Up to 95% of the zircon ages center around these two peaks. Both samples also contain zircon age populations of ~1860 Ma and 2080 Ma. A two-sample Kolmogorov-Smirnov test of the detrital zircon populations from both samples, incorporating errors for each grain, produced a P-value of 0.9 (Appendix 2).

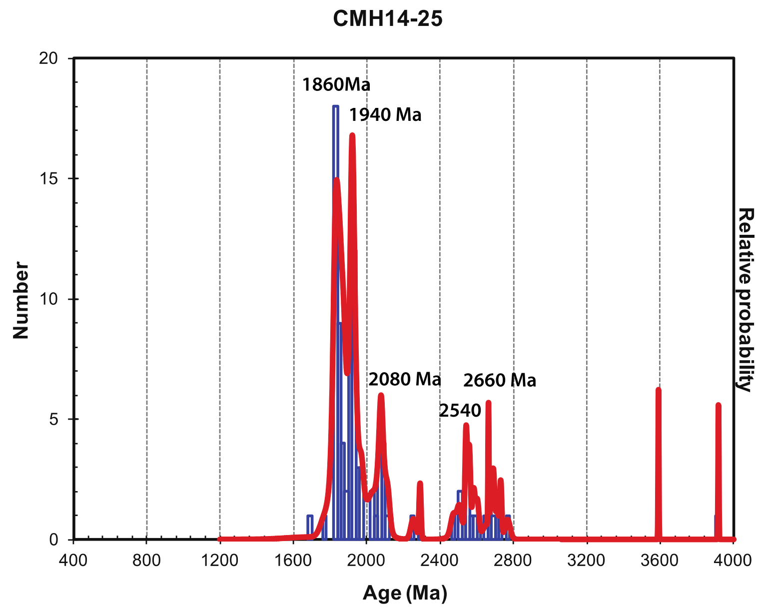


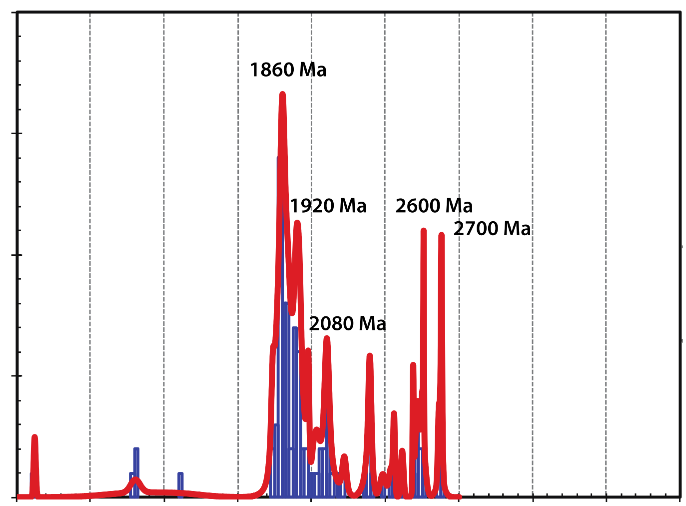


*Figure 6. Probability density plots for the detrital zircon populations of samples CMH14-25 (n=96) and CMH14-29 (n=95).*

*Zircon (U-Th)/He thermochronometry*

For the mylonitic quartzite sample collected to the south of Poison Peak, six detrital zircons produced a weighted mean zircon (U-Th)/He age of 68.4 ± 0.9 Ma (weighted mean age and 2σ standard error here and henceforth; Table 1). Five grains from the pluton produced an age of 56.8 ± 0.7 Ma. The older age was obtained from a sample collected from a higher elevation. Given that the samples were not collected along a vertical transect, they cannot be used to calculate exhumation rates. However, they are consistent with ongoing exhumation occurring from ~68-57 Ma in the hanging wall of the Poison Creek thrust.

*Thin sections*

Thin sections made from oriented samples collected along the Poison Creek thrust show clear S-C fabrics (Fig.8; Passchier and Trouw, 2005) and domino-type fragmenting of porphyroclasts (Fig 7; Passchier and Trouw, 2005) is also consistent with top-to-the-northeast displacement.

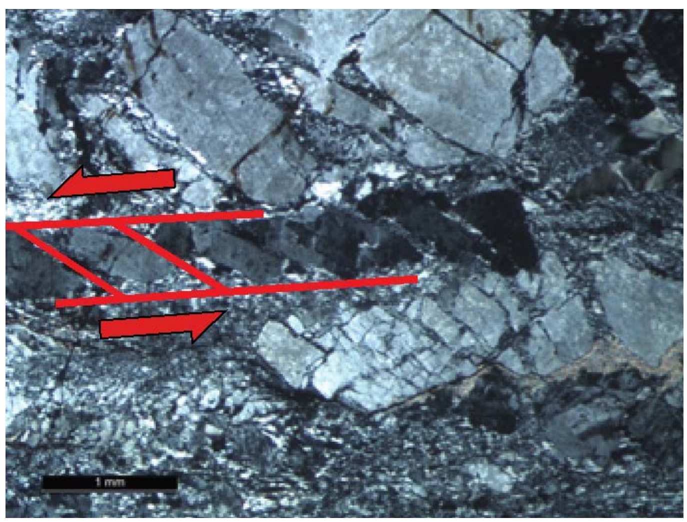

*Figure 7. Photomicrographs of sample CMH13-2 cross-polarized light at 2X magnification. Domino-type fragmentation of porphroclasts is evidence of shearing with a top to the left sense (Passchier and Trouw, 2005). The view looks toward the southeast with the horizontal equating to a ~43° dip to the southwest. Red lines highlight fractures.*

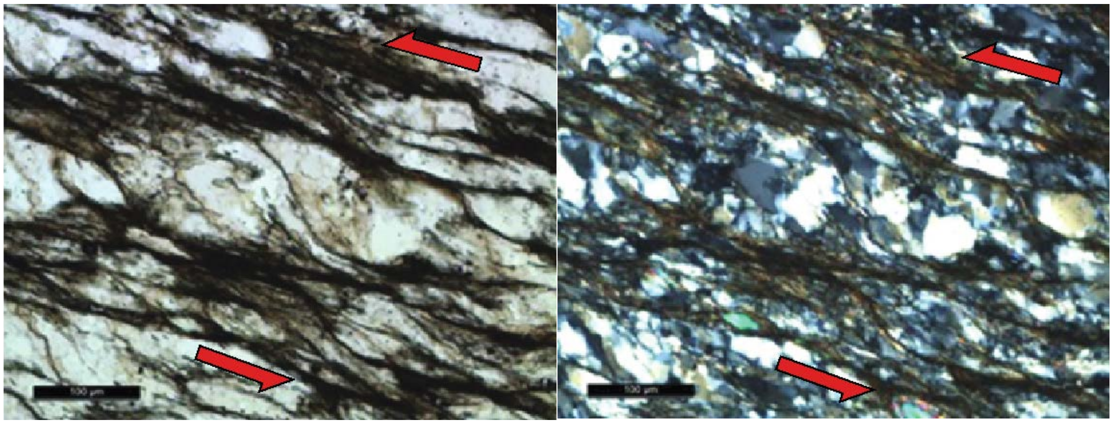

*Figure 8. Photomicrographs of sample CMH14-35 in plane-polarized light (left) and cross-polarized light at 10X magnification. These views look toward the southeast along the Poison Creek thrust. S-C fabrics show a top to the left (northeast) sense-of-shear.*

Outcrops of altered Saturday Mountain Formation on the north-trending ridge coming off of Poison Peak and within the 20 m thick altered horizon inside the Saturday Mountain Formation show folding (Fig. 9). A thin section from the horizon within the Saturday Mountain Formation, however, shows no signs of shear strain (Fig. 8). This indicates that the silicified horizon was not a significant fault zone but rather a lithologic layer that was preferentially altered.

*Figure 9. Outcrop of the silicified horizon within the Saturday Mountain Formation where coloration in the silicified horizon defines folds. Photo was taken on the ridge to the north of Poison Peak, just to the north of the folds found in the Saturday Mountain Formation in the footwall of the Goldbug thrust.*

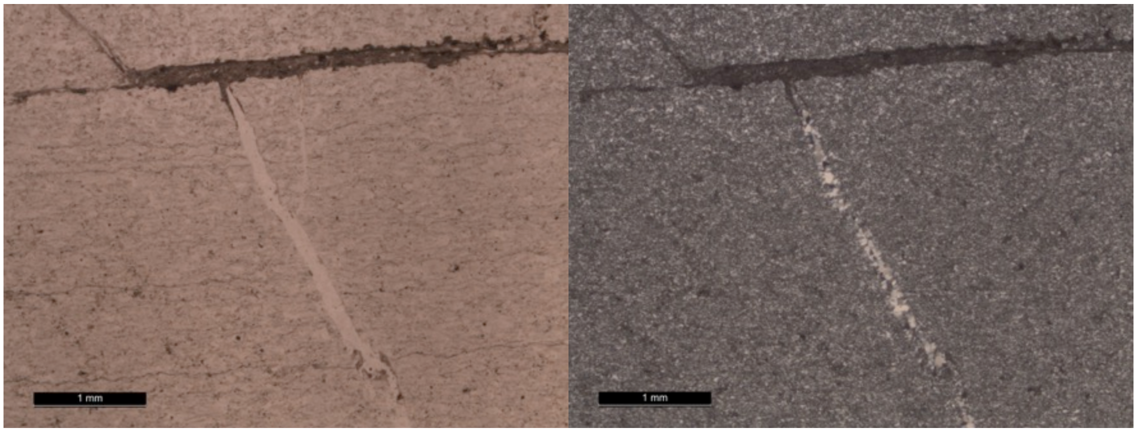


*Figure 10. Photomicrographs of Sample CMH14-01 in plane-polarized (left) and cross-polarized (right) light at 2X magnification. In the middle of the photo is a quartz vein. Very fine quartz grains and undeformed veins show a lack of clear shear strain.*

## Chapter V: Discussion

*Paleozoic-Mesoproterozoic contact and implications for the Lemhi Arch*

The angular contact separating Paleozoic and Mesoproterozoic units is interpreted to be an angular unconformity. Restoration of Paleozoic strata back to horizontal yields a pre-Ordovician 15-30° northeastward dip of underlying Mesoproterozoic strata. This suggests tilting and erosion occurred between Mesoproterozoic and Ordovician time. While there are no constraints on the timing of the erosion of the arch observed in the map area, elsewhere within the Lemhi Arch, exhumation occurred during Late Cambrian time (Todt, 2014). In the study area, Lemhi Arch exhumation was characterized by erosion of >5 km of strata above Swauger Formation prior to Ordovician deposition. Rotation of Mesoproterozoic strata likely occurred at the same time.

*The Poison Creek thrust's offset*

Given the updated Lemhi subbasin stratigraphy (Burmester et al., 2013), the net stratigraphic offset of Mesoproterozoic strata by the Poison Creek thrust is more consistent with a normal fault. However, Mesoproterozoic strata overlie Paleozoic strata in a clear thrust relationship. S-C fabrics and other shear sense indicators observed in thin section are also consistent with this thrust sense of displacement (Fig. 8). Therefore, deformation prior to Mesozoic shortening is required to create these observed geometries.

Although folding prior to Poison Creek thrusting could have lowered a portion of the Apple Creek Formation to the southwest relative to the Swauger Formation, there is no recognized pre-Mesozoic, post Ordovician shortening in the region (Tysdal, 2002). Thus, pre-Ordovician extension is more likely the mechanism to lower the Apple Creek relative to the Swauger Formation, suggesting that the Poison Creek thrust is an inverted normal fault. In the regional tectonic history, Rodinian rifting is the best candidate for formation of this normal fault (Lund et al., 2010). This extension may be temporally comparable to formation of the Lemhi Arch and could explain regional northeastward tilting beneath the unconformity.

*Thrust geometries*

Observations from the field show flat-on-flat thrust fault geometries for the Poison Creek thrust. The orientations of the Apple Creek Formation in the hanging-wall of the Poison Creek thrust consistently demonstrate a hanging-wall flat geometric relationship. Additionally, the strata of the Poison Creek footwall lie nearly parallel to the fault plane. These relationships hold true for both the northwestern and southeastern portions of the map area.

Despite the more complex geometry of the Goldbug thrust, flat on flat relationships are still observed. A local anticline is observed in the hanging-wall of the Goldbug thrust, probably representing a fault bend fold caused by a hanging-wall ramp on a footwall flat in the northwestern portion of the map area. This ramp and related anticline apparently did not fold the Poison Creek thrust to the southwest. The Goldbug fault is interpreted to cut down toward the southwest through the Swauger Formation at a very low angle as shown in Figure 13.

In the southeastern portion of the map area, the Goldbug thrust cuts along the unconformity between the Paleozoic and Mesoproterozoic strata. This interpretation is supported by the presence of the complete thickness of the Kinnikinic Quartzite, with no underlying Swauger Formation in the hanging-wall of the thrust. It is typical for weak stratigraphic horizons to be exploited by thrust faults. In this case, the angular unconformity between the Mesoproterozoic and the Paleozoic may have provided the most suitable weakness. Stratigraphic boundaries within the Mesoproterozoic strata were likely not exploited by Mesozoic deformation due to their northeast-dipping orientations. This suggests that not only the mechanical stratigraphy but also a favorable pre-thrust orientation of stratigraphy strongly controls the geometry of thrusting.

The current dips of 45-85° for strata and fault surfaces in the map area likely are not originally from deformation along the Poison Creek and Goldbug thrusts alone or Cenozoic extension because the strata and faults both dip toward the southwest at similar angles. Basin and Range extension, predominantly accommodated along southwest-dipping normal faults and associated rotation, would decrease the dip angles by rotating the fault blocks down toward the northeast (clockwise) due to southwest-dipping range bounding faults. Instead, the counterclockwise rotation likely resulted during thrusting structurally below the Poison Creek thrust. Upon displacement of newer thrusts farther toward the foreland, thrusts closer to the hinterland are commonly rotated to steeper angles (Fig. 11; e.g., Boyer and Elliott, 1982). The most likely faults to root down below the Poison Creek and Goldbug thrusts include the Brushy Gulch fault and the North Fork and Freeman thrusts, which are all exposed to the northeast of the map area (Schmidt et al., 2013; Lonn et al., 2013a; Lonn et al., 2013b).

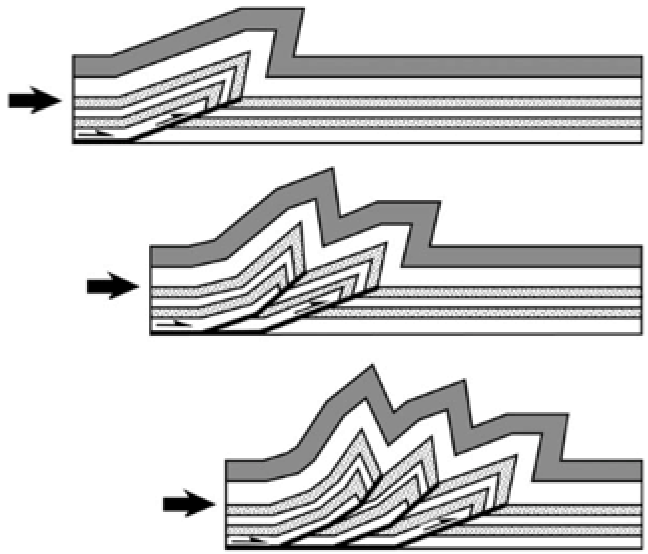

*Figure 11. Schematic rotation of more hinterland-ward structures to steeper angles during slip along newer thrusts (from Poblet and Lisle, 2011; modified from Mitra and Boyer, 1986).*

*Detrital zircon analysis*

The detrital zircon age populations of the two samples are visually similar and the P-value obtained from a two-sample K-S test provides confirmation that the sources of the two samples are statistically similar. This suggests that the samples represent the same stratigraphic unit and that the section is duplicated by a thrust fault. The continuity of the Kinnikinic Quartzite along-strike to the northwest suggests that the Goldbug thrust continues along-strike across the field area, rather than being two different faults along-strike.

The detrital zircon analysis also recognized two age populations, at ~1860 Ma and 2080 Ma, that are not recognized in early Paleozoic and Proterozoic strata found in the area (Link et al., 2013). The Lower Ordovician Summerhouse and Cambrian Wilbert formations are both believed to be recycled from local strata (Ruppel, 1986; Baar, 2009). However, the ~1860 Ma and 2080 Ma populations found in both samples analyzed as part of this study are not present in the Mesoproterozoic strata of the region (Link, unpublished). These ages point toward the contribution of sediment from distal or unrecognized local sources. Additionally, the absence of pre-1800 Ma grains differs from the age populations of the Belt Supergroup. The young (~490 Ma) grain observed in CMH14-29 is likely to have come from the late Cambrian plutons found along the trace of the Lemhi Arch (Lund et al., 2010).

*Proposed model for the Poison Creek thrust*

To better constrain the kinematic history of deformation in the study area, schematic step-by-step models were constructed. Three models were tested using the Move2014.2 software (Appendix 1). In the preferred model (Fig. 13), rifting of Rodinia during late Proterozoic to early Paleozoic time (Fig. 13B) followed deposition of Lemhi subbasin strata during Mesoproterozoic time (Fig. 13C and D). The model suggests that on the Laurentian margin, southeast-striking listric normal faults initiated during this rifting. These faults rotated the Mesoproterozoic strata down toward the northeast, creating topographic relief, which formed the Lemhi Arch (Fig. 12). This rotation was concurrent with or followed by erosion of over five km of the Apple Creek and Lawson Creek Formations in order to expose the Swauger Formation by the Ordovician Period.

By the Ordovician Period, the margin had subsided to the point that the remaining Lemhi Arch was submerged and sedimentation on top of the arch initiated. Following Ordovician to Jurassic quiescence, Mesozoic shortening initially reactivated a normal fault as a thrust fault ramp (Fig. 13E). Within the hanging-wall of the reactivated fault and the overlying Paleozoic strata, fault-propagation folding occurred as evidenced by a
and the overlying Paleozoic strata, fault-propagation folding occurred as evidenced by a
syncline and anticline previous workers recognized to the southwest of the map area

(Evans and Green, 2003). Reconstructions in Move 2014.2 suggest these folds are inconsistent with fault bend folding alone; instead, the tri-shear algorithm (fault propagation folding; Erslev, 1991) was able to better restore the folded strata to an undeformed state, with fault bend folding also contributing to the formation of the syncline to the southeast of the Poison Creek thrust fault (Appendix 1).

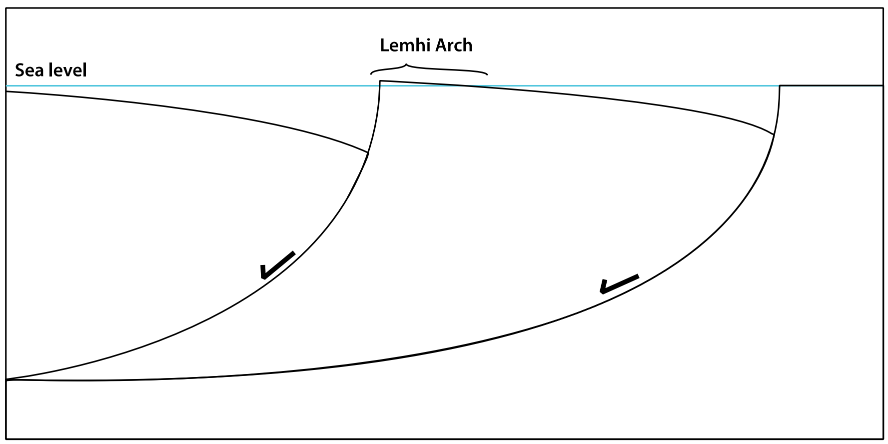


*Figure 12. A schematic regional-scale southwest-northeast cross-section showing the proposed genesis of the Lemhi Arch as a large rotated fault block within the Laurentian rifted margin.*

Initially, the Poison Creek thrust brought a hanging-wall flat of Apple Creek Formation over the top of a Paleozoic footwall flat (Fig. 13F). As shortening continued, the Goldbug thrust formed as an imbricate below the Poison Creek thrust (Fig. 13G). Motion continued on the Goldbug thrust until the thrust wedge reached critical taper and new structures formed to the northeast. The Goldbug and Poison Creek thrusts were then rotated counterclockwise to greater southwestward dips as movement was accommodated on the more foreland-ward structures (Fig. 13H).


*Figure 13A. A southwest-northeast oriented cross-sectional schematic time step showing the undeformed section of the Mesoproterozoic upper Lemhi subbasin strata. Yab- the banded siltite member of the Apple Creek Formation; Yac- coarse siltite member of the Apple Creek Formation; Yad- diamictite member of the Apple Creek Formation; Yaf- fine siltite member of the Apple Creek Formation; Yajl- Jahnke Lake member of the Apple Creek Formation; Ylc- Lawson Creek Formation; Ys- Swauger Formation (not shown in 13A: Yg- Gunsight Formation).*

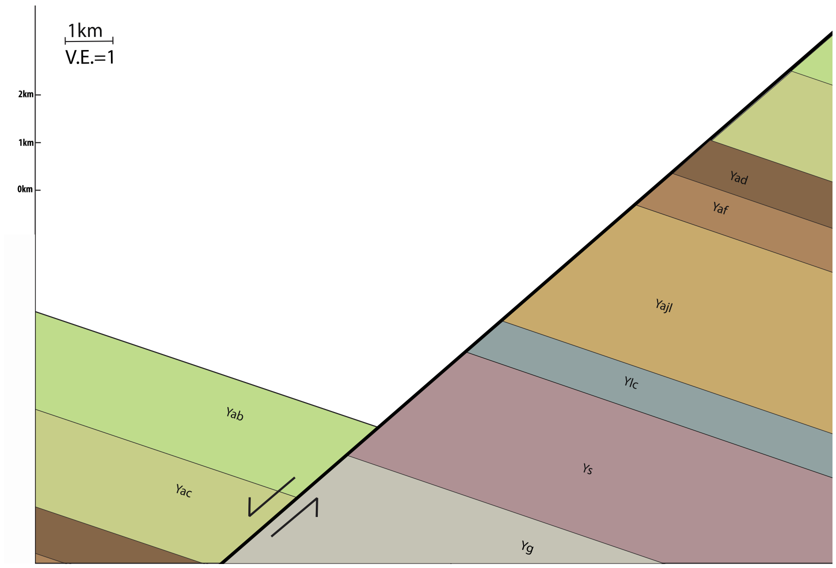


*Figure 13B. Southwest-northeast extension was accommodated on southwest dipping normal faults. Rotation of 15-30° (20° pictured here) down toward the northeast occurred as a result of the extension.*

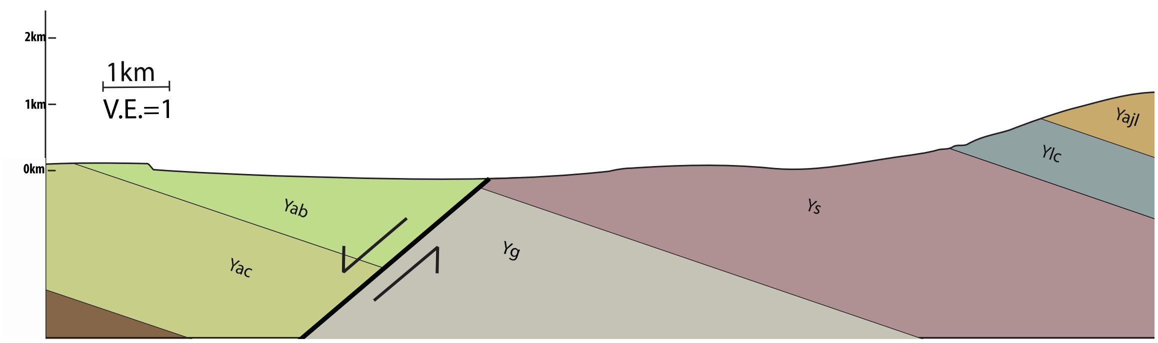


*Figure 13C. Following extension, weathering and erosion removed >5 km to expose the Swauger Formation by Middle Ordovician time.*

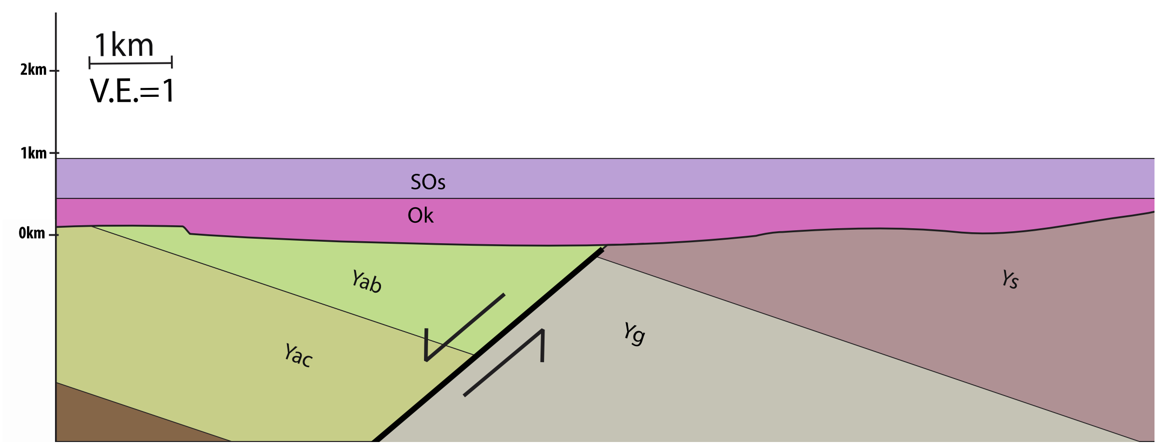


*Figure 13D. During the middle Ordovician through early Silurian time the Kinnikinic Quartzite and Saturday Mountain Formation were deposited unconformably on top of the Mesoproterozoic Lemhi subbasin stratigraphy.*

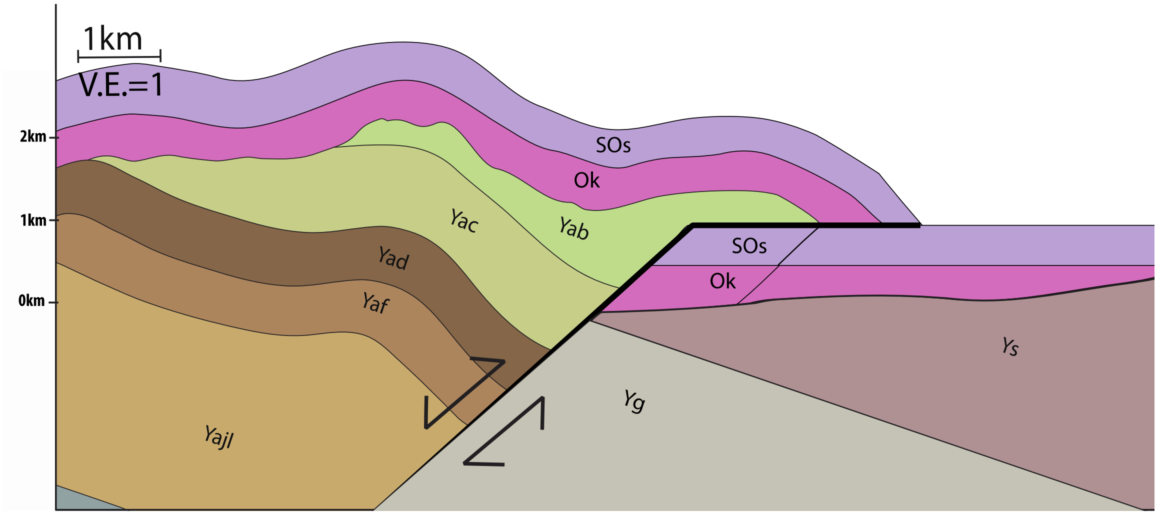


*Figure 13E. In the Mesozoic Period, shortening initially reactivated a normal fault. The Poison Creek thrust cut up through the Ordovician Kinnikinic and Ordovician-Silurian Saturday Mountain Formations using the pre-existing fault surface and the Paleozoic strata as a thrust fault ramp before forming a thrust fault flat o the Saturday Mountain Formation. Hanging-wall strata were deformed via fault propagation folding, as well as, fault bend folding.*

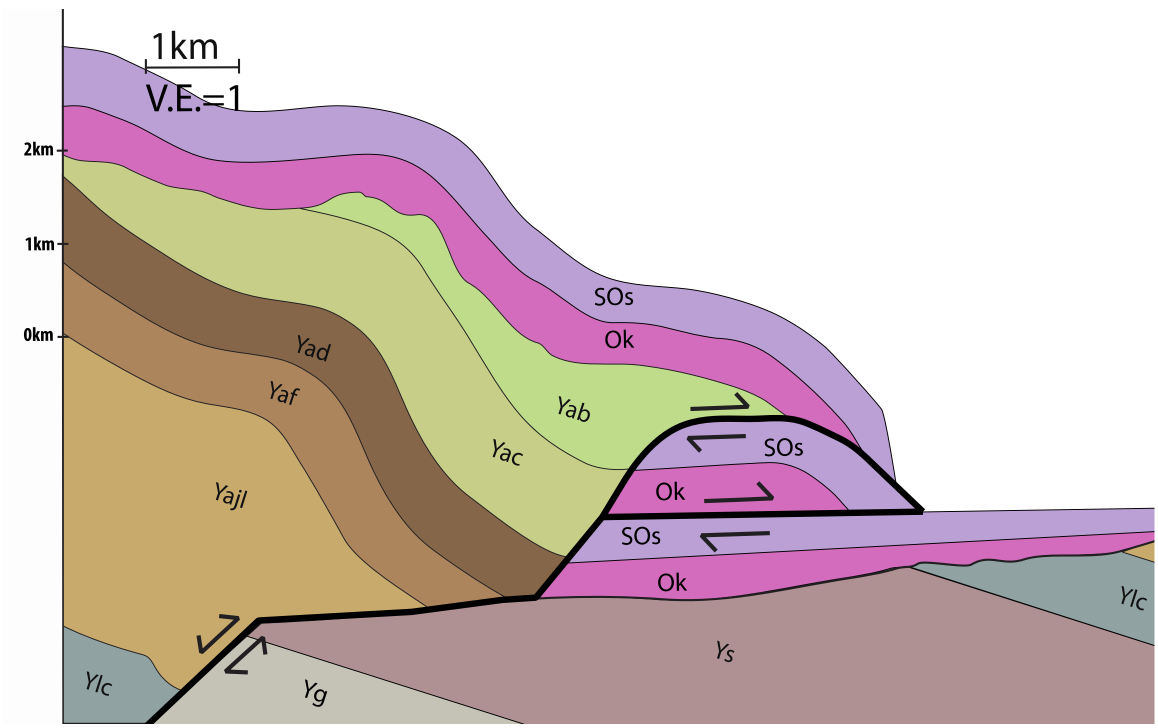


*Figure 13F. Continued shortening led to the formation of a footwall imbricate fault (the Goldbug thrust fault) that cut along the Mesoproterozoic-Paleozoic angular unconformity before ramping up into the Saturday Mountain Formation.*

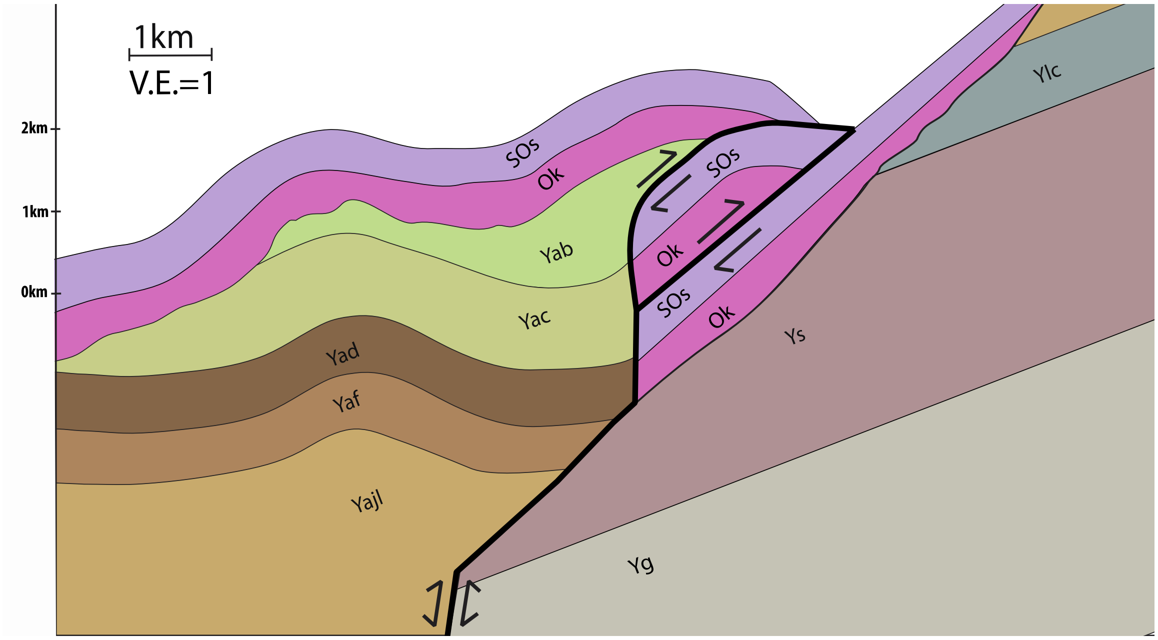

*Figure 13G. Following displacement on the Goldbug thrust fault, structurally lower faults formed or became active. Motion along these faults resulted in the rotation of the strata and the Poison Creek and Goldbug thrust faults.*

*(U-Th)/He zircon thermochronometry*

The two cooling ages from the hanging-wall of the Poison Creek thrust suggest that the thrusts did not form during early Sevier orogenesis (Late Jurassic; Table 1; Fig 14). This implies thrust faults farther to the west, including the Iron Lake fault, the Pioneer thrust, and the Copper Basin thrust, are likely older Sevier-aged structures. Future thermochronometry of these thrusts can determine if the age of motion along these faults fall within the timing of the Sevier orogeny.

The ages of cooling present a good indication of the timing of motion along the Poison Creek thrust fault (Fig. 14; Table 1). The difference between the two cooling ages is to be expected as the samples were collected from different elevations. Despite two significant exhumational events within east-central Idaho since 57 Ma, the zircon (U-Th)/He cooling ages obtained in this study preserve an age corresponding to thrusting in the Sevier fold-thrust belt. Coupled with a preliminary zircon (U-Th)/He cooling age of ~82 Ma from the hanging-wall of the Iron Lake fault to the southwest (Fig. 14; Pearson, unpublished), these dates are consistent with an overall eastward propagation of deformation.

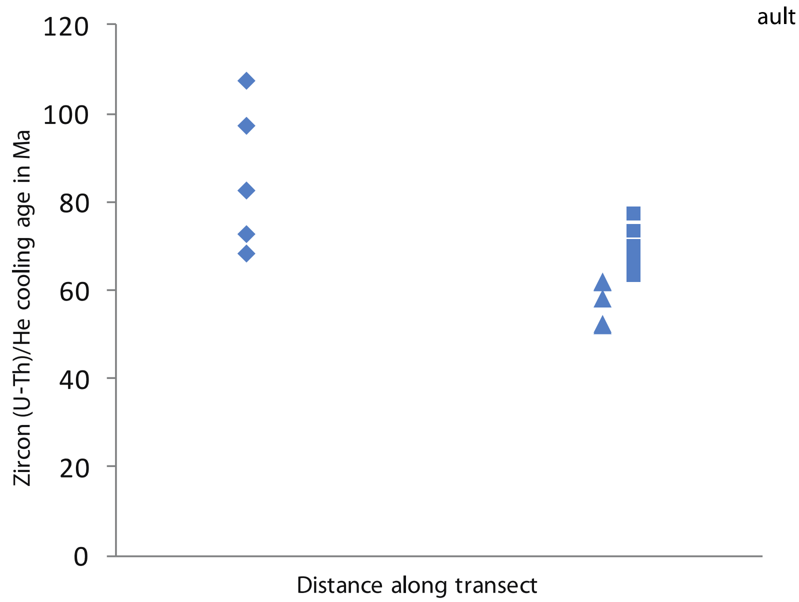


*Figure 14. (U-Th)/He zircon thermochronometry data represented on a transect across the Iron Lake fault (Pearson, unpublished) and the Poison Creek thrust.*

Apatite fission track cooling ages obtained for the Absaroka thrust by Burtner et al. (1994) across the Snake River Plain are ~60 Ma (closure temperature of 90-120°C; Ketcham et al., 1999). The similar ages of exhumation on both the Absaroka and the Poison Creek thrust suggests along-strike continuity in timing of displacement within the Wyoming salient, despite major changes in the orientations of thrusts. Future work correlating other thrusts across the Snake River Plain will provide further context for evaluating the spacing and styles of deformation in the southwest Montana reentrant relative to the Wyoming salient.

*The southwest Montana reentrant and the Lemhi Arch*

Davis et al. (1983) proposed that increased friction on a basal décollement will tend toward greater internal deformation of the thrust wedge, decreased spacing of thrust faults, and a greater topographic slope. Increased friction can be obtained by decreased depth of the décollement and/or the absence of a low-strength horizon (Davis et al., 1983). The relative high of previously deformed Proterozoic rocks in the area of the Lemhi Arch would promote a higher taper angle and decreased spacing between thrusts due to increased strength of the basal décollement (Davis et al., 1983). This has been proposed to result from basement rocks functioning as a buttress (Weil et al., 2010). Skipp (1988) observed a decrease in thrust spacing in the Beaverhead Range of east-central Idaho relative to Sevier belt thrusts in southeastern Idaho. In east-central Idaho, an absence of Cambrian shale and a thin section of Paleozoic rocks within east-central Idaho may have promoted formation of a décollement at the brittle-ductile transition rather than at a stratigraphic weakness (Pearson and Becker, 2015), a similar scenario proposed for southwestern Montana (Kulik and Schmidt, 1988). The crystalline basement rocks within hanging-walls of thrusts in the Beaverhead Range by Skipp (1988) point toward the absence of a shallow weakness and the presence of a deeper décollement. The changes in deformational style may have allowed the fold-thrust belt to propagate farther in the areas around the Lemhi Arch (Pearson and Becker, 2015).

The similarity in cooling ages obtained from the Absaroka thrust in southeastern Idaho (Burtner et al., 1994) and those from the Poison Creek (this study) suggests that the deformation was synchronous and eastward-propagating in both areas, despite differing deformational styles (Pearson and Becker, 2015). More thermochronometry and geometric observations of thrust faults in and around the area of the Lemhi Arch will be needed in order to characterize the geometrical and temporal impacts of the arch on the Wyoming salient.

*Extension*

Three main normal faults or fault systems are recognized in the map area. Age constraints on these faults are limited. However, two of these faults, the northeast-striking and north-striking faults in the southeast portion of the map area, are likely to be middle Eocene in age, given that their orientations are consistent with northwest-southeast oriented Trans-Challis extension (Bennett, 1986). Although Trans-Challis extension has not previously been recognized in the northern Lemhi Range, previous work focused on the mid-Eocene trans-Challis extension only in areas to the west and southwest (Bennett, 1986).

At the southeastern edge of the map area, a north-striking normal fault dropped the Challis volcanic deposits that make up the ridgeline of Watson Peak. The mafic lava flows of this ridge line likely correlate to the mafic lava flows of the Salmon River Valley on the west side of the Salmon River fault system based on the underlying correlated Tuff of Ellis Creek. These correlations of the volcanic deposits suggest the absence of a topographic barrier between the deposits during the time of their eruption. Assuming minimal paleotopography, relating the volcanic deposits in the hanging-wall to the deposits in the hanging-wall of the Salmon River fault system provides a tool for estimating minimum offset along both faults. The lack of volcanic deposits on Poison Peak Ridgeline and the immediate surrounding area suggests the north-striking fault likely dropped the Challis deposits from relative elevations higher than that of the Poison Peak ridgeline.

Cross cutting and map relationships suggest the Salmon River fault system is an old feature that has been reactivated multiple times (Hobbs, 1985). The system consists of west-dipping normal faults. In the study area, one of these faults dropped a block of Jahnke Lake member against the Swauger Formation. The magnitude of offset is only constrained by the thickness of the omitted Lawson Creek Formation (300 m to 1.2 km thick; Evans and Green, 2003; Burmester et al., 2013). Orientations of the angular unconformity and the Mesoproterozoic strata nearby the Jahnke Lake block suggest the overlying Jahnke Lake member in the area should have been eroded away prior to Ordovician Kinnikinic Qaurtzite deposition. Thus, pure dip-slip motion would have to be pre-date pre-Ordovician erosion given that the Jahnke Lake member in most of the area was eroded away during the time of Lemhi Arch.

Alternatively, the fault system could have accommodated a component of strike-slip motion allowing for the block to have originated from the north or south. An additional fault bounding the Jahnke Lake member block on the west side brought Challis volcanic deposits against the Jahnke Lake member, indicating the fault system was active after the Challis volcanic episode.

*Salmon River Lineament*

The footwall lateral ramps in both the Poison Creek and the Goldbug thrusts are suggestive of a single feature impacting the geometry of both structures. In the study area, the lateral ramps spatially coincide with the Salmon River lineament/fault system. The Salmon River fault system is hypothesized to have existed during early Paleozoic time (Hobbs, 1985). This spatial correlation of the lateral ramps with the older Salmon River fault system is similar to those observed by McDowell (1997) in southwestern

Montana. There, the Tendoy and Deadwood Gulch thrusts formed lateral ramps along the edge of the Blacktail-Snowcrest uplift (McDowell, 1997). Due to the absence of bedding dipping toward the west or northwest, a stratigraphic weakness is unlikely to be the feature influencing the fault geometries in the map area. This means pre-existing structures are the most plausible features to be the weakness exploited as lateral ramps. In addition to the lateral ramps, the imbricate thrust sheets of the Goldbug Ridge line up with the Salmon River fault system. A westward dipping system of pre-existing faults would be conducive for forming this imbricate thrust system.

At a more regional scale, the trace of the ~175 km long Salmon River fault system coincides with where Basin and Range valleys and mountain ranges end. Thomas (2006) demonstrates that similar regional-scale structures can have a strong influence on subsequent deformation. The steep dip of the feature, as determined from its linear map trace, leave open the possibility that it initially formed as a strike-slip fault. Furthermore, its linear NNE trace is nearly orthogonal to the proposed spreading center and related passive margin (Lister et al., 1986; Lund, 2008). Thus, the documentation of the Poison Creek thrust as an inverted, likely early Paleozoic normal fault, coupled with the possibility of the Salmon River fault system being a Rodinian transfer fault, suggest that prominent, previously undocumented extensional features associated with Neoproterozoic to early Paleozoic rifting are present in east-central Idaho.

## Chapter VI: Conclusions

The results of this study emphasize the role of reactivation of pre-existing structures and weaknesses in influencing the geometry of Sevier-aged structures in east-central Idaho. The primary conclusions to be drawn from this study include:

1. Mesoproterozoic strata were rotated down toward the northeast prior to the deposition of the Ordovician Kinnikinic Quartzite. This rotation may have occurred coincidentally with normal faulting during breakup of Rodinia and may have been responsible for formation of the Lemhi Arch.
2. Late Proterozoic to early Paleozoic extension in the area is responsible for the lowering of the Apple Creek Formation in the southwest prior to deposition of the Ordovician Kinnikinic Quartzite. The Poison Creek thrust likely reactivated this late Proterozoic to early Paleozoic normal fault.
3. Lateral ramps in the Goldbug and Poison Creek thrust faults spatially correlate to the Salmon River fault system, which has an early Paleozoic or older history. Similar lateral ramps have been observed in the Tendoy and Deadwood Gulch thrusts of southwestern Montana (McDowell, 1997). A westward dipping group of imbricate thrust sheets also line up with the Salmon River fault system, again suggesting an influence of pre-existing normal faults of the Salmon River fault system on Mesozoic thrust geometries.
4. The Salmon River fault system may have been reactivated multiple times, as hypothesized by Hobbs (1985) in the Bayhorse region, and supported in the field area by preservation of a block of Jahnke Lake member within the area of the Lemhi Arch that requires pre-Ordovician normal faulting. This impacted the geometry of

Mesozoic shortening structures and lowered Challis volcanic deposits against Mesoproterozoic and Paleozoic strata.

5. Zircon (U-Th)/He cooling ages suggest that exhumation of the Poison Creek's hanging-wall occurred from 68-57 Ma. This is coincident with displacement along the Absaroka thrust and suggests along-strike continuity in the timing of thrusting within the northern margin of the Wyoming salient.
6. Trans-Challis extension is present in the northern Lemhi Range, represented by two faults observed in the map area. Trans-Challis faulting lowered both the Goldbug and Poison Creek thrust faults down toward the south.
7. The combination of ~1860 Ma and 2080 Ma detrital zircon populations and the absence of pre-1800 Ma grains found in the Ordovician Kinnikinic Quartzite point toward the contribution of sediment from distal or unrecognized local sources.

## References


Aleinikoff, J.N., Slack, J.F., Lund, K., Evans, K.E., Fanning, C.M., Mazdab, F.K., Wooden, J.L., Pillers, R.M., 2012, Constraints on the timing of Co-Cu ± Au mineralization in the Blackbird District, Idaho, using SHRIMP U-Pb ages of monazite and xenotime plus zircon ages of related Mesoproterozoic orthogneisses and metasedimentary rocks: Economic Geology, v. 107, p. 1143–1175.

Allen, J. R., and Allen, P. A., 2005, Basin Analysis - Principles and Application: Blackwell Publishing Ltd., 532 p.

Armstrong, F.C., and Oriel, S.S., 1965, Tectonic development of Idaho-Wyoming thrust belt: AAPG Bulletin, v. 49, p. 1847–1861.

Armstrong, R.L., 1968, Sevier orogenic belt in Nevada and Utah: Geological Society of America Bulletin, v. 79, p. 429–458.

Armstrong, R.L., 1975, Precambrian (1500 M.Y. old) rocks of central Idaho- The Salmon River Arch and its role in Cordilleran sedimentation and tectonics: American Journal of Science, v. 275, p. 437–457.

Baar, E.E., 2009, Determining the regional-scale detrital zircon provenance of the Middle-Late Ordovician Kinnikinic (Eureka) Quartzite, east-central Idaho, U.S., (M.S. Thesis): Spokane, Washington State University, 76 p.

Bennett, E.H., 1986, Relationship of the trans-Challis fault system in central Idaho to Eocene and Basin and Range extensions: Geology, v. 14, no. 6, p. 481–484.

Boyer, S.E., and Elliott, D., 1982, Thrust systems: AAPG Bulletin, v. 66, no. 9, p. 1196-1230.

Burmester, R.F., Lonn, J.D., Lewis, R.S., and McFadden, M.D., 2013, Toward a grand unified theory for stratigraphy of the Lemhi subbasin of the Belt Supergroup: Northwest Geology, v. 42, p. 1–20.

Burmester, R.F. Lonn, J.D., Lewis, R.S., and McFadden, M.D., (in press) Stratigraphy of the Lemhi subbasin of the Belt Supergroup, *in* MacLean, J., and Sears, J.W., eds., Geological Society of America, Special Publication.

Burtner, R.L., Nigrini, A., and Donelick, R.A., 1994, Thermochronology of Lower Cretaceous source rocks in the Idaho-Wyoming thrust belt: AAPG Bulletin, v. 78, p. 1613–1636.

Coney, P.J., and Evenchick, C. A., 1994, Consolidation of the American Cordilleras: Journal of South American Earth Sciences, v. 7, p. 241–262.

Coney, P.J., and Harms, T.A., 1984, Cordilleran metamorphic core complexes: Cenozoic extensional relics of Mesozoic compression: Geology, v. 12, p. 550–554.

Crosby, G.W., 1969, Radial movements in the western Wyoming Salient of the Cordilleran overthrust belt: Geological Society of America Bulletin, v. 80, p. 1061–1078.

Davis, D., Suppe, J., and Dahlen, F.A., 1983, Mechanics of fold-and-thrust belts and accretionary wedges: Journal of Geophysical Research, v. 88, p. 1153–1172.

DeCelles, P.G., 2004, Late Jurassic to Eocene evolution of the Cordilleran: American Journal of Science, v. 304, p. 105–168.

DeCelles, P.G., and Mitra, G., 1995, History of the Sevier orogenic wedge in terms of critical taper models, northeast Utah and southwest Wyoming: Geological Society of America Bulletin, v. 107, p. 454–462.

Ekren, E.B., 1988, Stratigraphic and structural relations of the Hoodoo Quartzite and Yellowjacket Formation of the middle Proterozoic Age from Hoodoo Creek eastward to Mount Taylor, central Idaho: U.S. Geological Survey Bulletin, v. 1570. p. 1-16.

Erslev, E. A, 1991, Trishear fault-propagation folding: Geology, v. 19, p. 617–620.

Evans, K. V., and Green, G.N., 2003, Geologic map of the Salmon national forest and vicinity, eastern-central Idaho: Geologic Investigation Series I-2765, United States Geological Survey, 1:100,000.

Evans, K. V, Aleinikoff, J.N., Obradovich, J.D., and Fanning, C.M., 2000, SHRIMP U-Pb geochronology of volcanic rocks, Belt Supergroup, western Montana: evidence for rapid deposition of sedimentary strata: Canadian Journal of Earth Sciences, v. 37, p. 1287–1300.

Fisher, F.S., McIntyre, D.H., and Johnson, K.M., 1983, Geologic Map of the Challis 1° X 2° Quadrangle, Idaho: Miscellaneous Investigation Series Map I-1819, United States Geological Survey, 1:250,000.

Guynn, J., and Gehrels, G., 2010, Comparison of Detrital Zircon Age Distributions Using the K-S Test: University of Arizona, http://www.geo.arizona.edu/alc.

Harrison, J.E., 1972, Precambrian Belt Basin of northwestern United States: Its geometry, sedimentation, and copper occurrences: Geological Society of America Bulletin, v. 83, p. 1215–1240.

Hobbs, S.W., 1985. Precambrian and Paleozoic sedimentary terranes in the Bayhorse area of the Challis quadrangle, *in* McIntyre, D. H., eds., Symposium on the geology and mineral deposits of the Challis 1 degree x 2 degree quadrangle, Idaho: U.S. Geological Survey Bulletin, v. 1658, p. 59–68.

Humphreys, E.D., 1995, Post-Laramide removal of the Farallon slab, western United States: Geology, v. 23, p. 1–4.

James, C., and Oaks, R., 1977, Petrology of the Kinnikinic Quartzite (middle Ordovician), east-central Idaho: Journal of Sedimentary Petrology, v. 47, p. 1491–1511.

Janecke, S.U., and Snee, L.W., 1993, Timing and episodicity of middle Eocene volcanism and onset of conglomerate deposition, Idaho: The Journal of Geology, p. 603–621.

Janecke, S.U., Vandenburg, C.J., Blankenau, J.J., and Gonigle, J.W.M., 2000, Long-distance longitudinal transport of gravel across the Cordilleran thrust belt of Montana and Idaho: Geology, v. 28, p. 439–442.

Ketcham, R.A., Donelick, R.A., and Carlson, W.D., 1999, Variability of apatite fission-track annealing kinetics: III. Extrapolation to geological time scales: American Mineralogist, v. 84, p. 1235–1255.

Kulik, D.M., and Schmidt, C.J., 1988, Region of overlap and style of interaction of Cordilleran thrust belt and Rocky Mountain foreland, *in* Schmidt, C.J., and Perry, W.J. Jr., eds., Interaction of the Rocky Mountain foreland and the Cordilleran thrust belt: Geological Society of America Memoirs, v. 171, p. 75–98.

Lewis, R.S., Vervoort, J.D., Burmester, R.F., and Oswald, P.J., 2010, Detrital zircon analysis of Mesoproterozoic and Neoproterozoic metasedimentary rocks of north-central Idaho: implications for development of the Belt–Purcell basin: Canadian Journal of Earth Sciences, v. 47, p. 1383–1404.

Lewis, R.S., Burmester, R.F., Othberg, K.L., Lonn, J.D., Stanford, L.R., and McFadden, M.D., 2015, Geologic map of the Salmon 30 x 60 minute quadrangle, Idaho: Idaho Geological Survey, 1:100,000 (in press).

Link, P.K., Janecke, S.U., 1999, Geologic Roadlogs for the Big and Little Lost River, Lemhi, and Salmon River Valleys, *in* Hughes, S.S., and Thackray, G.D., eds. Guidebook to the Geology of Eastern Idaho: Idaho Museum of Natural History, v. 1, p. 295-334.

Link, P.K., and Janecke, S.U., 2009, Mantle drip from the rising Lemhi Arch: 500 Ma plutons and detrital zircons in upper Cambrian sandstones, eastern Idaho: Geological Society of America Abstracts with Programs, v. 41, No 7, p. 181.

Link, P.K., Steel, T.D., Stewart, E.S., Sherwin, J.A., Hess, L.R., and McDonald, C., 2013, Detrital zircons in the Mesoproterozoic upper Belt Supergroup in the Beaverhead and Lemhi Ranges, MT and ID: Northwest Geology, v. 42, p. 39–44.

Lister, G.S., Etheridge, M.A, and Symonds, P.A., 1986, Detachment faulting and the evolution of passive continental margins Detachment faulting and the evolution of passive continental margins: Geology, v. 14, p. 246–250.

Lonn, J.D., Lewis, R.S., and Burmester, R.F., 2013a, Geologic Field Guide to the Freeman Creek Area Near Salmon, Idaho: Northwest Geology, v. 42, p. 199–204.

Lonn, J.D., Lewis, R.S., Burmester, R.F., and McFadden, M.D., 2013b, Geologic Field Guide to the Trail Gulch Area Near North Fork, Idaho: Northwest Geology, v. 42, p. 205–214.

Ludwig, K.R., 2003, User's manual for Isoplot 3.00: a geochronological toolkit for Microsoft Excel. No. 4.

Lund, K., 2008, Geometry of the Neoproterozoic and Paleozoic rift margin of western Laurentia: Implications for mineral deposit settings: Geosphere, v. 4, p. 429.

Lund, K., Aleinikoff, J.N., Evans, K. V., duBray, E.A., Dewitt, E.H., and Unruh, D.M., 2010, SHRIMP U-Pb dating of recurrent Cryogenian and Late Cambrian-Early Ordovician alkalic magmatism in central Idaho: Implications for Rodinian rift tectonics: Geological Society of America Bulletin, v. 122, p. 430–453.

Lydon, J.W., 2007, Geology and metallogeny of the Belt-Purcell basin: Mineral Deposits of Canada, *in* Goodfellow, W.D., eds., A Synthesis of Major Deposit-types, District Metallogeny, the Evolution of Geological Provinces, and Exploration Methods: Geological Association of Canada, Mineral Deposits Division, Special Publication No. 5, p. 581-607.

McDowell, R.J., 1997, Evidence for synchronous thin-skinned and basement deformation in the Cordilleran fold-thrust belt: the Tendoy Mountains, southwestern Montana: Journal of Structural Geology, v. 19, p. 77–87.

McIntyre, D.H., Ekren, E.B., and Hardyman, R.F., 1982, Stratigraphic and structural framework of the Challis volcanics in the eastern half of the Challis 1 x 2 quadrangle, Idaho: Cenozoic geology of Idaho: Idaho Bureau of Mines and Geology Bulletin, v. 26, p. 3–22.

Meyers, J., 2014, Eocene magmatic evolution and synchronous to subsequent extensional faulting, Little Wood River Reservoir Quadrangle, Blaine County Idaho, (M.S. Thesis): Pocatello, Idaho State University, 64 p.

Mitra, G., and Boyer, S.E., 1986, Energy balance and deformation mechanisms of duplexes: Journal of Structural Geology, v. 8, p. 291–304.

Passchier, C.W., Trouw, R.A.J., 2005, Microtectonics - 2 edition: Springer. 366 p.

Payne, S.J., McCaffrey, R., and King, R.W., 2008, Strain rates and contemporary deformation in the Snake River Plain and surrounding Basin and Range from GPS and seismicity: Geology, v. 36, p. 647–650.

Pearson, D.M., and Becker, T.P., 2015, Proterozoic rift systems and their influence on the formation of the Late Cretaceous- early Cenozoic Wyoming Salient: Geological Society of America Abstracts with Programs, v. 47, p. 9.

Poblet, J., and Lisle, R.J., 2011, Kinematic evolution and structural styles of fold-and-thrust belts, *in* Poblet, J., and Lisle, R. J., eds., Kinematic Evolution and Structural Styles of Fold-and-Thrust Belts: Geological Society of London, Special Publications, v. 349, p. 1-24.

Proffett, J.M., 1977, Cenozoic geology of the Yerington district, Nevada, and implications for the nature and origin of Basin and Range faulting: Geological Society of America Bulletin, v. 88, p. 247-266.

Reiners, P.W., Spell, T.L., Nicolescu, S., and Zanetti, K.A., 2004, Zircon (U-Th)/He thermochronometry: He diffusion and comparisons with 40Ar/39Ar dating: Geochimica et Cosmochimica Acta, v. 68, p. 1857–1887.

Reiners, P.W., 2005, Zircon (U-Th)/He thermochronometry, *in* Reiners, P.W., and Ehlers, T.A., eds., Thermochronology: Reviews in Mineralogy and Geochemistry, v. 58, p. 151–176.

Rodgers, D.W., and Janecke, S.U., 1992, Tertiary paleogeographic maps of the western Idaho-Wyoming-Montana thrust belt: *in* Link, P.K., Kuntz, M.A., and Platt, L.B. eds., Regional Geology of Eastern Idaho and Western Wyoming: Geological Society of America Memoirs, v. 179, p. 83–94.

Ross, C. P., 1947, Geology of the Borah Peak quadrangle, Idaho: Geological Society of America Bulletin, v. 58, p. 1085-1160.

Royse, F., Warner, M.A., and Reese, D.L., 1975, Thrust belt structural geometry and related stratigraphic problems Wyoming-Idaho-Northern Utah: Rocky Mountain Association of Geologists 1975 Symposium, p. 41-54.

Ruppel, E.T., 1975, Precambrian and Lower Ordovician rocks in east-central Idaho: U.S. Geological Survey Professional Paper, v. 889, 22 p.

Ruppel, E.T., 1980, Geologic map of the Patterson Quadrangle: U.S. Geological Survey Map GQ-1529, 1:24,000

Ruppel, E.T., 1986, The Lemhi Arch: A Late Proterozoic and Early Paleozoic landmass in central Idaho, *in* Peterson, J.A., eds., Paleotectonics and sedimentation in the Rocky Mountain Region, United States: AAPG Memoir, v. 41, p. 119–130.

Ruppel, E.T., and Lopez, D. A., 1988, Regional geology and mineral deposits in and near the central part of the Lemhi Range, Lemhi County, Idaho: U.S. Geological Survey Professional Paper, v. 1480, 118 p.

Ruppel, E.T., O'Neill, J.M., and Lopez, D.A., 1993, Geologic map of the Dillon 1° x2° quadrangle, Idaho and Montana: United States Geological Survey, 1:250,000.

Schmidt, K.L., Lewis, R.S., and Burmester, R.F., 2013, Into the River of No Return corridor: Mesoproterozoic rocks along the Salmon River from North Fork to Corn Creek, east-central Idaho: Northwest Geology, v. 42, p. 215–228.

Scholten, R., 1957, Paleozoic evolution of the geosynclinal margin north of the snake river plain, Idaho-Montana: Bulletin of the Geological Society of America, v. 68, p. 151–170.

Skipp, B., 1988, Cordilleran thrust belt and faulted foreland in the Beaverhead Mountains, Idaho and Montana, *in* Schmidt, C.J., and Perry, W.J. Jr., eds., Interaction of the Rocky Mountain foreland and the Cordilleran thrust belt: Geological Society of America Memoirs, v. 171, p. 237–266.

Skipp, B., and Hait, M.H.J., 1977, Allochthons along the northeast margin of the Snake River Plain, Idaho: Wyoming Geological Association Guidebook, v. 29, p. 499-515

Skipp, B., and Link, P. K., 1992, Middle and Late Proterozoic rocks and Late Proterozoic tectonics in the southern Beaverhead Mountains, Idaho and Montana: A preliminary report, *in* Link, P.K., Kuntz, M.A., and Platt, L.B. eds., Regional Geology of Eastern Idaho and Western Wyoming: Geological Society of America Memoirs, No 179, p. 141-154.

Sloss, L.L., 1954, Lemhi Arch, a mid-Paleozoic positive element in south-central Idaho: Geological Society of America Bulletin, v. 66, p. 365–368.

Stewart, E.D., Link, P.K., Fanning, C.M., Frost, C.D., and McCurry, M., 2010, Paleogeographic implications of non-North American sediment in the Mesoproterozoic upper Belt Supergroup and Lemhi Group, Idaho and Montana, USA: Geology, v. 38, p. 927–930.

Stewart, J.H., 1972, Initial deposits in the Cordilleran geosyncline: Evidence of a late Precambrian (< 850 my) continental separation: Geological Society of America Bulletin, v. 83, p. 1345–1360.

Taylor, J.R., 1982, An Introduction to Error Analysis: The Study of Uncertainties in Physical Measurements: Univ. Sci. Books, Mill Valley, Calif., 327.

Thomas, W.A., 2006, Tectonic inheritance at a continental margin; GSA Today, v. 16, p. 4–11.

Todt, M.K., 2014, U-Pb and Hf Analysis of zircon grains from the Nounan Dolomite and Worm Creek Quartzite, Idaho and their potential magmatic source: Implications for Cambrian Laurentian tectonics, (M.S. Thesis): Pocatello, Idaho State University, 166 p.

Tysdal, R.G., 2002, Structural geology of western part of Lemhi Range, east-central Idaho: U.S. Geological Survey Professional Paper, v. 1659, 31p..

Weil, A.B., and Yonkee, W.A., 2012, Layer-parallel shortening across the Sevier fold-thrust belt and Laramide foreland of Wyoming: spatial and temporal evolution of a complex geodynamic system: Earth and Planetary Science Letters, v. 357-358, p. 405–420.

Weil, A.B., Yonkee, A., and Sussman, A., 2010, Reconstructing the kinematic evolution of curved mountain belts: A paleomagnetic study of Triassic red beds from the Wyoming salient, Sevier thrust belt, U.S.A: Geological Society of America Bulletin, v. 122, p. 3–23.

Wiltschko, D. V., and Dorr, J.A.J., 1983, Timing of deformation in overthrust belt and foreland of Idaho, Wyoming, and Utah: AAPG bulletin, v. 67, p. 1304–1322.

Winston, D., 1986, Middle Proterozoic tectonics of the Belt Basin, western Montana and northern Idaho: Montana Bureau of Mines and Geology, p. 245–257.

Winston, D., Link, P.K., and Hathaway, N., 1999, The Yellowjacket is not the Prichard and other heresies: Belt Supergroup correlations, structure and paleogeography, east-central Idaho, *in* Hughes, S.S., and Thackray, G.D., eds., Guidebook to the Geology of Eastern Idaho: Idaho Museum of Natural History, v. 1, p. 3–20.

Yonkee, W.A., Parry, W.T., Bruhn, R.L., and Cashman, P.H., 1989, Thermal models of thrust faulting: Constraints from fluid-inclusion observations, Willard thrust sheet, Idaho-Utah-Wyoming thrust belt.: Geological Society of America Bulletin, v. 101, p. 304–313.

**Table 1.** Thermochronometry results.

Weighted average calculations for zircon (U-Th)/He cooling ages based on Taylor (1982).

| | U (ppm) | Th (ppm) | Th/U (atomic) | 4He (nmol/g) | Mass (µg) | Half Width (µm) | HAC (FT) | Cooling Age (Ma) | 2σ (Ma) |
|---|---|---|---|---|---|---|---|---|---|
| CMH13-02 Poison Creek shear zone (44.877675°N, 113.893068°W) | | | | | | | | | |
| Grain | | | | | | | | | |
| 14B790_DP_AC_CMH_01_Z1 | 809 | 149 | 0.18 | 233 | 2.34 | 44.0 | 0.694 | 70.1 | 2.31 |
| 14B791_DP_AC_CMH_01_Z2 | 884 | 317 | 0.36 | 279 | 2.84 | 44.8 | 0.700 | 73.6 | 2.57 |
| 14B792_DP_AC_CMH_01_Z3 | 612 | 132 | 0.22 | 188 | 2.42 | 39.1 | 0.660 | 77.5 | 2.76 |
| 14B793_DP_AC_CMH_01_Z4 | 366 | 112 | 0.30 | 97.4 | 1.12 | 36.7 | 0.642 | 67.7 | 2.58 |
| 14B794_DP_AC_CMH_01_Z5 | 447 | 168 | 0.38 | 135 | 1.91 | 62.9 | 0.781 | 63.6 | 1.92 |
| 14B795_DP_AC_CMH_01_Z6 | 368 | 362 | 0.98 | 111 | 2.07 | 39.1 | 0.668 | 65.5 | 1.83 |
| Average | | | | | | | | 69.7 | 2.33 |
| Weighted Average | | | | | | | | 68.4 | 2.22 |
| 1LBK12 Deep Creek Pluton (45.126159°N, 114.214251°W) | | | | | | | | | |
| Grain | | | | | | | | | |
| 14B801_DP_1LBK12_Z1 | na | na | na | na | na | 92.9 | na | 58.6 | 1.60 |
| 14B802_DP_1LBK12_Z2 | 13.8 | 3.87 | 0.28 | 1.38 | 183 | 83.8 | 0.109 | 52.8 | 1.53 |
| 14B803_DP_1LBK12_Z3 | 31.0 | 12.9 | 0.42 | 0.39 | 18.0 | 64.8 | 0.142 | 62.4 | 1.83 |
| 14B804_DP_1LBK12_Z4 | na | na | na | na | na | 87.9 | na | 62.2 | 1.82 |
| 14B805_DP_1LBK12_Z5 | 14.1 | 6.73 | 0.48 | 0.34 | 64.9 | 59.3 | 0.157 | 52.5 | 1.40 |
| Average | | | | | | | | 57.7 | 1.64 |
| Weighted Average | | | | | | | | 56.8 | 1.60 |

**Table 2:** U-Pb data and NUagecalc ages for Samples CMH14-25 and CMH14-29

CMH14-25 (44.91874801°N, 113.887837°W)

| Analysis | U | 206Pb | U/Th | 206Pb* | ± | 206Pb* | ± | 207Pb* | ± | 206Pb* | ± | Best age | ± | Conc |
|---|---|---|---|---|---|---|---|---|---|---|---|---|---|---|
| | (ppm) | 204Pb | | 207Pb* | (%) | 238U | (%) | 235U | (Ma) | 207Pb* | (Ma) | (Ma) | (Ma) | (%) |
| CMH14-25-67 | 25 | 22872 | 1.7 | 8.7348 | 2.6 | 0.3307 | 3.5 | 1855.8 | 37.3 | 1871.8 | 47.5 | 1871.8 | 47.5 | 98.4 |
| CMH14-25-1 | 194 | 186279 | 2.0 | 8.7332 | 0.5 | 0.3373 | 0.8 | 1872.9 | 7.6 | 1872.1 | 8.4 | 1872.1 | 8.4 | 100.1 |
| CMH14-25-40 | 93 | 154827 | 1.7 | 8.6933 | 0.9 | 0.3343 | 0.6 | 1869.2 | 9.3 | 1880.4 | 16.2 | 1880.4 | 16.2 | 98.9 |
| CMH14-25-33 | 165 | 250152 | 0.9 | 8.6879 | 0.5 | 0.3429 | 1.0 | 1891.4 | 9.4 | 1881.5 | 8.9 | 1881.5 | 8.9 | 101.0 |
| CMH14-25-27 | 85 | 69964 | 2.2 | 8.5878 | 1.0 | 0.3421 | 1.2 | 1899.5 | 14.0 | 1902.3 | 18.7 | 1902.3 | 18.7 | 99.7 |
| CMH14-25-52 | 36 | 40312 | 1.0 | 8.5614 | 1.4 | 0.3460 | 2.0 | 1911.9 | 20.7 | 1907.8 | 24.5 | 1907.8 | 24.5 | 100.4 |
| CMH14-25-54 | 29 | 18108 | 0.7 | 8.5592 | 2.0 | 0.3551 | 1.5 | 1934.3 | 21.3 | 1908.3 | 35.4 | 1908.3 | 35.4 | 102.6 |
| CMH14-25-49 | 104 | 83257 | 1.1 | 8.5473 | 0.9 | 0.3466 | 1.2 | 1914.6 | 12.6 | 1910.8 | 15.7 | 1910.8 | 15.7 | 100.4 |
| CMH14-25-3 | 66 | 48655 | 1.6 | 8.5253 | 1.3 | 0.3539 | 1.5 | 1934.9 | 17.1 | 1915.5 | 22.6 | 1915.5 | 22.6 | 102.0 |
| CMH14-25-4 | 279 | 380288 | 2.3 | 8.5206 | 0.4 | 0.3449 | 1.4 | 1913.3 | 12.4 | 1916.4 | 6.4 | 1916.4 | 6.4 | 99.7 |
| CMH14-25-29 | 103 | 64968 | 1.1 | 8.5162 | 0.5 | 0.3504 | 1.3 | 1927.3 | 12.4 | 1917.4 | 9.7 | 1917.4 | 9.7 | 101.0 |
| CMH14-25-65 | 65 | 59656 | 1.6 | 8.5084 | 1.0 | 0.3458 | 0.8 | 1916.7 | 10.9 | 1919.0 | 17.4 | 1919.0 | 17.4 | 99.8 |
| CMH14-25-20 | 101 | 41790 | 1.0 | 8.5076 | 0.8 | 0.3416 | 0.6 | 1906.2 | 8.9 | 1919.2 | 14.6 | 1919.2 | 14.6 | 98.7 |
| CMH14-25-80 | 92 | 92523 | 1.0 | 8.5048 | 0.7 | 0.3473 | 1.6 | 1920.7 | 15.2 | 1919.8 | 12.2 | 1919.8 | 12.2 | 100.1 |
| CMH14-25-39 | 86 | 62163 | 0.9 | 8.5011 | 0.7 | 0.3504 | 0.8 | 1928.7 | 9.3 | 1920.5 | 13.4 | 1920.5 | 13.4 | 100.8 |
| CMH14-25-71 | 111 | 172937 | 2.9 | 8.5006 | 0.7 | 0.3506 | 2.0 | 1929.3 | 18.4 | 1920.7 | 12.4 | 1920.7 | 12.4 | 100.9 |
| CMH14-25-6 | 54 | 56070 | 0.6 | 8.4991 | 0.9 | 0.3466 | 1.0 | 1919.6 | 11.9 | 1921.0 | 16.5 | 1921.0 | 16.5 | 99.9 |
| CMH14-25-88 | 64 | 57876 | 0.8 | 8.4979 | 2.0 | 0.3442 | 1.4 | 1913.7 | 21.1 | 1921.2 | 36.2 | 1921.2 | 36.2 | 99.3 |
| CMH14-25-36 | 237 | 221284 | 1.3 | 8.4898 | 0.4 | 0.3534 | 1.3 | 1937.2 | 11.4 | 1922.9 | 6.4 | 1922.9 | 6.4 | 101.4 |
| CMH14-25-23 | 53 | 102726 | 1.5 | 8.4707 | 1.4 | 0.3423 | 0.9 | 1911.8 | 14.7 | 1927.0 | 26.0 | 1927.0 | 26.0 | 98.5 |
| CMH14-25-46 | 131 | 109156 | 2.6 | 8.4666 | 0.5 | 0.3507 | 0.7 | 1933.1 | 7.9 | 1927.8 | 9.8 | 1927.8 | 9.8 | 100.5 |
| CMH14-25-51 | 223 | 281331 | 1.5 | 8.4536 | 0.5 | 0.3477 | 0.6 | 1926.9 | 6.5 | 1930.6 | 8.5 | 1930.6 | 8.5 | 99.6 |
| CMH14-25-98 | 37 | 29742 | 0.8 | 8.4426 | 1.7 | 0.3467 | 0.8 | 1925.5 | 16.7 | 1932.9 | 31.1 | 1932.9 | 31.1 | 99.3 |
| CMH14-25-17 | 96 | 98547 | 1.0 | 8.4320 | 0.9 | 0.3397 | 1.1 | 1909.2 | 12.0 | 1935.1 | 16.0 | 1935.1 | 16.0 | 97.4 |
| CMH14-25-97 | 86 | 99671 | 1.4 | 8.4112 | 1.0 | 0.3441 | 0.7 | 1922.4 | 10.7 | 1939.6 | 18.6 | 1939.6 | 18.6 | 98.3 |
| CMH14-25-76 | 25 | 18885 | 0.7 | 8.4093 | 1.9 | 0.3424 | 3.2 | 1918.3 | 32.2 | 1940.0 | 34.5 | 1940.0 | 34.5 | 97.8 |
| CMH14-25-2 | 16 | 19225 | 1.0 | 8.3661 | 2.7 | 0.3501 | 3.6 | 1941.9 | 39.2 | 1949.2 | 48.7 | 1949.2 | 48.7 | 99.3 |
| CMH14-25-75 | 38 | 39653 | 0.9 | 8.3624 | 2.6 | 0.3501 | 0.4 | 1942.3 | 22.9 | 1950.0 | 46.8 | 1950.0 | 46.8 | 99.2 |
| CMH14-25-48 | 16 | 9852 | 0.6 | 8.3269 | 3.4 | 0.3625 | 2.8 | 1976.3 | 37.8 | 1957.6 | 60.0 | 1957.6 | 60.0 | 101.9 |
| CMH14-25-70 | 16 | 12476 | 0.9 | 8.3076 | 4.2 | 0.3614 | 3.1 | 1975.7 | 45.8 | 1961.7 | 75.4 | 1961.7 | 75.4 | 101.4 |
| CMH14-25-69 | 135 | 110488 | 2.2 | 8.2609 | 0.6 | 0.3650 | 1.0 | 1989.0 | 10.3 | 1971.8 | 10.1 | 1971.8 | 10.1 | 101.7 |
| CMH14-25-13 | 30 | 48850 | 0.6 | 8.2504 | 1.6 | 0.3514 | 3.0 | 1957.2 | 29.6 | 1974.0 | 29.3 | 1974.0 | 29.3 | 98.3 |
| CMH14-25-42 | 66 | 57919 | 1.8 | 7.9860 | 1.0 | 0.3704 | 0.7 | 2031.5 | 10.8 | 2031.9 | 18.0 | 2031.9 | 18.0 | 100.0 |

Table 2 Continued

| Analysis | U | 206Pb | U/Th | 206Pb* | ± | 206Pb* | ± | error | 207Pb* | ± | 206Pb* | ± | Best age | ± | Conc |
|---|---|---|---|---|---|---|---|---|---|---|---|---|---|---|---|
| | (ppm) | 204Pb | | 207Pb* | (%) | 238U | (%) | corr. | 235U | (Ma) | 207Pb* | (Ma) | (Ma) | (Ma) | (%) |
| CMH14-25-47 | 14 | 20057 | 0.9 | 9.6541 | 6.7 | 0.3089 | 2.4 | 0.33 | 1714.6 | 58.6 | 1689.3 | 123.1 | 1689.3 | 123.1 | 102.7 |
| CMH14-25-50 | 75 | 72236 | 1.3 | 9.2606 | 1.2 | 0.3170 | 1.1 | 0.67 | 1770.6 | 14.0 | 1765.7 | 22.6 | 1765.7 | 22.6 | 100.5 |
| CMH14-25-63 | 172 | 125537 | 4.1 | 8.9616 | 0.5 | 0.3324 | 1.9 | 0.97 | 1838.4 | 16.5 | 1825.4 | 9.2 | 1825.4 | 9.2 | 101.3 |
| CMH14-25-72 | 68 | 51973 | 1.1 | 8.9609 | 1.7 | 0.3335 | 1.2 | 0.57 | 1841.4 | 17.6 | 1825.5 | 30.9 | 1825.5 | 30.9 | 101.6 |
| CMH14-25-86 | 30 | 34984 | 1.1 | 8.9581 | 2.2 | 0.3369 | 2.7 | 0.77 | 1850.3 | 29.7 | 1826.1 | 40.4 | 1826.1 | 40.4 | 102.5 |
| CMH14-25-25 | 53 | 43228 | 1.3 | 8.9524 | 1.8 | 0.3340 | 1.2 | 0.57 | 1843.4 | 18.4 | 1827.3 | 32.3 | 1827.3 | 32.3 | 101.7 |
| CMH14-25-57 | 76 | 76797 | 1.1 | 8.9486 | 1.3 | 0.3361 | 1.6 | 0.77 | 1849.1 | 17.3 | 1828.0 | 23.6 | 1828.0 | 23.6 | 102.2 |
| CMH14-25-77 | 213 | 243933 | 1.8 | 8.9454 | 0.6 | 0.3305 | 0.8 | 0.79 | 1835.3 | 8.8 | 1828.7 | 11.5 | 1828.7 | 11.5 | 100.7 |
| CMH14-25-99 | 43 | 34622 | 1.1 | 8.9394 | 2.4 | 0.3356 | 1.2 | 0.46 | 1848.7 | 22.5 | 1829.9 | 42.6 | 1829.9 | 42.6 | 101.9 |
| CMH14-25-78 | 105 | 142561 | 1.7 | 8.9385 | 0.8 | 0.3333 | 1.0 | 0.79 | 1843.0 | 10.6 | 1830.1 | 13.9 | 1830.1 | 13.9 | 101.3 |
| CMH14-25-26 | 51 | 60881 | 0.4 | 8.9352 | 1.6 | 0.3274 | 1.4 | 0.67 | 1828.2 | 18.4 | 1830.8 | 29.2 | 1830.8 | 29.2 | 99.7 |
| CMH14-25-37 | 107 | 187122 | 1.0 | 8.9326 | 0.8 | 0.3347 | 1.6 | 0.89 | 1847.1 | 14.9 | 1831.3 | 14.6 | 1831.3 | 14.6 | 101.6 |
| CMH14-25-30 | 50 | 52258 | 1.2 | 8.9254 | 0.9 | 0.3443 | 1.6 | 0.88 | 1871.9 | 15.8 | 1832.8 | 15.6 | 1832.8 | 15.6 | 104.1 |
| CMH14-25-94 | 55 | 49622 | 0.9 | 8.9199 | 1.0 | 0.3321 | 0.9 | 0.69 | 1841.7 | 11.5 | 1833.9 | 17.7 | 1833.9 | 17.7 | 100.8 |
| CMH14-25-64 | 131 | 101286 | 1.1 | 8.9196 | 0.5 | 0.3311 | 0.6 | 0.75 | 1839.1 | 6.5 | 1833.9 | 9.2 | 1833.9 | 9.2 | 100.5 |
| CMH14-25-66 | 54 | 39715 | 1.3 | 8.9178 | 1.0 | 0.3397 | 1.5 | 0.83 | 1861.2 | 15.4 | 1834.3 | 18.2 | 1834.3 | 18.2 | 102.8 |
| CMH14-25-41 | 90 | 105540 | 1.1 | 8.9123 | 1.0 | 0.3321 | 1.0 | 0.71 | 1842.5 | 11.8 | 1835.4 | 17.8 | 1835.4 | 17.8 | 100.7 |
| CMH14-25-14 | 40 | 48541 | 1.1 | 8.9010 | 1.7 | 0.3254 | 0.8 | 0.41 | 1826.3 | 16.1 | 1837.7 | 31.4 | 1837.7 | 31.4 | 98.8 |
| CMH14-25-91 | 67 | 77615 | 1.6 | 8.8963 | 1.2 | 0.3339 | 1.3 | 0.74 | 1848.5 | 14.6 | 1838.7 | 21.0 | 1838.7 | 21.0 | 101.0 |
| CMH14-25-38 | 91 | 61418 | 1.7 | 8.8943 | 1.2 | 0.3280 | 0.8 | 0.55 | 1833.5 | 12.4 | 1839.1 | 22.0 | 1839.1 | 22.0 | 99.4 |
| CMH14-25-62 | 53 | 27086 | 1.3 | 8.8824 | 0.9 | 0.3313 | 5.7 | 0.99 | 1843.2 | 48.9 | 1841.5 | 15.9 | 1841.5 | 15.9 | 100.2 |
| CMH14-25-31 | 39 | 47613 | 0.8 | 8.8694 | 1.3 | 0.3336 | 1.5 | 0.75 | 1850.3 | 16.6 | 1844.1 | 23.4 | 1844.1 | 23.4 | 100.6 |
| CMH14-25-11 | 51 | 56368 | 0.9 | 8.8237 | 1.3 | 0.3256 | 0.9 | 0.59 | 1834.0 | 13.3 | 1853.5 | 22.9 | 1853.5 | 22.9 | 98.0 |
| CMH14-25-15 | 101 | 141184 | 1.8 | 8.8200 | 0.8 | 0.3283 | 3.0 | 0.96 | 1841.5 | 26.9 | 1854.2 | 15.0 | 1854.2 | 15.0 | 98.7 |
| CMH14-25-83 | 90 | 93203 | 1.2 | 8.8177 | 0.8 | 0.3403 | 1.4 | 0.86 | 1872.2 | 13.9 | 1854.7 | 14.8 | 1854.7 | 14.8 | 101.8 |
| CMH14-25-85 | 200 | 292446 | 1.8 | 8.8136 | 0.6 | 0.3386 | 1.9 | 0.96 | 1868.4 | 16.7 | 1855.6 | 10.3 | 1855.6 | 10.3 | 101.3 |
| CMH14-25-73 | 51 | 88751 | 1.1 | 8.8065 | 1.3 | 0.3298 | 1.4 | 0.73 | 1846.7 | 15.9 | 1857.0 | 22.9 | 1857.0 | 22.9 | 99.0 |
| CMH14-25-8 | 134 | 107183 | 1.0 | 8.8062 | 0.9 | 0.3326 | 0.5 | 0.53 | 1853.9 | 8.7 | 1857.1 | 15.6 | 1857.1 | 15.6 | 99.7 |

Table 2 Continued

| Analysis | U | 206Pb | U/Th | 206Pb* | ± | 206Pb* | ± | error | 207Pb* | ± | 206Pb* | ± | Best age | ± | Conc |
|---|---|---|---|---|---|---|---|---|---|---|---|---|---|---|---|
| | (ppm) | 204Pb | | 207Pb* | (%) | 238U | (%) | corr. | 235U | (Ma) | 207Pb* | (Ma) | (Ma) | (Ma) | (%) |
| CMH14-25-12 | 61 | 63851 | 1.5 | 7.8221 | 0.7 | 0.3730 | 0.8 | 0.72 | 2056.1 | 9.5 | 2068.5 | 13.2 | 2068.5 | 13.2 | 98.8 |
| CMH14-25-56 | 28 | 28591 | 0.8 | 7.8103 | 2.9 | 0.3913 | 2.1 | 0.58 | 2099.7 | 31.8 | 2071.2 | 51.5 | 2071.2 | 51.5 | 102.8 |
| CMH14-25-93 | 69 | 137186 | 1.4 | 7.7899 | 0.7 | 0.3859 | 1.0 | 0.81 | 2089.7 | 10.5 | 2075.8 | 12.3 | 2075.8 | 12.3 | 101.4 |
| CMH14-25-21 | 139 | 265009 | 1.7 | 7.7805 | 0.4 | 0.3785 | 0.6 | 0.79 | 2073.5 | 6.4 | 2077.9 | 7.7 | 2077.9 | 7.7 | 99.6 |
| CMH14-25-74 | 81 | 70903 | 2.4 | 7.7578 | 1.3 | 0.3906 | 1.2 | 0.67 | 2104.0 | 15.3 | 2083.1 | 22.5 | 2083.1 | 22.5 | 102.0 |
| CMH14-25-10 | 80 | 104660 | 1.6 | 7.7424 | 0.8 | 0.3749 | 0.7 | 0.66 | 2069.5 | 8.9 | 2086.5 | 13.3 | 2086.5 | 13.3 | 98.4 |
| CMH14-25-100 | 53 | 138280 | 0.6 | 7.7410 | 1.5 | 0.3808 | 1.3 | 0.67 | 2083.5 | 17.9 | 2086.9 | 26.5 | 2086.9 | 26.5 | 99.7 |
| CMH14-25-9 | 61 | 46445 | 1.8 | 7.7279 | 1.3 | 0.3808 | 1.0 | 0.61 | 2085.0 | 14.3 | 2089.8 | 22.4 | 2089.8 | 22.4 | 99.5 |
| CMH14-25-96 | 174 | 227512 | 2.3 | 7.6188 | 0.6 | 0.3960 | 2.2 | 0.96 | 2132.3 | 19.9 | 2114.8 | 10.8 | 2114.8 | 10.8 | 101.7 |
| CMH14-25-53 | 76 | 68203 | 1.4 | 7.0342 | 0.8 | 0.4148 | 0.9 | 0.73 | 2245.6 | 10.6 | 2253.7 | 13.9 | 2253.7 | 13.9 | 99.2 |
| CMH14-25-32 | 187 | 158756 | 1.7 | 6.8872 | 0.3 | 0.4311 | 1.6 | 0.98 | 2299.7 | 14.5 | 2290.1 | 5.1 | 2290.1 | 5.1 | 100.9 |
| CMH14-25-68 | 64 | 56499 | 2.2 | 6.1889 | 0.9 | 0.4650 | 0.8 | 0.68 | 2467.5 | 10.8 | 2472.2 | 14.4 | 2472.2 | 14.4 | 99.6 |
| CMH14-25-16 | 36 | 40389 | 1.2 | 6.0876 | 2.3 | 0.4750 | 2.9 | 0.78 | 2502.5 | 34.3 | 2500.1 | 39.2 | 2500.1 | 39.2 | 100.2 |
| CMH14-25-89 | 89 | 148412 | 1.5 | 6.0738 | 0.7 | 0.4734 | 1.0 | 0.82 | 2501.5 | 11.2 | 2503.9 | 11.6 | 2503.9 | 11.6 | 99.8 |
| CMH14-25-24 | 91 | 89036 | 1.1 | 5.9456 | 0.3 | 0.4881 | 1.1 | 0.97 | 2549.8 | 10.3 | 2539.7 | 4.8 | 2539.7 | 4.8 | 100.9 |
| CMH14-25-60 | 61 | 68182 | 1.2 | 5.9230 | 0.5 | 0.4902 | 1.5 | 0.94 | 2557.4 | 14.4 | 2546.1 | 8.7 | 2546.1 | 8.7 | 101.0 |
| CMH14-25-61 | 110 | 280427 | 1.3 | 5.9091 | 0.5 | 0.4821 | 0.8 | 0.83 | 2544.0 | 9.1 | 2550.0 | 9.1 | 2550.0 | 9.1 | 99.5 |
| CMH14-25-35 | 120 | 843321 | 1.2 | 5.8744 | 0.3 | 0.4795 | 0.7 | 0.91 | 2544.4 | 7.2 | 2559.9 | 5.4 | 2559.9 | 5.4 | 98.6 |
| CMH14-25-58 | 22 | 26780 | 0.9 | 5.8366 | 1.9 | 0.4995 | 2.1 | 0.75 | 2588.6 | 26.8 | 2570.7 | 31.6 | 2570.7 | 31.6 | 101.6 |
| CMH14-25-95 | 134 | 335166 | 1.9 | 5.7974 | 0.4 | 0.4910 | 1.1 | 0.94 | 2578.9 | 11.3 | 2581.9 | 7.2 | 2581.9 | 7.2 | 99.7 |
| CMH14-25-81 | 100 | 120235 | 1.1 | 5.7286 | 0.5 | 0.4991 | 1.1 | 0.90 | 2605.5 | 11.2 | 2601.9 | 8.5 | 2601.9 | 8.5 | 100.3 |
| CMH14-25-59 | 36 | 61697 | 0.3 | 5.5534 | 1.2 | 0.5057 | 1.5 | 0.79 | 2646.9 | 18.1 | 2653.5 | 19.6 | 2653.5 | 19.6 | 99.4 |
| CMH14-25-7 | 176 | 276762 | 0.6 | 5.5231 | 0.1 | 0.5098 | 1.3 | 0.99 | 2659.6 | 12.4 | 2662.6 | 2.3 | 2662.6 | 2.3 | 99.7 |
| CMH14-25-55 | 121 | 198739 | 0.8 | 5.4689 | 0.4 | 0.5151 | 0.3 | 0.67 | 2678.6 | 4.8 | 2678.9 | 6.2 | 2678.9 | 6.2 | 100.0 |
| CMH14-25-5 | 124 | 168157 | 1.3 | 5.4315 | 0.3 | 0.5072 | 1.1 | 0.96 | 2670.5 | 10.7 | 2690.2 | 5.3 | 2690.2 | 5.3 | 98.3 |
| CMH14-25-22 | 55 | 71050 | 1.3 | 5.3706 | 0.6 | 0.5195 | 0.8 | 0.80 | 2703.8 | 9.5 | 2708.9 | 9.9 | 2708.9 | 9.9 | 99.6 |
| CMH14-25-79 | 92 | 117651 | 0.7 | 5.3036 | 0.3 | 0.5332 | 1.0 | 0.95 | 2740.4 | 9.7 | 2729.6 | 5.2 | 2729.6 | 5.2 | 100.9 |
| CMH14-25-45 | 59 | 85572 | 1.3 | 5.1865 | 0.9 | 0.5324 | 2.6 | 0.95 | 2760.1 | 25.7 | 2766.3 | 14.4 | 2766.3 | 14.4 | 99.5 |
| CMH14-25-44 | 159 | 341248 | 1.3 | 3.0874 | 0.1 | 0.6931 | 0.6 | 0.98 | 3517.6 | 5.7 | 3588.4 | 1.9 | 3588.4 | 1.9 | 94.6 |
| CMH14-25-84 | 170 | 446301 | 1.8 | 2.4898 | 0.1 | 0.8418 | 0.6 | 0.98 | 3922.6 | 6.4 | 3915.2 | 2.0 | 3915.2 | 2.0 | 100.6 |
| CMH14-25-90 | 133 | 105514 | 1.5 | 8.7772 | 0.8 | 0.3326 | 0.3 | 0.37 | 1856.6 | 7.5 | 1863.0 | 14.8 | 1863.0 | 14.8 | 99.3 |
| CMH14-25-34 | 59 | 66615 | 0.7 | 8.7743 | 1.8 | 0.3333 | 0.5 | 0.27 | 1858.8 | 15.7 | 1863.6 | 32.0 | 1863.6 | 32.0 | 99.5 |

Table 2 Continued

| Analysis | U | 206Pb | U/Th | 206Pb* | ± | 206Pb* | ± | error | 207Pb* | ± | 206Pb* | ± | Best age | ± | Conc |
|---|---|---|---|---|---|---|---|---|---|---|---|---|---|---|---|
| | (ppm) | 204Pb | | 207Pb* | (%) | 238U | (%) | corr. | 235U | (Ma) | 207Pb* | (Ma) | (Ma) | (Ma) | (%) |
| CMH14-25-67 | 25 | 22872 | 1.7 | 8.7348 | 2.6 | 0.3307 | 3.5 | 0.80 | 1855.8 | 37.3 | 1871.8 | 47.5 | 1871.8 | 47.5 | 98.4 |
| CMH14-25-18 | 92 | 116340 | 1.2 | 8.7972 | 1.0 | 0.3333 | 0.9 | 0.69 | 1856.6 | 11.2 | 1858.9 | 17.2 | 1858.9 | 17.2 | 99.8 |

CMH14-29 (44.89298598°N, 113.877021°W)

| Analysis | U | 206Pb | U/Th | 206Pb* | ± | 206Pb* | ± | error | 207Pb* | ± | 206Pb* | ± | Best age | ± | Conc |
|---|---|---|---|---|---|---|---|---|---|---|---|---|---|---|---|
| | (ppm) | 204Pb | | 207Pb* | (%) | 238U | (%) | corr. | 235U | (Ma) | 207Pb* | (Ma) | (Ma) | (Ma) | (%) |
| CMH14-29-64 | 183 | 17708 | 1.0 | 17.3464 | 2.9 | 0.0798 | 1.2 | 0.38 | 498.7 | 12.4 | 516.4 | 63.7 | 494.8 | 5.6 | 95.8 |
| CMH14-29-88 | 38 | 15424 | 0.7 | 13.5672 | 7.2 | 0.1792 | 2.2 | 0.29 | 1053.0 | 49.7 | 1033.4 | 146.7 | 1033.4 | 146.7 | 102.8 |
| CMH14-29-BSMALL1 | 119 | 63112 | 1.3 | 13.5149 | 1.3 | 0.1717 | 0.7 | 0.49 | 1028.0 | 9.6 | 1041.2 | 26.2 | 1041.2 | 26.2 | 98.1 |
| CMH14-29-77 | 38 | 25825 | 0.7 | 13.4791 | 8.7 | 0.1790 | 2.5 | 0.27 | 1056.8 | 59.6 | 1046.6 | 176.1 | 1046.6 | 176.1 | 101.4 |
| CMH14-29-8 | 97 | 25296 | 2.6 | 11.9258 | 6.2 | 0.2093 | 7.9 | 0.79 | 1248.5 | 72.4 | 1289.1 | 120.7 | 1289.1 | 120.7 | 95.0 |
| CMH14-29-54 | 139 | 131040 | 1.6 | 9.1544 | 0.4 | 0.3191 | 0.7 | 0.88 | 1786.0 | 6.9 | 1786.7 | 7.0 | 1786.7 | 7.0 | 99.9 |
| CMH14-29-85 | 106 | 75453 | 1.9 | 9.1477 | 0.9 | 0.3215 | 0.7 | 0.61 | 1792.8 | 9.2 | 1788.0 | 15.8 | 1788.0 | 15.8 | 100.5 |
| CMH14-29-67 | 50 | 31626 | 0.7 | 9.0751 | 1.3 | 0.3272 | 1.3 | 0.70 | 1814.4 | 16.0 | 1802.6 | 24.4 | 1802.6 | 24.4 | 101.2 |
| CMH14-29-44 | 105 | 204711 | 1.6 | 9.0645 | 0.7 | 0.3217 | 0.7 | 0.71 | 1801.2 | 8.7 | 1804.7 | 13.3 | 1804.7 | 13.3 | 99.6 |
| CMH14-29-30 | 45 | 54991 | 1.1 | 9.0319 | 1.1 | 0.3371 | 1.5 | 0.79 | 1843.9 | 15.7 | 1811.2 | 20.5 | 1811.2 | 20.5 | 103.4 |
| CMH14-29-33 | 43 | 41984 | 0.7 | 8.9879 | 1.9 | 0.3343 | 1.4 | 0.59 | 1840.8 | 19.9 | 1820.1 | 34.3 | 1820.1 | 34.3 | 102.1 |
| CMH14-29-95 | 31 | 13284 | 0.5 | 8.9542 | 2.9 | 0.3326 | 1.5 | 0.45 | 1839.7 | 27.3 | 1826.9 | 51.8 | 1826.9 | 51.8 | 101.3 |
| CMH14-29-BSMALL2 | 53 | 87466 | 1.0 | 8.9428 | 1.4 | 0.3307 | 0.8 | 0.51 | 1835.9 | 14.0 | 1829.2 | 25.7 | 1829.2 | 25.7 | 100.7 |
| CMH14-29-20 | 104 | 146719 | 1.6 | 8.9369 | 1.1 | 0.3293 | 0.6 | 0.51 | 1832.7 | 10.4 | 1830.4 | 19.1 | 1830.4 | 19.1 | 100.2 |
| CMH14-29-89 | 52 | 70339 | 0.9 | 8.9302 | 1.8 | 0.3448 | 3.2 | 0.87 | 1872.8 | 30.9 | 1831.8 | 31.9 | 1831.8 | 31.9 | 104.3 |
| CMH14-29-51 | 77 | 77482 | 1.1 | 8.9245 | 0.8 | 0.3339 | 1.7 | 0.89 | 1845.9 | 15.9 | 1832.9 | 15.2 | 1832.9 | 15.2 | 101.3 |
| CMH14-29-55 | 63 | 76916 | 1.0 | 8.9229 | 1.0 | 0.3302 | 2.4 | 0.92 | 1836.5 | 21.7 | 1833.3 | 18.0 | 1833.3 | 18.0 | 100.3 |
| CMH14-29-24 | 119 | 112704 | 1.8 | 8.9194 | 0.7 | 0.3317 | 0.8 | 0.76 | 1840.8 | 8.7 | 1834.0 | 12.0 | 1834.0 | 12.0 | 100.7 |
| CMH14-29-91 | 70 | 62502 | 0.9 | 8.9107 | 1.2 | 0.3334 | 1.4 | 0.74 | 1845.9 | 15.6 | 1835.7 | 22.2 | 1835.7 | 22.2 | 101.0 |

Table 2 Continued

| Analysis | U | 206Pb | U/Th | 206Pb* | ± | 206Pb* | ± | error | 207Pb* | ± | 206Pb* | ± | Best age | ± | Conc |
|---|---|---|---|---|---|---|---|---|---|---|---|---|---|---|---|
| | (ppm) | 204Pb | | 207Pb* | (%) | 238U | (%) | corr. | 235U | (Ma) | 207Pb* | (Ma) | (Ma) | (Ma) | (%) |
| CMH14-29-4 | 97 | 50267 | 1.3 | 8.7979 | 1.1 | 0.3412 | 1.3 | 0.78 | 1876.5 | 14.7 | 1858.8 | 19.4 | 1858.8 | 19.4 | 101.8 |
| CMH14-29-50 | 34 | 43278 | 0.7 | 8.7905 | 2.0 | 0.3310 | 2.5 | 0.78 | 1851.2 | 27.7 | 1860.3 | 36.8 | 1860.3 | 36.8 | 99.1 |
| CMH14-29-53 | 63 | 38286 | 1.1 | 8.7874 | 0.9 | 0.3346 | 0.6 | 0.52 | 1860.8 | 9.3 | 1860.9 | 16.8 | 1860.9 | 16.8 | 100.0 |
| CMH14-29-92 | 67 | 47098 | 1.6 | 8.7684 | 1.2 | 0.3422 | 0.8 | 0.54 | 1881.7 | 12.6 | 1864.8 | 22.4 | 1864.8 | 22.4 | 101.7 |
| CMH14-29-21 | 68 | 29022 | 1.5 | 8.7668 | 1.2 | 0.3363 | 0.9 | 0.60 | 1867.1 | 12.5 | 1865.2 | 21.0 | 1865.2 | 21.0 | 100.2 |
| CMH14-29-14 | 54 | 61547 | 0.9 | 8.7656 | 1.2 | 0.3334 | 1.3 | 0.74 | 1859.8 | 15.0 | 1865.4 | 21.4 | 1865.4 | 21.4 | 99.4 |
| CMH14-29-42 | 19 | 20711 | 0.5 | 8.7511 | 2.8 | 0.3314 | 1.2 | 0.38 | 1856.2 | 26.3 | 1868.4 | 51.4 | 1868.4 | 51.4 | 98.8 |
| CMH14-29-68 | 152 | 101437 | 2.3 | 8.7416 | 0.5 | 0.3178 | 1.0 | 0.88 | 1821.3 | 9.8 | 1870.4 | 9.8 | 1870.4 | 9.8 | 95.1 |
| CMH14-29-11 | 19 | 17229 | 0.6 | 8.7199 | 4.3 | 0.3347 | 3.7 | 0.65 | 1867.7 | 48.4 | 1874.9 | 77.7 | 1874.9 | 77.7 | 99.3 |
| CMH14-29-97 | 129 | 125533 | 1.8 | 8.6481 | 0.7 | 0.3411 | 0.8 | 0.76 | 1891.0 | 8.7 | 1889.7 | 12.0 | 1889.7 | 12.0 | 100.1 |
| CMH14-29-58 | 42 | 39293 | 0.9 | 8.6126 | 1.8 | 0.3481 | 0.8 | 0.40 | 1911.9 | 16.7 | 1897.1 | 31.9 | 1897.1 | 31.9 | 101.5 |
| CMH14-29-87 | 56 | 109944 | 1.8 | 8.5901 | 1.3 | 0.3549 | 1.6 | 0.77 | 1930.7 | 17.8 | 1901.8 | 23.7 | 1901.8 | 23.7 | 102.9 |
| CMH14-29-92 | 83 | 122953 | 1.5 | 8.5511 | 0.7 | 0.3541 | 0.8 | 0.74 | 1932.9 | 9.5 | 1910.0 | 13.2 | 1910.0 | 13.2 | 102.3 |
| CMH14-29-61 | 66 | 57241 | 0.6 | 8.5397 | 0.9 | 0.3511 | 2.8 | 0.95 | 1926.5 | 25.3 | 1912.4 | 15.8 | 1912.4 | 15.8 | 101.4 |
| CMH14-29-56 | 84 | 81979 | 1.8 | 8.5263 | 0.5 | 0.3510 | 1.2 | 0.92 | 1927.6 | 11.4 | 1915.2 | 9.5 | 1915.2 | 9.5 | 101.2 |
| CMH14-29-82 | 51 | 98985 | 1.1 | 8.5228 | 1.3 | 0.3489 | 1.5 | 0.76 | 1923.0 | 17.6 | 1916.0 | 23.8 | 1916.0 | 23.8 | 100.7 |
| CMH14-29-10 | 101 | 117384 | 0.9 | 8.5150 | 0.6 | 0.3547 | 0.9 | 0.81 | 1937.9 | 9.6 | 1917.6 | 11.6 | 1917.6 | 11.6 | 102.1 |
| CMH14-29-31 | 85 | 139416 | 1.4 | 8.5105 | 0.7 | 0.3529 | 1.2 | 0.84 | 1934.0 | 12.1 | 1918.6 | 13.4 | 1918.6 | 13.4 | 101.6 |
| CMH14-29-2 | 44 | 45312 | 0.5 | 8.4833 | 1.9 | 0.3550 | 1.7 | 0.66 | 1941.8 | 21.8 | 1924.3 | 33.8 | 1924.3 | 33.8 | 101.8 |
| CMH14-29-62 | 95 | 106046 | 0.8 | 8.4684 | 0.7 | 0.3504 | 1.1 | 0.84 | 1932.2 | 11.3 | 1927.5 | 12.6 | 1927.5 | 12.6 | 100.5 |
| CMH14-29-28 | 46 | 28725 | 0.5 | 8.4638 | 1.4 | 0.3528 | 1.2 | 0.67 | 1938.5 | 15.8 | 1928.4 | 24.3 | 1928.4 | 24.3 | 101.0 |
| CMH14-29-35 | 95 | 102677 | 0.9 | 8.4430 | 0.7 | 0.3541 | 1.0 | 0.83 | 1943.8 | 10.8 | 1932.8 | 12.3 | 1932.8 | 12.3 | 101.1 |
| CMH14-29-86 | 96 | 136436 | 1.2 | 8.4406 | 0.5 | 0.3562 | 2.1 | 0.98 | 1949.2 | 18.6 | 1933.3 | 8.3 | 1933.3 | 8.3 | 101.6 |
| CMH14-29-75 | 54 | 87857 | 1.0 | 8.4204 | 0.9 | 0.3566 | 1.2 | 0.80 | 1952.3 | 13.1 | 1937.6 | 16.1 | 1937.6 | 16.1 | 101.5 |
| CMH14-29-74 | 29 | 8023 | 1.1 | 8.4055 | 4.0 | 0.3627 | 3.7 | 0.69 | 1968.5 | 47.5 | 1940.8 | 71.0 | 1940.8 | 71.0 | 102.8 |
| CMH14-29-6 | 117 | 116684 | 1.1 | 8.3321 | 0.6 | 0.3629 | 1.5 | 0.92 | 1976.7 | 14.2 | 1956.5 | 11.6 | 1956.5 | 11.6 | 102.0 |
| CMH14-29-81 | 163 | 135100 | 0.8 | 8.2397 | 0.4 | 0.3581 | 0.5 | 0.77 | 1974.7 | 5.7 | 1976.3 | 7.5 | 1976.3 | 7.5 | 99.8 |
| CMH14-29-37 | 285 | 478462 | 1.4 | 8.2233 | 0.3 | 0.3670 | 1.4 | 0.98 | 1998.0 | 12.3 | 1979.9 | 4.7 | 1979.9 | 4.7 | 101.8 |
| CMH14-29-38 | 43 | 46456 | 1.3 | 8.2069 | 1.6 | 0.3680 | 1.2 | 0.60 | 2001.9 | 17.1 | 1983.4 | 27.8 | 1983.4 | 27.8 | 101.8 |
| CMH14-29-66 | 117 | 145166 | 1.4 | 8.0830 | 0.6 | 0.3633 | 1.6 | 0.94 | 2004.0 | 15.3 | 2010.5 | 10.3 | 2010.5 | 10.3 | 99.4 |

Table 2 Continued

| Analysis | U | 206Pb | U/Th | 206Pb* | ± | 206Pb* | ± | error | 207Pb* | ± | 206Pb* | ± | Best age | ± | Conc |
|---|---|---|---|---|---|---|---|---|---|---|---|---|---|---|---|
| | (ppm) | 204Pb | | 207Pb* | (%) | 238U | (%) | corr. | 235U | (Ma) | 207Pb* | (Ma) | (Ma) | (Ma) | (%) |
| CMH14-29-65 | 40 | 42659 | 1.0 | 7.8769 | 1.5 | 0.3892 | 0.9 | 0.53 | 2087.5 | 15.8 | 2056.2 | 26.8 | 2056.2 | 26.8 | 103.1 |
| CMH14-29-3 | 36 | 44813 | 1.1 | 7.8153 | 2.5 | 0.3935 | 1.4 | 0.48 | 2104.1 | 25.2 | 2070.0 | 43.8 | 2070.0 | 43.8 | 103.3 |
| CMH14-29-27 | 83 | 89970 | 0.9 | 7.7903 | 0.6 | 0.3824 | 1.2 | 0.88 | 2081.4 | 11.7 | 2075.7 | 11.0 | 2075.7 | 11.0 | 100.6 |
| CMH14-29-22 | 69 | 83285 | 1.0 | 7.7709 | 0.6 | 0.3885 | 1.1 | 0.85 | 2097.8 | 11.0 | 2080.1 | 11.4 | 2080.1 | 11.4 | 101.7 |
| CMH14-29-43 | 146 | 234468 | 2.8 | 7.7603 | 0.6 | 0.3799 | 0.5 | 0.65 | 2079.1 | 6.8 | 2082.5 | 10.3 | 2082.5 | 10.3 | 99.7 |
| CMH14-29-60 | 54 | 85936 | 0.2 | 7.7537 | 1.1 | 0.3715 | 1.3 | 0.77 | 2060.2 | 14.9 | 2084.0 | 18.8 | 2084.0 | 18.8 | 97.7 |
| CMH14-29-47 | 66 | 61968 | 1.2 | 7.7534 | 0.8 | 0.3936 | 2.1 | 0.93 | 2111.5 | 19.6 | 2084.1 | 13.9 | 2084.1 | 13.9 | 102.7 |
| CMH14-29-15 | 48 | 60993 | 1.3 | 7.6598 | 1.1 | 0.3922 | 1.2 | 0.74 | 2119.0 | 14.5 | 2105.4 | 19.2 | 2105.4 | 19.2 | 101.3 |
| CMH14-29-69 | 57 | 175667 | 2.0 | 7.4398 | 1.8 | 0.3973 | 1.8 | 0.69 | 2156.4 | 22.9 | 2156.4 | 32.3 | 2156.4 | 32.3 | 100.0 |
| CMH14-29-78 | 108 | 114288 | 1.0 | 7.3587 | 0.6 | 0.4036 | 0.9 | 0.83 | 2180.4 | 10.0 | 2175.5 | 10.8 | 2175.5 | 10.8 | 100.5 |
| CMH14-29-18 | 47 | 67372 | 1.4 | 6.8858 | 1.5 | 0.4379 | 1.8 | 0.77 | 2314.2 | 21.0 | 2290.5 | 25.2 | 2290.5 | 25.2 | 102.2 |
| CMH14-29-71 | 29 | 25250 | 0.8 | 6.8382 | 0.8 | 0.4363 | 1.3 | 0.86 | 2317.1 | 13.4 | 2302.4 | 13.1 | 2302.4 | 13.1 | 101.4 |
| CMH14-29-40 | 94 | 98347 | 1.9 | 6.7991 | 0.5 | 0.4396 | 1.2 | 0.94 | 2329.3 | 12.1 | 2312.2 | 8.1 | 2312.2 | 8.1 | 101.6 |
| CMH14-29-59 | 108 | 154610 | 1.2 | 6.7915 | 0.4 | 0.4425 | 1.3 | 0.96 | 2336.4 | 12.6 | 2314.1 | 6.8 | 2314.1 | 6.8 | 102.1 |
| CMH14-29-13 | 56 | 117608 | 1.4 | 6.7646 | 0.7 | 0.4412 | 1.9 | 0.94 | 2337.2 | 18.5 | 2320.9 | 11.7 | 2320.9 | 11.7 | 101.5 |
| CMH14-29-26 | 138 | 100300 | 1.8 | 6.5184 | 0.9 | 0.4161 | 2.3 | 0.94 | 2317.6 | 22.5 | 2384.3 | 14.7 | 2384.3 | 14.7 | 94.1 |
| CMH14-29-52 | 91 | 228683 | 1.5 | 6.3477 | 0.7 | 0.4621 | 0.4 | 0.53 | 2438.2 | 7.4 | 2429.4 | 11.5 | 2429.4 | 11.5 | 100.8 |
| CMH14-29-79 | 287 | 295270 | 2.2 | 6.2886 | 0.3 | 0.4577 | 0.8 | 0.94 | 2437.9 | 7.4 | 2445.2 | 4.7 | 2445.2 | 4.7 | 99.3 |
| CMH14-29-94 | 86 | 137557 | 1.2 | 6.1269 | 0.4 | 0.4666 | 0.8 | 0.88 | 2479.9 | 8.4 | 2489.2 | 7.3 | 2489.2 | 7.3 | 99.2 |
| CMH14-29-80 | 156 | 28482 | 2.1 | 5.9140 | 0.2 | 0.4371 | 1.6 | 0.99 | 2452.3 | 14.8 | 2548.7 | 2.8 | 2548.7 | 2.8 | 91.7 |
| CMH14-29-45 | 99 | 15654 | 2.0 | 5.8584 | 0.7 | 0.4768 | 1.3 | 0.89 | 2541.7 | 13.9 | 2564.5 | 11.4 | 2564.5 | 11.4 | 98.0 |
| CMH14-29-72 | 78 | 132216 | 1.1 | 5.8404 | 0.5 | 0.4896 | 0.7 | 0.81 | 2569.2 | 8.5 | 2569.6 | 9.0 | 2569.6 | 9.0 | 100.0 |
| CMH14-29-19 | 94 | 115865 | 1.9 | 5.8100 | 0.5 | 0.5022 | 1.5 | 0.95 | 2598.0 | 14.4 | 2578.3 | 8.0 | 2578.3 | 8.0 | 101.7 |
| CMH14-29-32 | 224 | 497452 | 1.9 | 5.7384 | 0.4 | 0.5081 | 1.5 | 0.97 | 2620.6 | 14.7 | 2599.0 | 6.0 | 2599.0 | 6.0 | 101.9 |
| CMH14-29-25 | 35 | 43417 | 0.9 | 5.7379 | 0.7 | 0.4834 | 1.7 | 0.92 | 2574.0 | 17.6 | 2599.2 | 12.3 | 2599.2 | 12.3 | 97.8 |
| CMH14-29-98 | 204 | 233035 | 1.2 | 5.7155 | 0.1 | 0.5000 | 0.5 | 0.98 | 2609.2 | 5.2 | 2605.7 | 1.8 | 2605.7 | 1.8 | 100.3 |
| CMH14-29-12 | 60 | 73919 | 0.7 | 5.7132 | 0.8 | 0.5002 | 1.5 | 0.87 | 2610.0 | 15.8 | 2606.3 | 14.0 | 2606.3 | 14.0 | 100.3 |
| CMH14-29-17 | 146 | 286473 | 1.7 | 5.4395 | 0.3 | 0.5224 | 0.7 | 0.90 | 2697.0 | 6.8 | 2687.8 | 5.2 | 2687.8 | 5.2 | 100.8 |
| CMH14-29-29 | 25 | 45547 | 0.8 | 5.4109 | 1.2 | 0.5191 | 1.9 | 0.84 | 2696.1 | 21.8 | 2696.5 | 20.5 | 2696.5 | 20.5 | 100.0 |
| CMH14-29-63 | 87 | 205106 | 0.9 | 5.3983 | 0.4 | 0.5306 | 1.5 | 0.96 | 2719.0 | 14.4 | 2700.4 | 6.8 | 2700.4 | 6.8 | 101.6 |
| CMH14-29-41 | 76 | 106564 | 0.7 | 5.3923 | 0.3 | 0.5321 | 1.9 | 0.99 | 2722.6 | 17.9 | 2702.2 | 5.0 | 2702.2 | 5.0 | 101.8 |
| CMH14-29-70 | 219 | 94762 | 6.6 | 5.3909 | 0.2 | 0.5311 | 2.0 | 1.00 | 2721.2 | 18.9 | 2702.6 | 2.6 | 2702.6 | 2.6 | 101.6 |

Table 2 Continued

| Analysis | U | 206Pb | U/Th | 206Pb* | ± | 206Pb* | ± | error | 207Pb* | ± | 206Pb* | ± | Best age | ± | Conc |
|---|---|---|---|---|---|---|---|---|---|---|---|---|---|---|---|
| | (ppm) | 204Pb | | 207Pb* | (%) | 238U | (%) | corr. | 235U | (Ma) | 207Pb* | (Ma) | (Ma) | (Ma) | (%) |
| CMH14-29-34 | 150 | 81980 | 1.9 | 8.8935 | 0.5 | 0.3348 | 1.6 | 0.95 | 1851.1 | 14.0 | 1839.2 | 9.7 | 1839.2 | 9.7 | 101.2 |
| CMH14-29-16 | 121 | 120426 | 1.5 | 8.8924 | 0.6 | 0.3368 | 1.1 | 0.89 | 1856.2 | 10.7 | 1839.5 | 10.4 | 1839.5 | 10.4 | 101.7 |
| CMH14-29-39 | 16 | 19435 | 7.9 | 8.8899 | 4.2 | 0.3371 | 1.9 | 0.41 | 1857.3 | 39.3 | 1840.0 | 76.0 | 1840.0 | 76.0 | 101.8 |
| CMH14-29-76 | 60 | 59185 | 1.3 | 8.8855 | 0.8 | 0.3337 | 0.7 | 0.66 | 1849.0 | 8.5 | 1840.9 | 13.7 | 1840.9 | 13.7 | 100.8 |
| CMH14-29-84 | 74 | 66970 | 1.4 | 8.8794 | 1.3 | 0.3338 | 0.9 | 0.56 | 1849.9 | 13.8 | 1842.1 | 24.3 | 1842.1 | 24.3 | 100.8 |
| CMH14-29-83 | 32 | 31279 | 0.8 | 8.8676 | 3.6 | 0.3334 | 1.3 | 0.33 | 1849.9 | 32.4 | 1844.5 | 65.0 | 1844.5 | 65.0 | 100.6 |
| CMH14-29-49 | 35 | 49639 | 0.9 | 8.8533 | 3.0 | 0.3317 | 1.2 | 0.38 | 1847.1 | 27.6 | 1847.4 | 54.3 | 1847.4 | 54.3 | 100.0 |
| CMH14-29-96 | 43 | 20569 | 0.7 | 8.8377 | 1.9 | 0.3319 | 1.2 | 0.54 | 1849.0 | 19.4 | 1850.6 | 34.7 | 1850.6 | 34.7 | 99.8 |

**Table 3**

Two Sample K-S test results from Excel macro obtained from the University of Arizona Laserchron lab (Guynn and Gehrels, 2010)

| | | | | | |
|---|---|---|---|---|---|
| | **K-S P-values using error in the CDF** | | | **D-values using error in the CDF** | |
| | CMH14-25 | CMH14-29 | | CMH14-25 | CMH14-29 |
| CMH14-25 | | **0.936** | | | 0.078 |
| CMH14-29 | **0.936** | | | 0.078 | |
| | | | | | |
| | **K-S P-values for no error** | | | **D-values for no error** | |
| | CMH14-25 | CMH14-29 | | CMH14-25 | CMH14-29 |
| CMH14-25 | | 0.782 | | | 0.095 |
| CMH14-29 | 0.782 | | | 0.095 | |
| | | | | | |
| | **Average K-S P-values using Monte-Carlo** | | | **Two std devs. of P-values using Monte-Carlo** | |
| | CMH14-25 | CMH14-29 | | CMH14-25 | CMH14-29 |
| CMH14-25 | | 0.581 | | | 0.447 |
| CMH14-29 | 0.581 | | | 0.447 | |

**Table 4**

Transcribed field notes for notable samples collected. GPS coordinates were gathered with a Garmin Etrex using the WGS84 datum.

| Sample_ Collected | Lat | | Lon | | Date | Altitude (m) | Rock type | Dip direct ion | Dip | Notes |
|---|---|---|---|---|---|---|---|---|---|---|
| BC hand samples | 44.94594 997 | N | -113.944 325 | W | 2014-07-19T17:21:36Z | 1606.31 2378 | Ybc? | | | Float collected from large talus pile. Appear to be from a rock fall. No obvious Tcv&Ys (other rocks in the area). Collected ~4lb of varrying sizes (5 cm- 25cm) and textures (dark mineral laminae, green hued, dark grey to black, weathered grains (feldspar?)). |
| CMH-14-01 | 44.89361 7 | N | -113.862 514 | W | 6/3/14 11:52 | 2587.73 4863 | SOs | 209 | 56 | "Shear-Zone" black, red and yellow silicic band within the carb with local NE-verging folds. Very small crystals. Photo taken*. Folds: Axial surface 232/73; fold axis 39/170. Lineation of sriation (?) 16/291. Does not react to HCl or scratch with knife blade. |
| CMH-14-03 | 44.91340 8 | N | -113.844 382 | W | 6/4/14 8:41 | 2349.57 0068 | Tii | | | Amphibole rich, grey Qtz and altered feldspar. Overall weathers/stains dark green. Local alteration (?). Grains 1-4mm. Joint sets: ~5-10cm spacing 017/64; 078/65; 235/26 |
| CMH-14-05 | 44.91227 | N | -113.857 843 | W | 6/5/14 8:49 | 2257.52 4414 | Tci | 180 | 3 | Flow banding in welded tuff/ignimbrite. Biotite ~3%(?) ~65% glass. Qtz & Sanidine +lithics (1cm to >15cm (bigger than protractor)) flattened fiamme. Weathers grey to beige |
| CMH-14-06 | 44.88338 5 | N | -113.842 319 | W | 6/5/14 15:55 | 2550.96 4844 | Tcl | 26 | 12 | Olivine & CPX phynocrysts. ~80% groundmass mafic flow |

| | | | | | | | | | | |
|---|---|---|---|---|---|---|---|---|---|---|
| CMH-14-07 | 44.905496 | N | -113.909972 | W | 6/7/14 12:23 | 2273.38623 | Ok | 206 | 45 | On ridge...duplicated qtzite fins? (Repeated fracture 235/26) breccia clasts stretched (?) |
| CMH-14-09 | 44.936398 | N | -113.908962 | W | 6/11/14 11:19 | 2699.487305 | Ok? | 274 | 64 | Weird texture in Qtzite… What Jeff Lonn emailed Dave about. Are grains picked out? (Photo) Staining could be hydrothermal. Vitreous bits almost look like sigma clasts (Photo). No discernable trend to them. Vitreous boudins? |
| CMH-14-10 | 44.915466 | N | -113.920724 | W | 6/12/14 8:34 | 2122.460205 | SOs? | 210 | 65 | Carb coated Qtzite. Faint layering that are resistant to weathering. Fine grained medium grey Qtzite |
| CMH-14-11 | 44.968042 | N | -113.977501 | W | 6/13/14 14:07 | 2137.120361 | Ys | 89 | 90 | Apparent ripples from weathered out S-C fabric(?). In coarse grained Ys. I see striations (slicks?) that are parallel to outcrop |
| CMH-14-15 | 44.899393 | N | -113.900607 | W | 6/20/14 15:21 | 2345.724854 | Sos | 262 | 40 | "flakey" light grey dolo with alteration. Qtz and Carb veins. Qtz veins offset (top to right) ~2-3 cm (plain of offset 169/16) |
| CMH-14-16 | 44.893265 | N | -113.89523 | W | 6/20/14 18:15 | 2586.292969 | Ok | 285 | 58 | Sheared qtzite ? |
| CMH-14-20 | 44.98210397 | N | -113.985024 | W | 2014-07-12T17:47:15Z | 2021.503296 | Ys | | | Piece of float "Bad Ys" i.e. pure white sndstn with a few chert pebbles |
| CMH-14-22 | 44.97129902 | N | -113.998719 | W | 2014-07-16T17:42:01Z | 1934.140869 | Ok? Ys? | 118 | 50 | (slicked surface 092/82, slicks raking 89 from NW) Sample/outcrop appears to have more feldspar than others in area. Locally banded, fine to medium subangular white qtzite. (photo) slicked surface dipping E-NE |
| CMH-14-23 | 44.97019898 | N | -114.003 | W | 2014-07-16T19:02: | 1951.038086 | Ys | 240 | 40 | (fracture sets 028/68, 357/86) Banded green phylite? Contains purple qtz grains |

| | | | | | | | | | | |
|---|---|---|---|---|---|---|---|---|---|---|
| | | | 748 | | 55Z | | | | | |
| CMH-14-25 | 44.91874801 | N | -113.887837 | W | 2014-08-02T15:59:41Z | 2112.431396 | Ok? | | | Sample from "knob" for Dzs. Well sorted pure white, stains yellow vitreous. Reed- "could be Neoprot overlain by 'dirty carb'. could be fault contact. Would correlate to Big Creek (?), possibly don't need second (northern thrust)" |
| CMH-14-28 | 44.90911301 | N | -113.879308 | W | 2014-08-02T20:59:10Z | 2491.389648 | SOs | | | Sample of fossiliferous Carb in float to show Leif. Above is bioturbated and sed breccia (karst collapse?). Some Laminated carb in float as well. |
| CMH-14-29 | 44.89298598 | N | -113.877021 | W | 2014-08-02T23:19:27Z | 2717.285645 | Ok | | | "Upper Qtzite". White fine-grained. Nearby float has ripples |
| CMH-14-32 | 44.92689103 | N | -113.902059 | W | 2014-08-19T19:53:29Z | 2397.145508 | Ys | | | Lots of "Zebra fabric" (weird texture on Goldbug Ridge noted by Lonn to Dave). Fine to med grained light grey vitreous to white. Near contact that's obscured by talus… fault contact? Sample appears sheared. |
| CMH-14-35 | 44.975869 | N | -114.015717 | W | 2014-09-06T18:31:24Z | 2206.449219 | Yac | 304 | 26 | Schistosic Yac(?) in shearzone… grain reduction? |
| CMH-14-36 | 44.97567999 | N | -114.014112 | W | 2014-09-06T18:57:54Z | 2156.751953 | Yac? | 296 | 42 | Very fine grained. Same stuff as CMH14-35 but different elevation/height in shearzone |
| CMH-14-37 | 44.97570002 | N | -114.014801 | W | 2014-09-06T19:13:59Z | 2165.242188 | Yac? | 290 | 47 | (lineation 36/279) Same as CMH14-35&37 |
| CMH-14-38 | 44.97499502 | N | -114.011668 | W | 2014-09-06T21:28:40Z | 2127.82373 | Ok? | 271 | 61 | odd strain near foliations? Xbedding in Ys across contact. No strain in Ys |

**Appendix 1**
**Move Reconstruction** (Midland Valley software v. 2014.2)
Move reconstructions along the A-A' transect (extended beyond cross section)
*Model A* uses a combination of tri-shear and fault-parallel flow algorithms

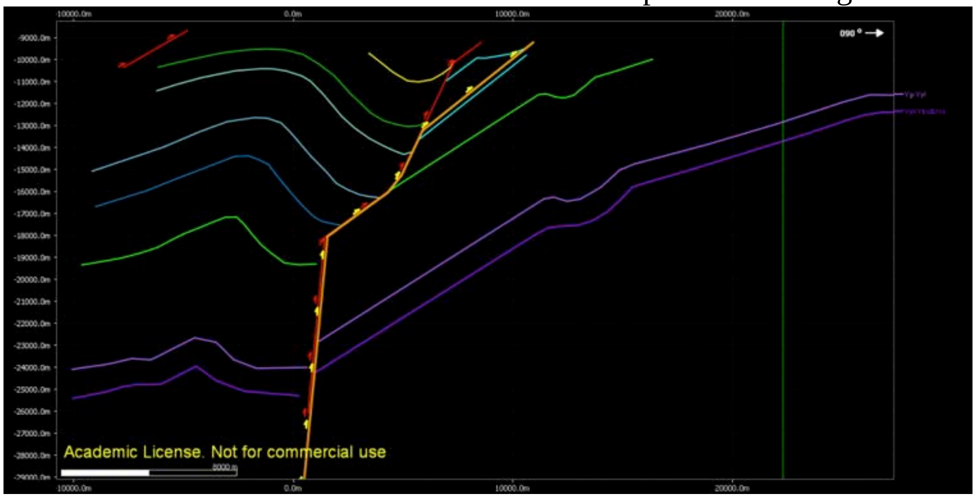

Current geometry (faults are colored red)

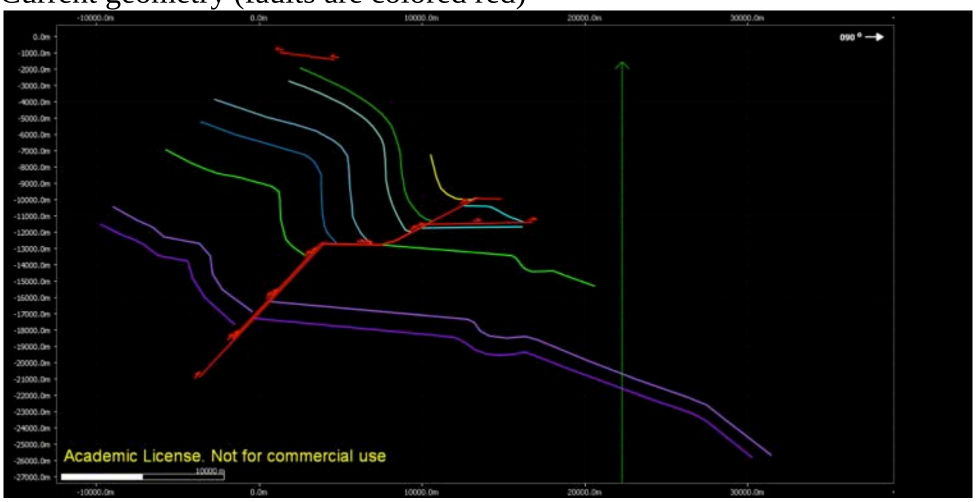

Current geometry restored to Paleozoic horizontal

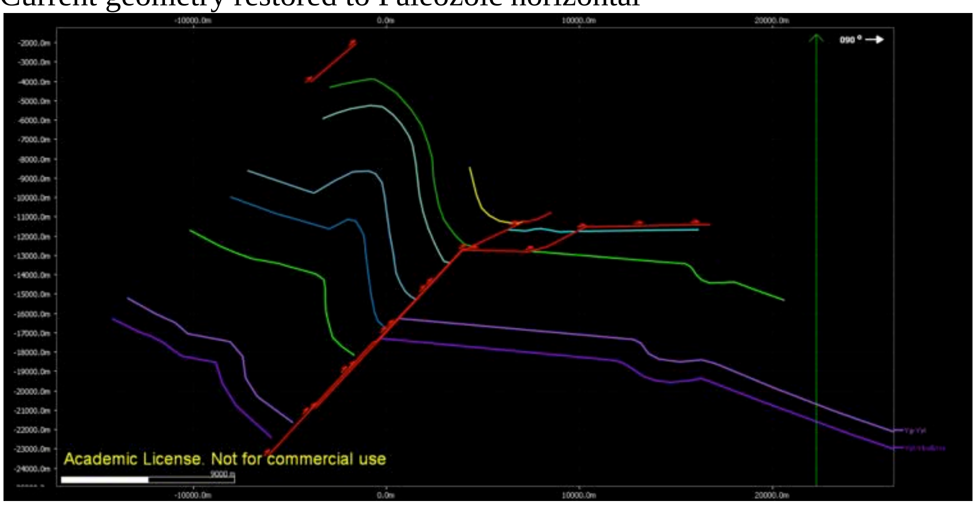

Motion along the Goldbug thrust restored using fault-parallel flow

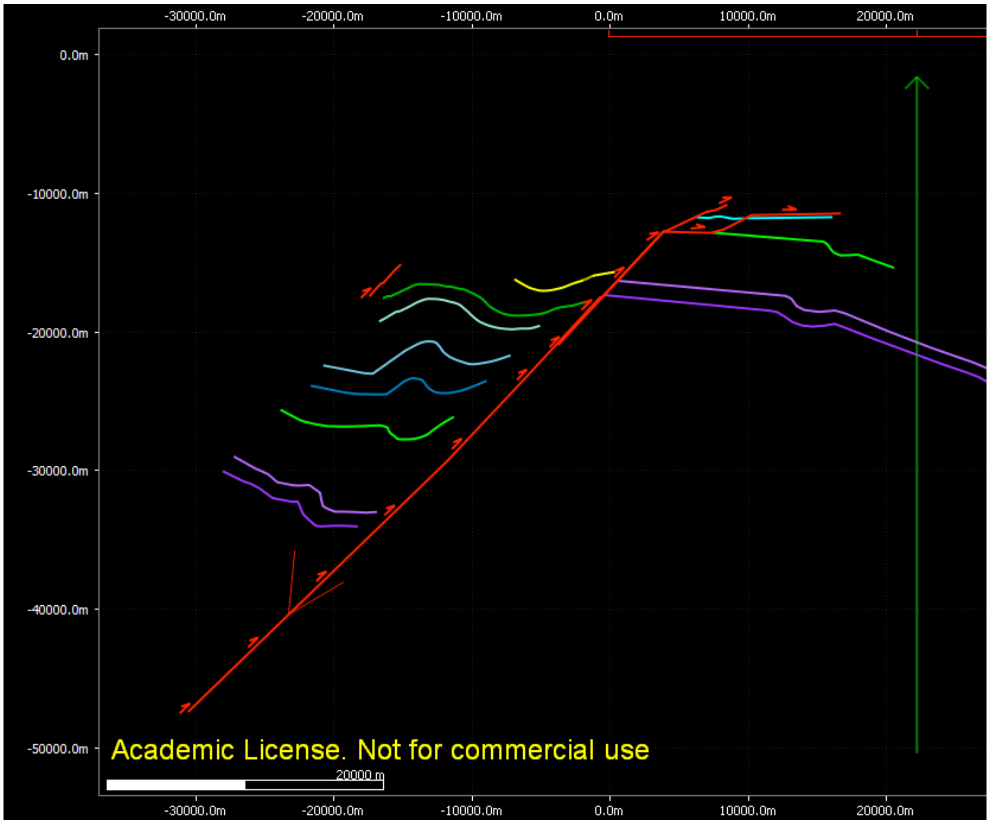


Restoring movement on the reactivated portion of the Poison Creek thrust using the tri-shear algorithm

**Move forward modeling**

Move forward modeling along the A-A' transect (extended beyond cross section) from pre-shortened state using tri-shear and fault-parallel flow

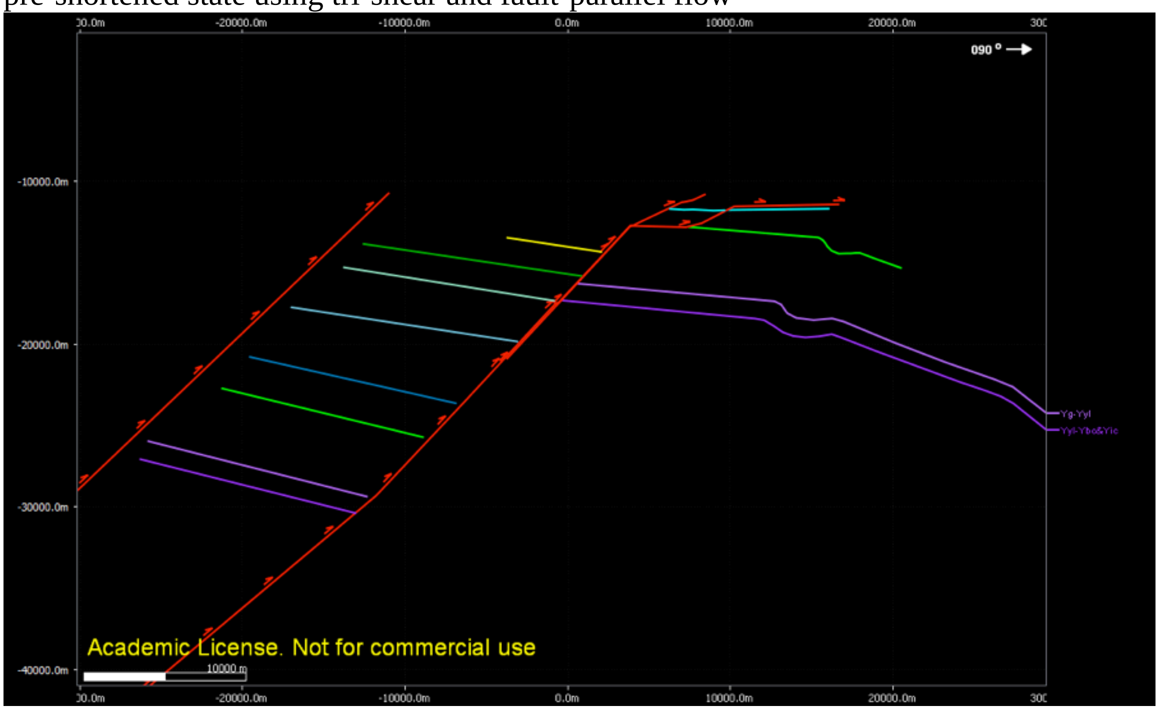

The assumed pre-shortening state of the area. Strata in the hanging-wall of the Poison Creek thrust lie in flat plains. The fault to the southwest above the hanging-wall of the Poison Creek is the Iron Lake. This assumes in-sequence faulting in the region (which is confirmed by a zircon (U-Th)/He date by Pearson, unpublished).

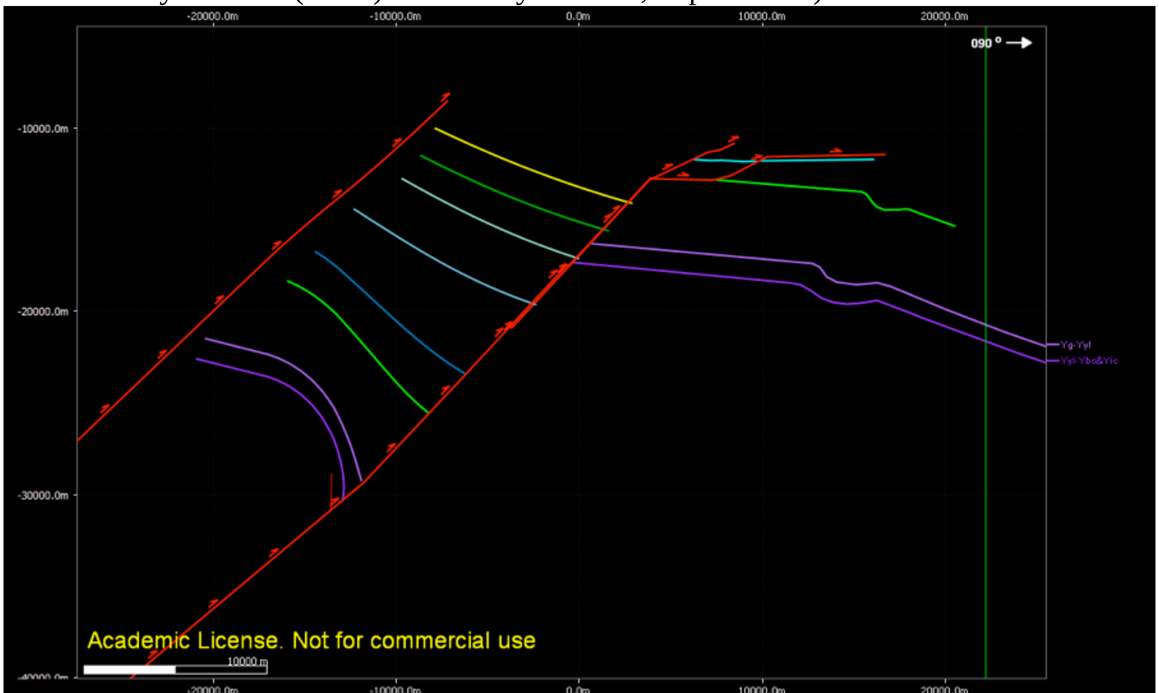


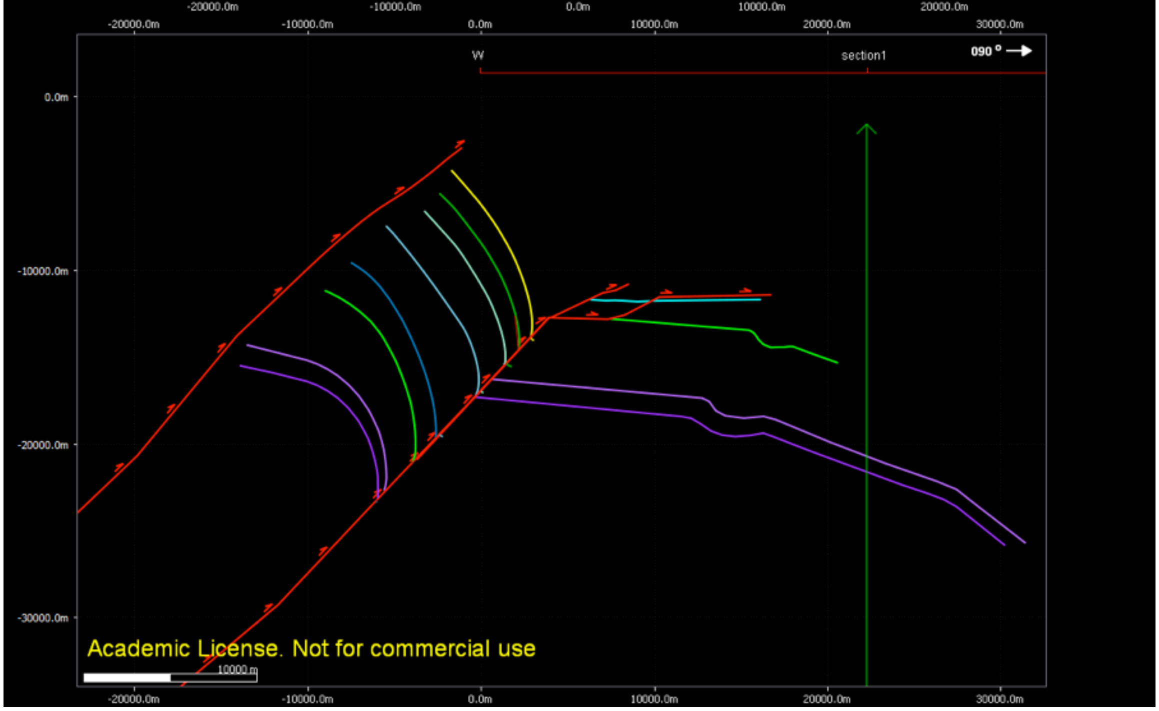


Tri-shear is employed mimicking the propagation of motion along the fault starting at depth and progressing to shallower depth.

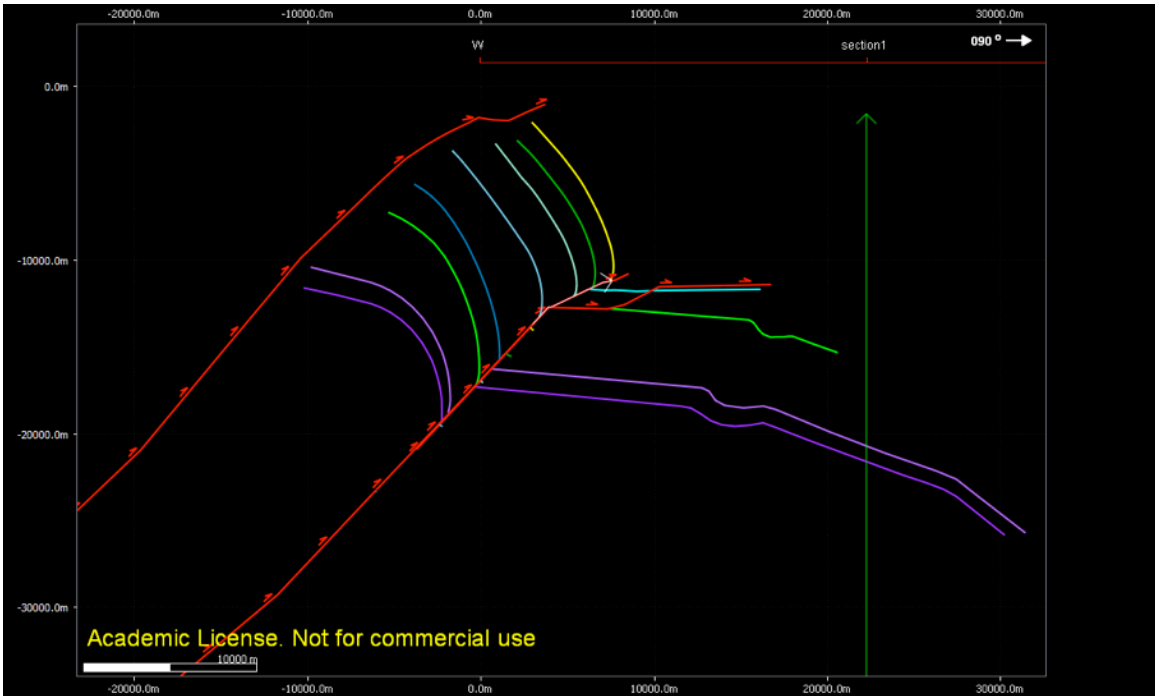


A combination of tri-shear and fault-parallel flow is used during the propagation of the fault tip through the Paleozoic strata. Tri-shear is used first before fault-parallel flow in order to replicate the initial fracturing and strain of fault propagation. Fault –parallel flow is used during fault tip propagation along the hanging-wall flat

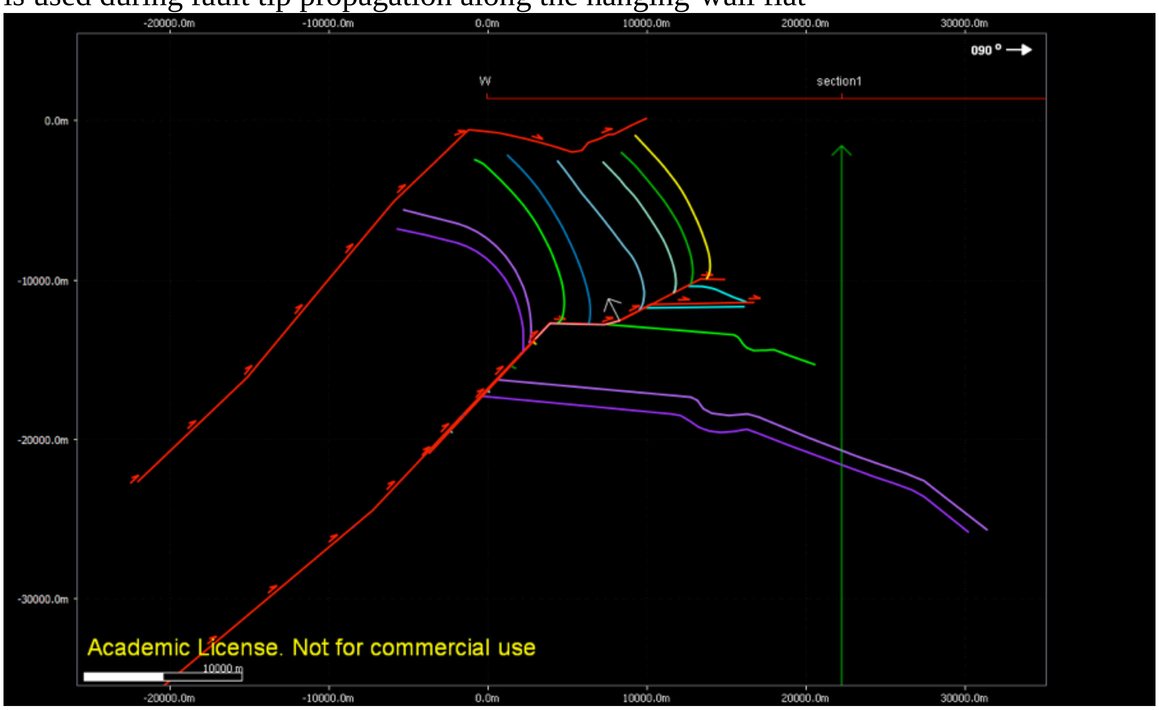


Fault-parallel flow is employed for motion along the Goldbug thrust fault

Model A: a tidied version

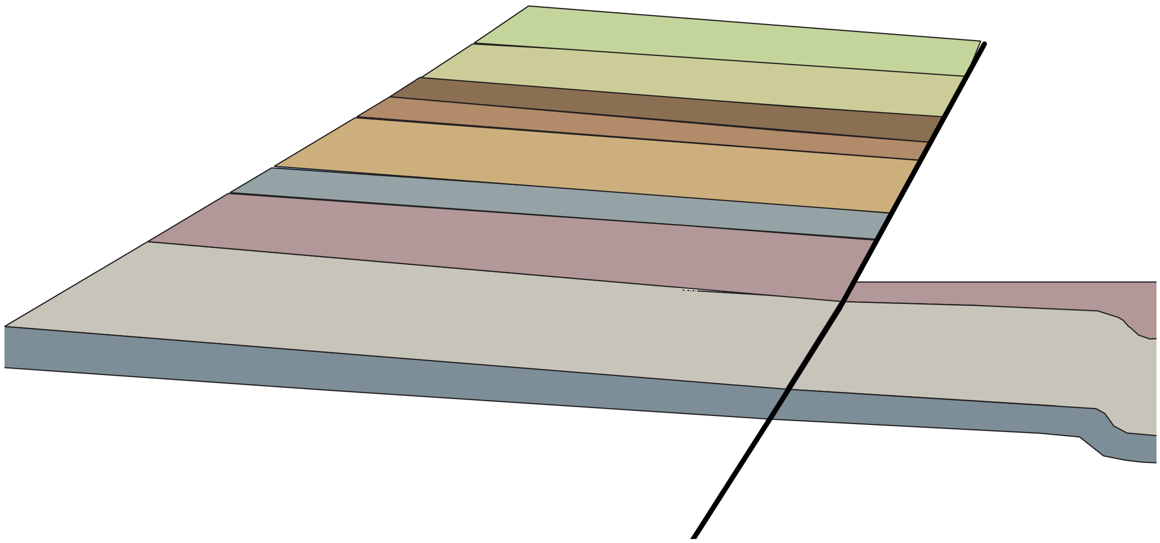

The normal fault is likely listric, however this is ignored beyond the simple rotation of the Lemhi subbasin strata being rotated (clockwise) down towards the northeast.

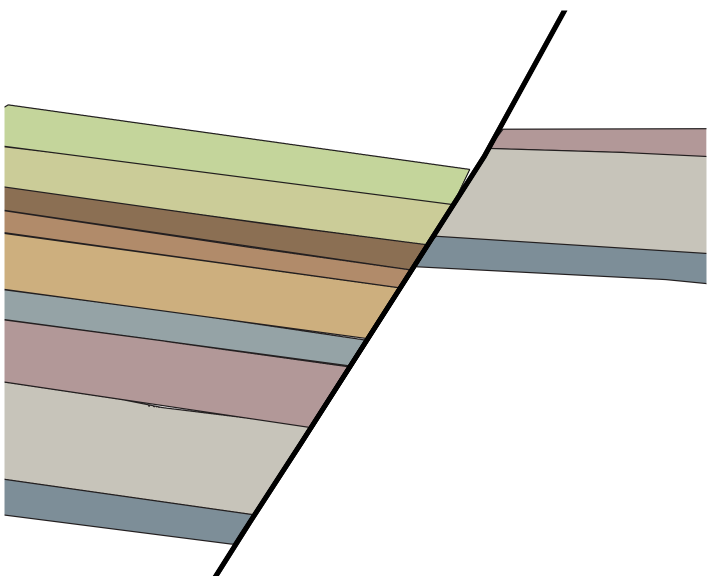

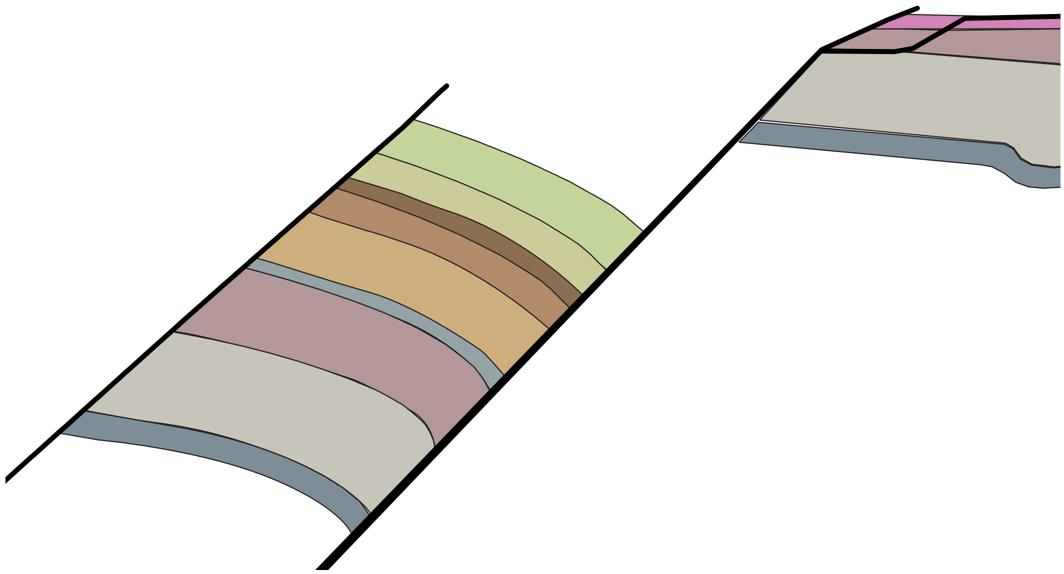

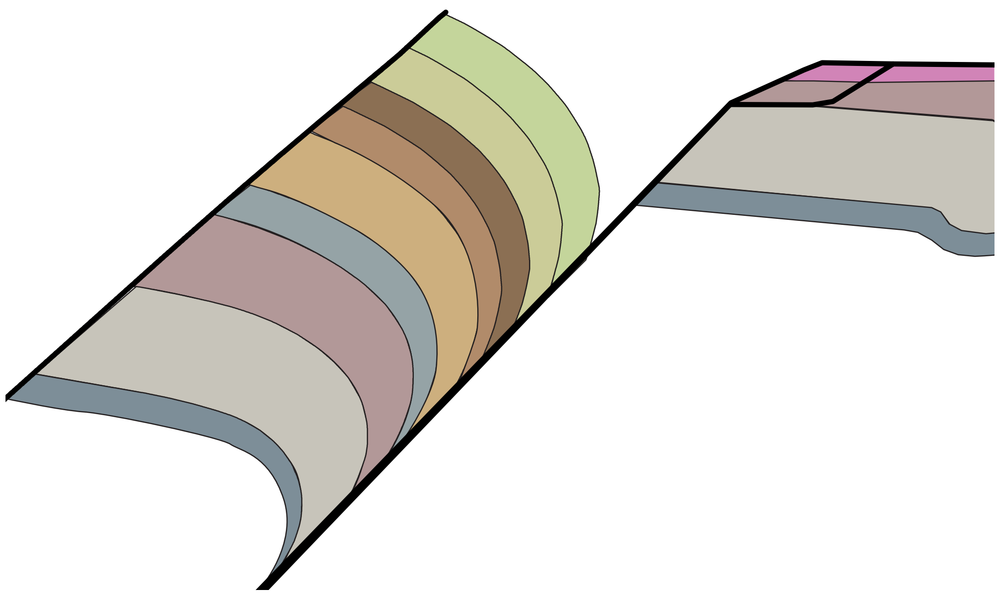

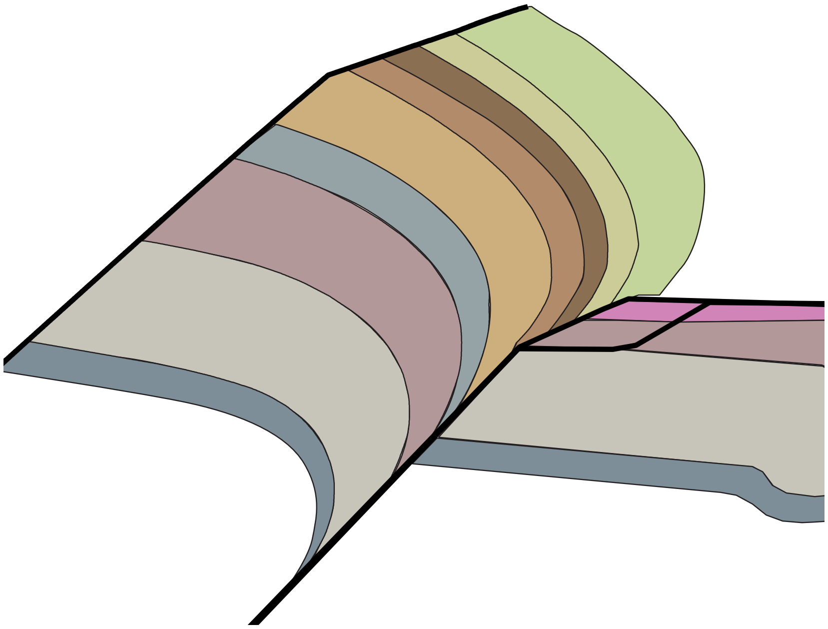

The Tri-shear algorithm is responsible for rotating the Lemhi subbasin strata near the hanging-wall cut off. This does not agree with the observations of the Poison Creek thrust's flat on flat geometric relationship.

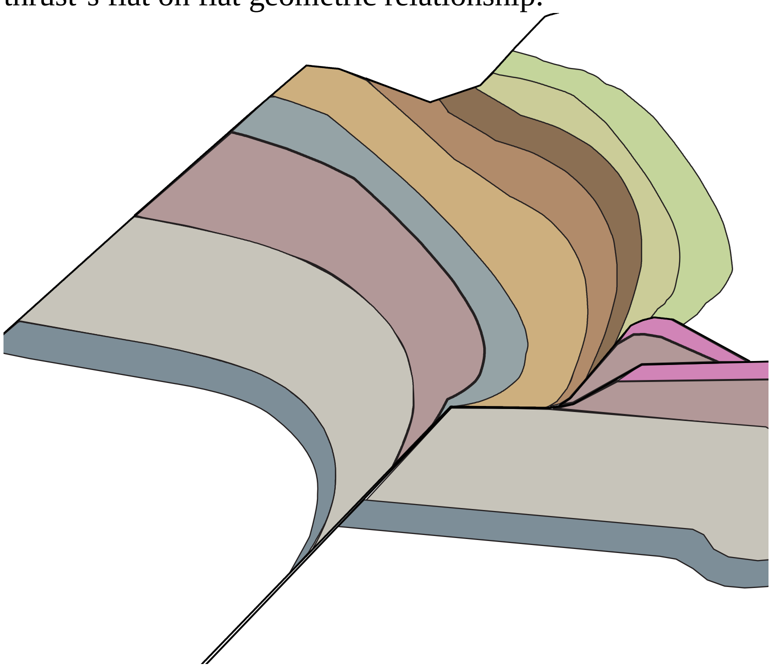

Model B. Forward modeling of a thrust fault propagating through the hanging wall of the rifting related normal fault. This model recreates the geometry observed within the map area and geometric data from the areas to the southwest of the map area. This model is complex and requires a very deep (>15km depth) detachment.

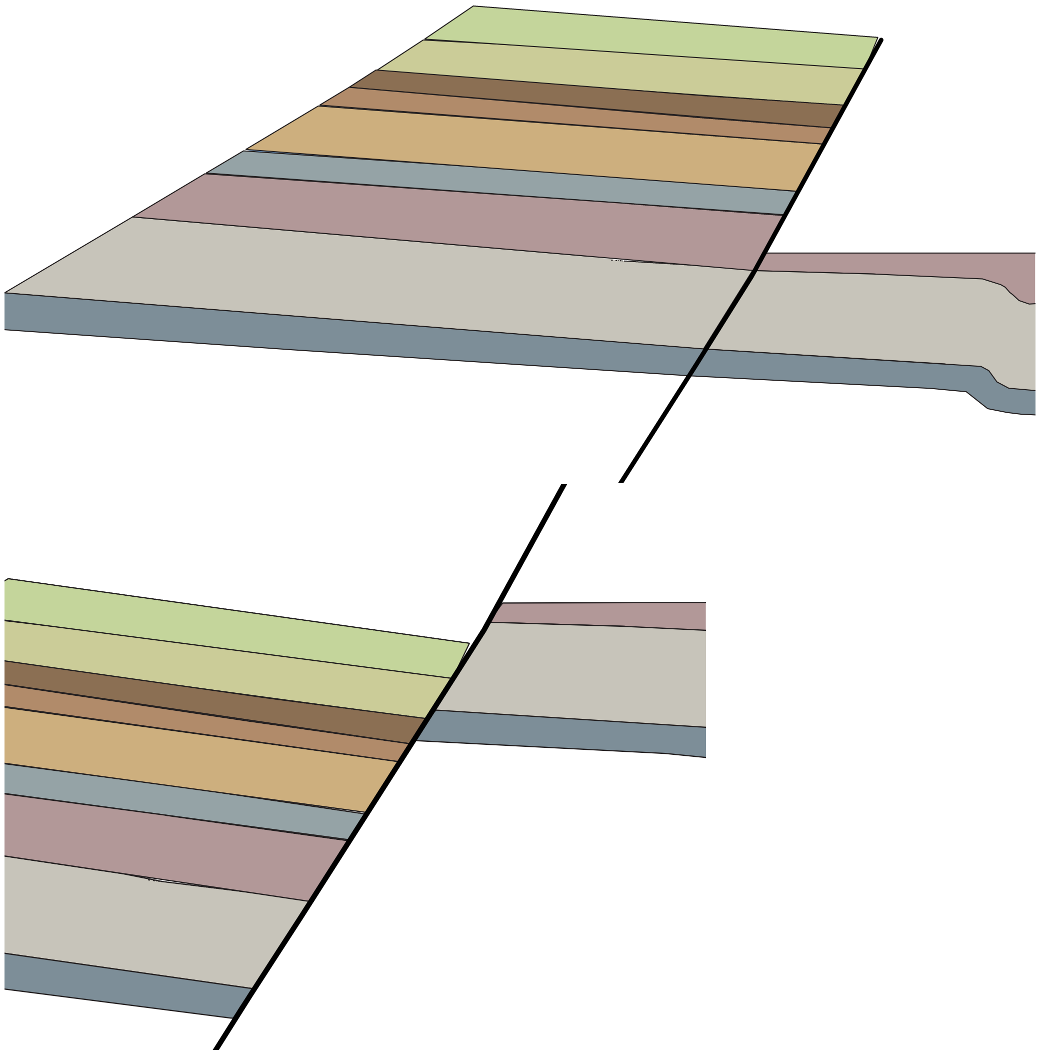

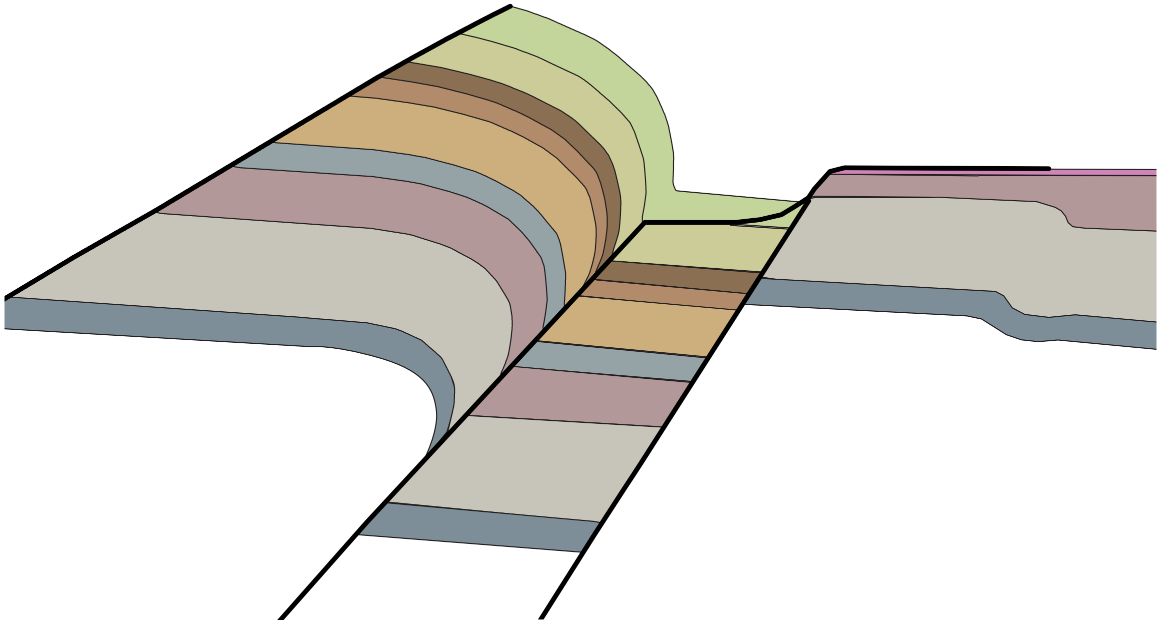

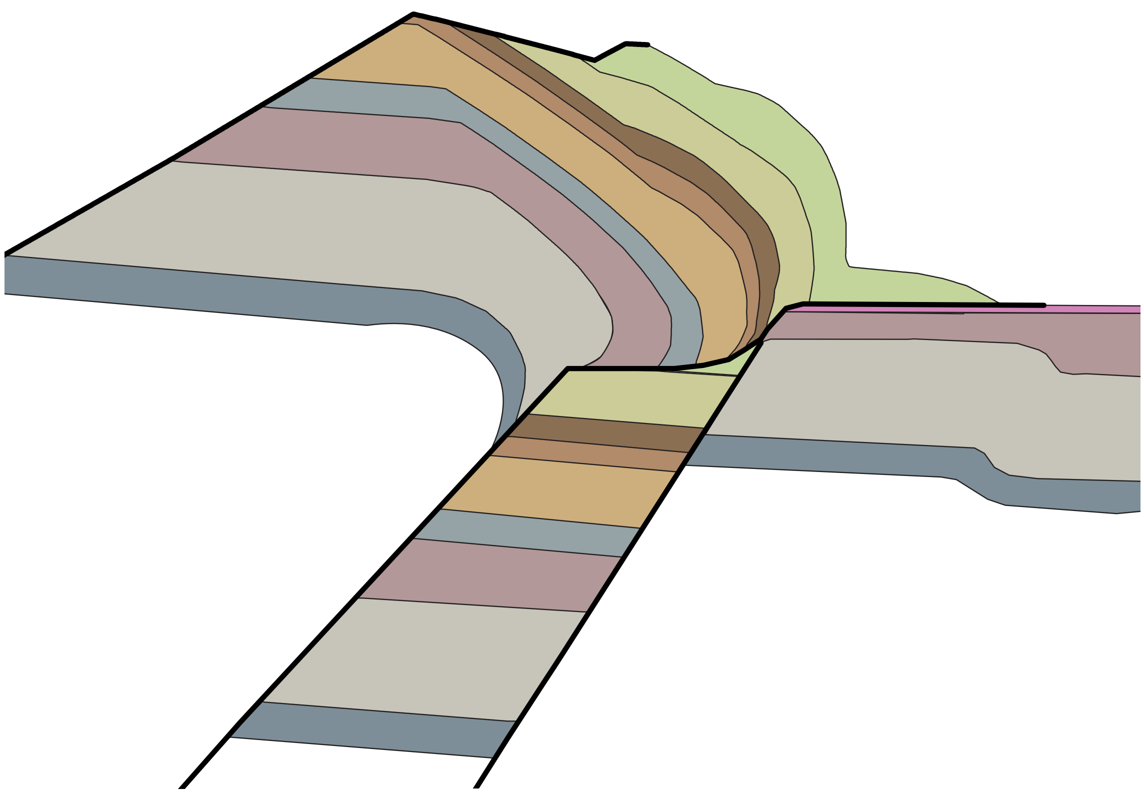

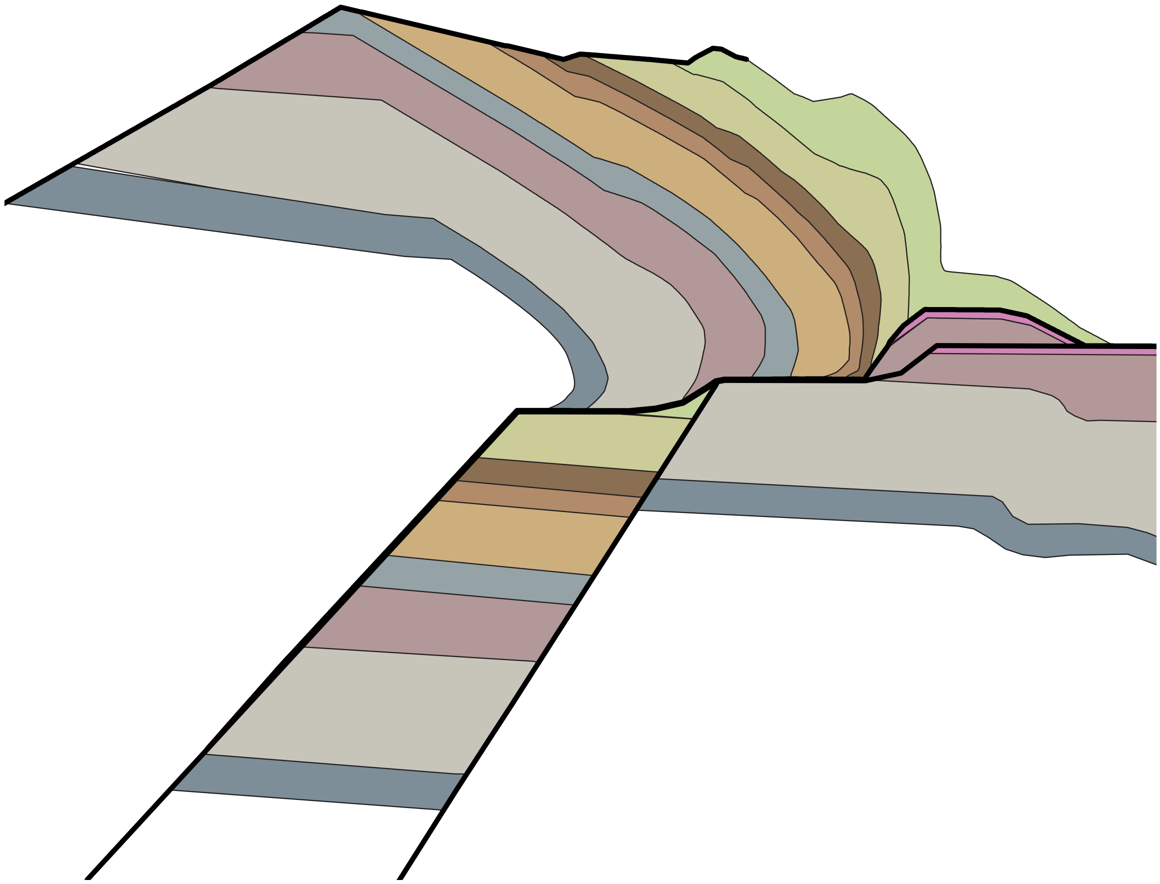

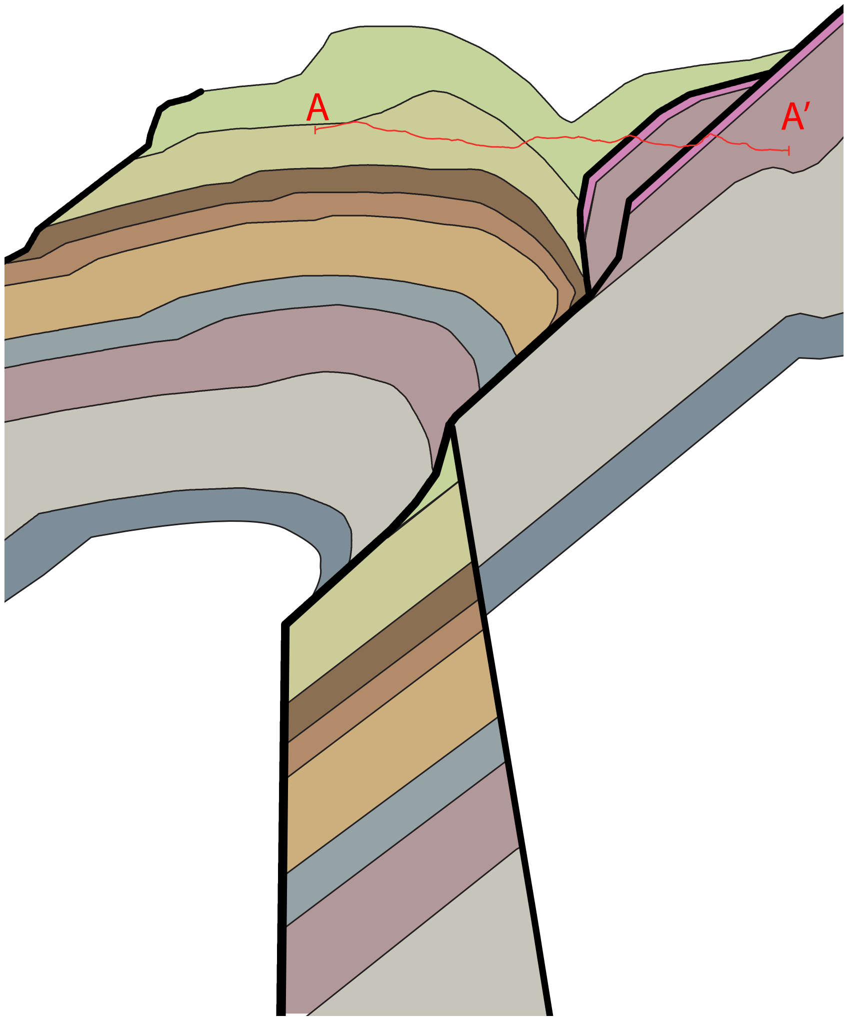


Model C. Forward modeling of a shallow (detachment at less than 10km depth) listric normal fault being reactivated during shortening. This model is similar to Model A, however the detachment of the reactivated normal fault is only 10km deep. This model only uses the fault parallel flow algorithm.

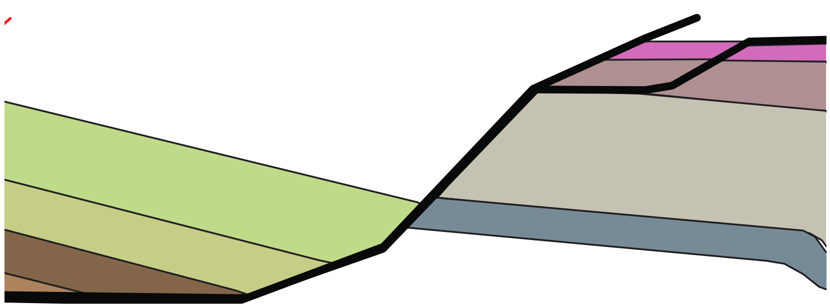

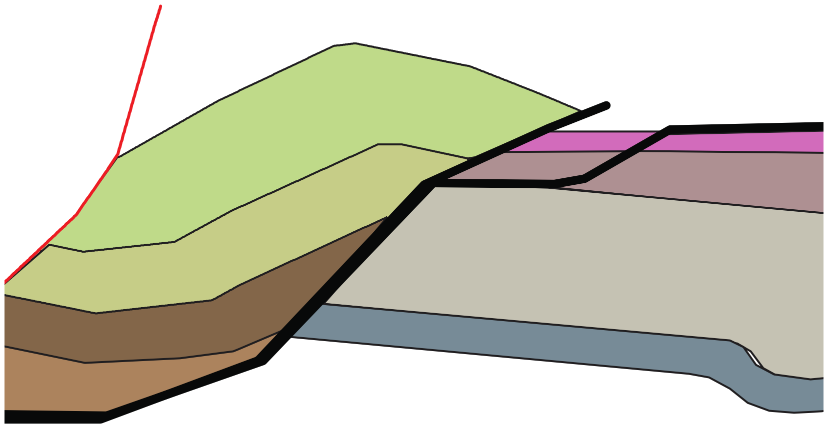

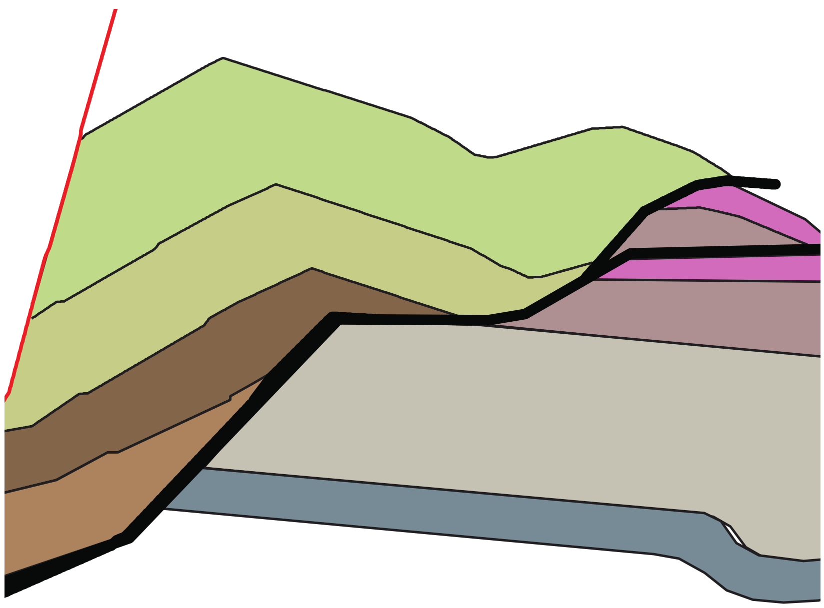

In the last step, everything is rotated 44 degrees counter clockwise. Despite the presence of the syncline and the anticline the Poison Creek hanging-wall, the amplitudes of the folds are not great enough to create the observed geometry of the region with a rotation of 44 degrees.

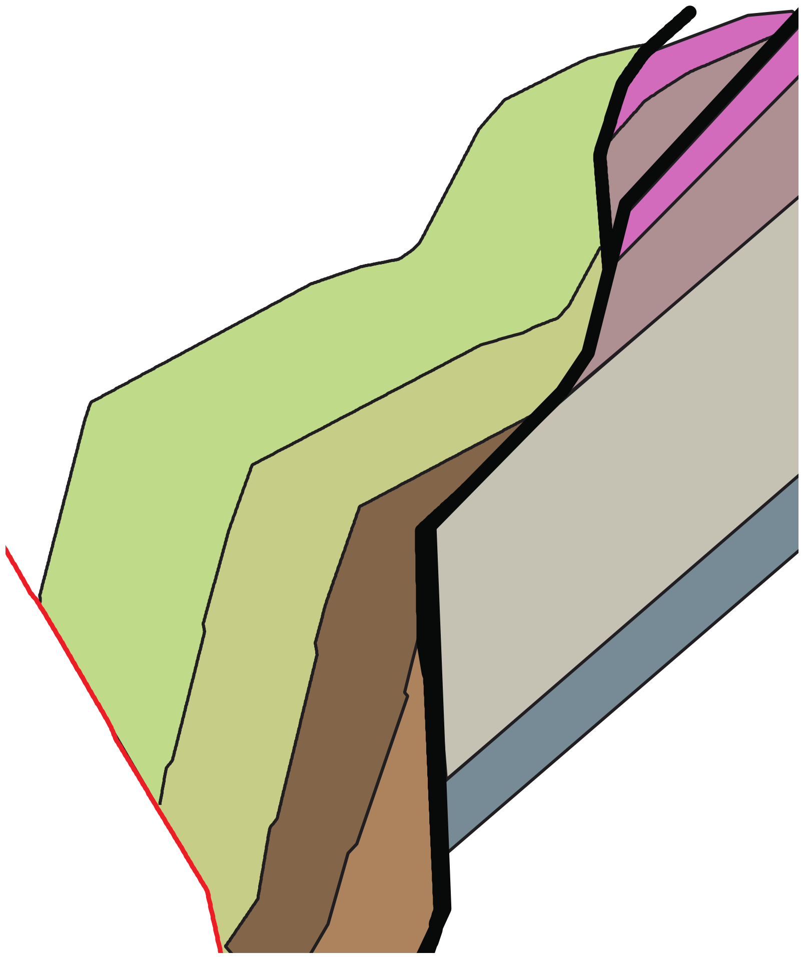

# Geologic Map of the Poison Creek Thrust Fault and vicinity near Poison Peak and Twin Peaks, Lemhi County, Idaho

Connor M. Hansen, and David M. Pearson
Idaho State University, Dept. of Geosciences
2015

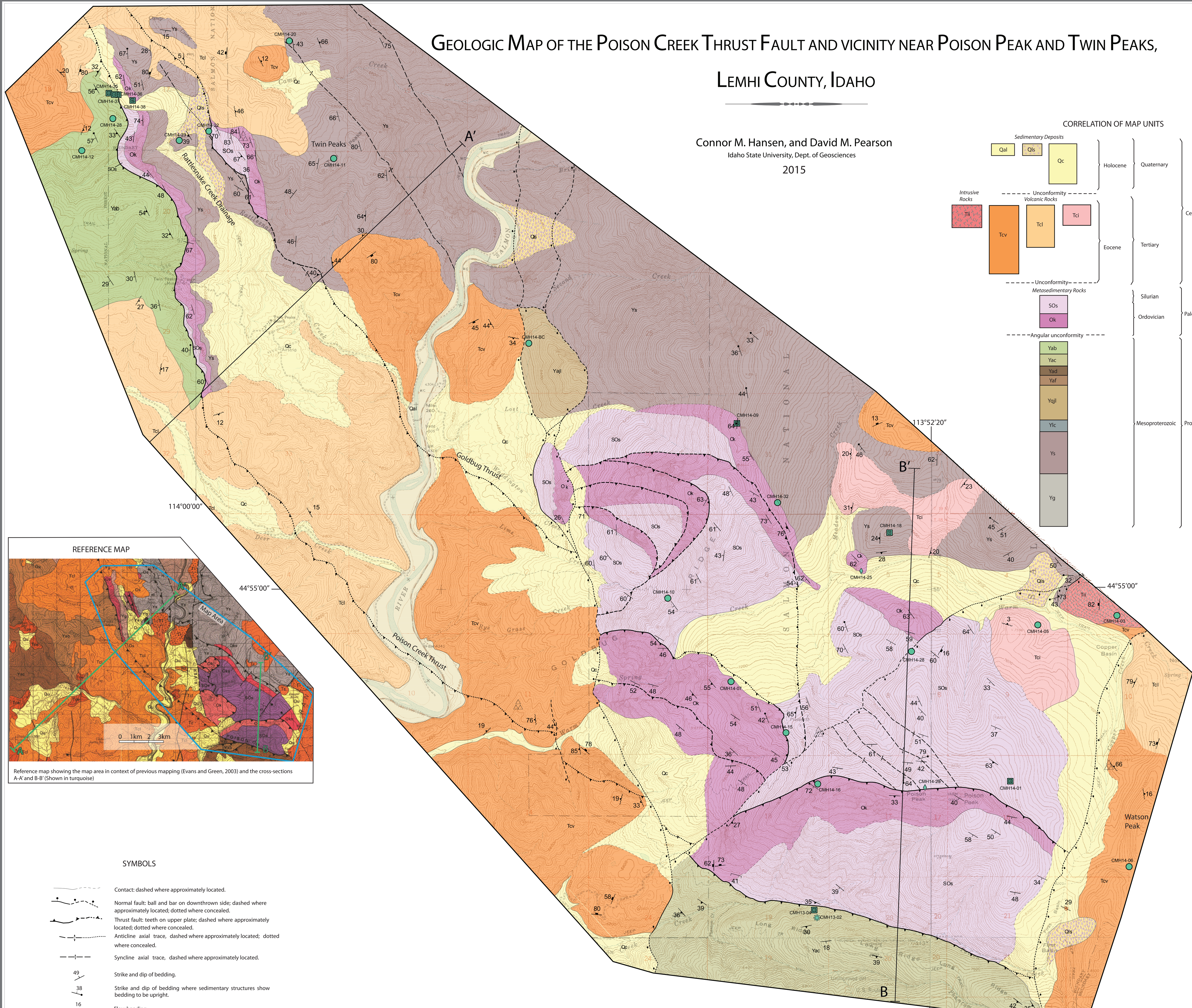


REFERENCE MAP

Reference map showing the map area in context of previous mapping (Evans and Green, 2003) and the cross-sections A-A' and B-B' (Shown in turquoise)

CORRELATION OF MAP UNITS



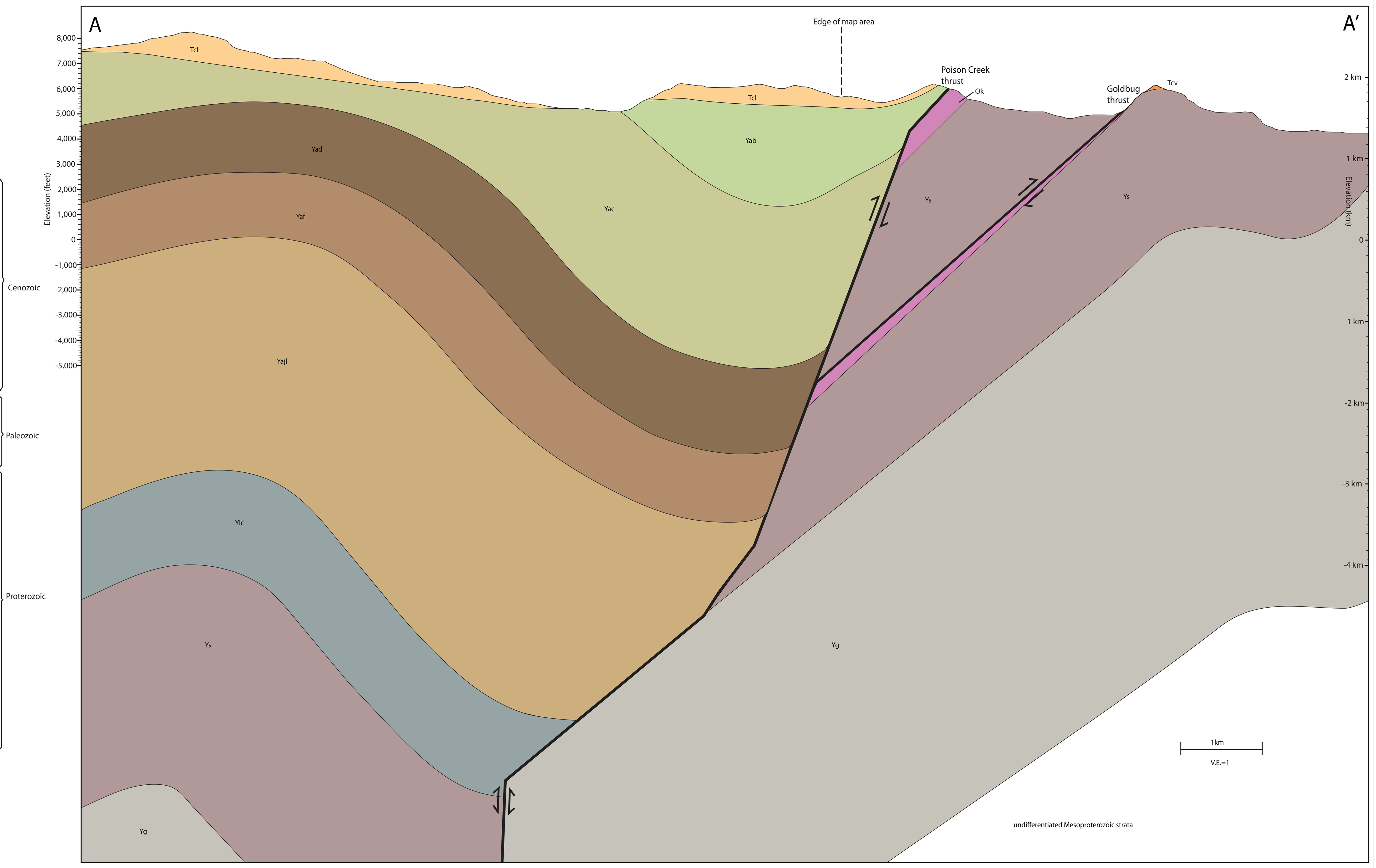


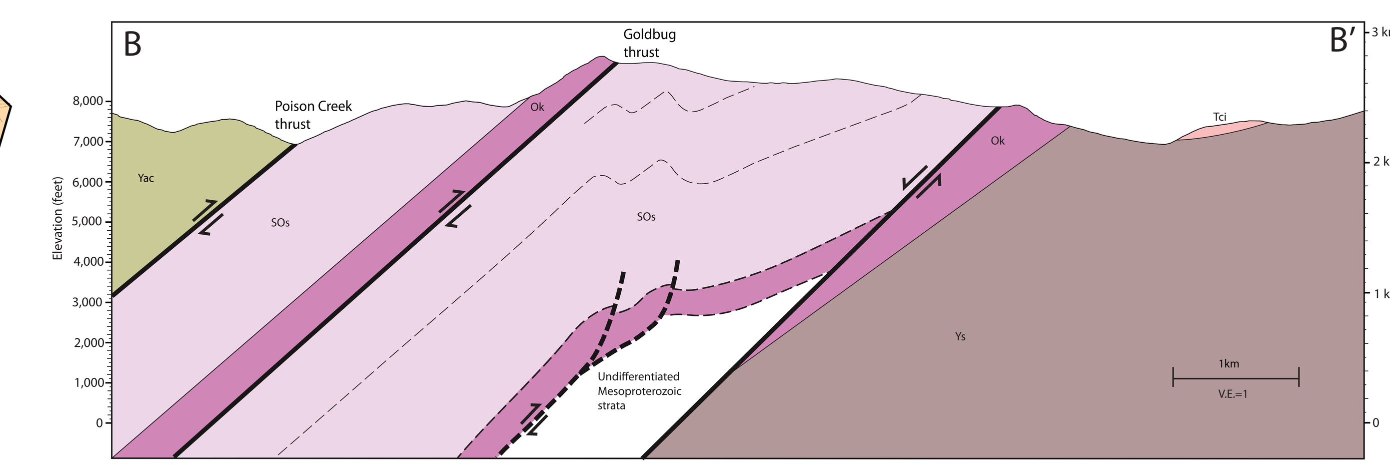


## SYMBOLS

- Contact: dashed where approximately located.
- Normal fault: ball and bar on downthrown side; dashed where approximately located; dotted where concealed.
- Thrust fault: teeth on upper plate; dashed where approximately located; dotted where concealed.
- Anticline axial trace, dashed where approximately located; dotted where concealed.
- Syncline axial trace, dashed where approximately located.
- 49 Strike and dip of bedding.
- 38 Strike and dip of bedding where sedimentary structures show bedding to be upright.
- 16 Flow banding
- 7 Strike and dip of foliation.
- 14 Strike and dip of cleavage.
- 34 Strike and dip of joint.
- Hand sample collected
- Sample collected for oriented thin section
- Zircon (U-Th)/He thermochronometry sample collected
- Detrital zircon sample
- Fault breccia observed



Research supported by the U. S. Geological Survey, National Cooperative Geologic Mapping Program, under USGS award number G14AC00162; and Idaho State Iniversity.The views and conclusions contained in this document are those of the authors and should not be interpreted as necessarily representing the official policies, either expressed or implied, of the U. S. Government

Base map from USGS Digital Raster Graphic.

Control by USGS and USC & GS.

Topography by photogrametric methods from aerial photographs taken 1957. Field checked 1962.

Projection: Idaho coordinate system, east zone (Transverse Mercator). 1927 North American Datum.

Datum is mean sea level.

UTM GRID AND 1962 MAGNETIC NORTH DECLINATION AT CENTER OF MAP

GN 1°59' MN 18.5°

SCALE: 1:24,000

1 1/2 0 1 MILE

1 0.5 0 1 KILOMETER

CONTOUR INTERVAL 40 FEET

DOTTED LINES REPRESENT 20-FOOT CONTOURS

MAP LOCATION

ADJOINING QUADRANGLES

HAT CREEK ALLISON CREEK LEM PEAK

## DESCRIPTION OF MAP UNITS

### Introduction

The geologic map of the area surrounding the Poison Creek thrust fault in the vicinity of Poison Peak and the Twin Peaks shows the distribution of rock units exposed at the surface, or buried under a thin veneer of soil and colluvium. Areas of thicker surficial alluvium and colluvium are mapped as their own map units (Quaternary Alluvium and Quaternary Colluvium).

The map is a result of field mapping conducted in 2013, 2014, and data from previous research by others. Concepts of the geologic units were based on the findings of the Idaho Geological Survey and the Montana Bureau of Mines and Geology as outlined by Burmester et al. (2013). Locally, attitudes from previous mapping as compiled by Evans and Green (2003) were used to supplement mapping.

The oldest rocks of the area are Mesoproterozoic metasedimentary rocks of the Lemhi subbasin. They make up most of the northern portion of the field area as well as the hanging wall of the Poison Creek thrust fault. Unconformably overlying the Mesoproterozoic metasedimentary rocks in the footwall of the Poison Creek thrust are Paleozoic metasedimentary rocks. Tertiary aged volcanic deposits of the Challis Volcanic Group overlie both the Mesoproterozoic and Paleozoic metasedimentary rocks.

**Qal** Alluvium (Quaternary) —Alluvium is found along the Salmon River in the middle of the map area. Clast sizes range from clay to boulders, and vary in roundness from round to angular. Clasts consist mostly of quartzite, siltite, volcanic detritus, dolomite, granite, granodiorite, and the occasional altered local rock. Deposits are moderately well-sorted and of unknown thicknesses.

**Qls** Landslide (Quaternary) —Landslide or slump deposits: made up of a variety of parent material, ranging from boulders and talus to soil and clay. Variable thicknesses.

**Qc** Colluvium (Quaternary) —Locally derived unconsodildated poorly sorted boulder, gravel, sand, and silt deposits. Clasts are typically angular to subrounded. Observed clast compositions are locally derived quartzite, dolomite, volcanic detritus, and altered carbonate and quartzite clasts.

### Challis Volcanic Group

During Eocene time, mafic lavas and lithic tuffs associated with Challis Group volcanism covered a large portion of the region that is now central Idaho (Fisher et al., 1983; Tysdal, 2002; Meyers, 2014). The stratigraphic section of the Challis volcanic deposits constructed to the northwest of the Lemhi Pass approximately 35 km to the east of the mapping area (Blankenau, 1999) was used to establish a correlation of isolated volcanic deposits.

**Tci** Intrusive rocks (Tertiary) —A locally altered phaneritic quartz diorite is found only to the north of Poison Peak in the southeastern portion of the map. Grains are typically 1-3 mm in diameter.

**Tcv** Challis volcanic deposits, undivided (Tertiary) —Challis volcanic deposits that have not been subdivided are shown as a composite map unit. The deposits are widespread within the map area. The undivided unit generally contains the following from base to top: welded lithic tuffs, and mafic lava flows with local volcaniclastic sandstones and the Tuff of Ellis Creek. Lahar deposits are found to the west of Watson Peak near the eastern point of the mapping area.

**Tcl** Mafic lava (Tertiary) —A dark gray to black series of mafic lava flows found mainly in the western half and eastern most edge of the map area. Compositions include basaltic, latitic, and andesitic lavas. The lava flows are occasionally interbedded with volcaniclastic sandstones. The stratigraphy of the mafic lavas in the area shows a general trend toward increasingly mafic compositions.

**Tii** Challis ignimbrite (Tertiary) —A lithic-rich welded tuff found unconformably overlying Mesoproterozoic and Paleozoic strata in the eastern portion of the map area. Contains ~8% quartz, 4% biotite, and 3% plagioclase phenocrysts and ~15% lithic fragments ranging from 1 mm to 10+ cm in diameter with in a fine-grained ash matrix. While off-white and light gray on fresh surfaces, the deposits weather to brownish medium gray.

### Paleozoic Strata

Sedimentary and low-grade metasedimentary rocks can be found in the footwall of the Poison Creek thrust. Exposed in the map area are Ordovician and Silurian aged rocks deposited unconformably upon the tilted Mesoproterozoic strata of the Lemhi subbasin. This unconformable contact is interpreted to be a representation of the Lemhi Arch as a paleo-topographic high during Neoproterozoic to Middle Ordovician time.

**SOs** Saturday Mountain Formation (Ordovician-Silurian) —A very fine- to medium-grained dolomitic limestone with local limy mudstone and dolomitic wackestone portions; ranges from a cream to medium blue-gray in color. Locally, the lowermost Saturday Mountain Formation is fossiliferous, containing abundant Rugosa horn corals and fossil hash. Farther up section are localized stromatolite deposits and dissolution collapse breccias. Above this is thick to massively bedded light gray dolomite that appears mottled when weathered. The uppermost portions of the Saturday Mountain Formation consist of laminated to finely bedded fine-grained dolostone. Evans and Green (2003) and Ruppel and Lopez (1988) document the Saturday Mountain Formation thinning to the southeast. In this area, the Saturday Mountain Formation is estimated to be at least 850 m thick, more than double the thickness in the central Lemhi Range (Evans and Green, 2003).

**Ok** Kinnikinic Quartzite (Ordovician) —A super-mature white fine- to medium-grained well-sorted vitreous quartzite that forms cliffs and ridges in the footwall of the Poison Creek thrust. Locally, the cement around the sub-rounded grains has been eroded away to produce orange to brown lenses of porous rock. The Kinnikinic Quartzite locally contains small argillaceous lenses. Kinnikinic Quartzite shares a sharp contact with the overlying Saturday Mountain Formation and unconformably overlies the Mesoproterozoic strata. In the Lemhi Range, Kinnikinic Quartzite is approximately 300 m thick, and marginally thinner across the Salmon River near the Twin Peaks.

### Mesoproterozoic strata

Low-grade metasedimentary rocks of the Mesoproterozoic Lemhi subbasin make up the Poison Creek thrust fault hanging wall and most of the northern portion of the footwall exposed in the mapping area. Mesoproterozoic strata are shown in the cross section A-A'. The thicknesses of these units and their descriptions are compiled from previous researchers. Relatively younger Apple Creek Formation in the hanging wall of the Poison Creek thrust compared to the Swauger Formation in the Poison Creek thrust footwall requires extension prior to movement on the thrust (likely post-Mesoproterozoic and pre-Ordovician).

**Yab** Banded siltite member of the Apple Creek Formation (Mesoproterozoic) — Exposed in the northwestern portion of the map area, the banded siltite consists of dark gray to black very fine-grained quartzite, argillite, and siltite. Bedding ranges from medium bedded to thinly laminated. A variety of sedimentary structures are preserved in the banded siltite of the Apple Creek Formation, including desiccation cracks and ripples. Although the top and bottom contacts are not observed in the map area, the member has a gradational contact with the coarse siltite member of the Apple Creek Formation and has an estimated thickness of 2,000 m (Evans and Green, 2003).

**Yac** Coarse siltite member of the Apple Creek Formation (Mesoproterozoic) — The coarse-grained quartz-rich siltite, green-gray to dark gray in color, is exposed extensively in the hanging wall of the Poison Creek thrust fault as Long Ridge to the east of the Salmon River in the mapping area. Locally the coarse siltite contains pebble-sized clasts and, in rare localities near the Poison Creek thrust, distinct abundant foliations. The coarse siltite grades upward into the banded siltite and has a total estimated thickness of 2,000 to 2,500 m (Evans and Green, 2003).

**Yad** Diamictite member of the Apple Creek Formation (Mesoproterozoic) — Observed only in cross section A-A'. The argillaceous siltite to matrix-supported poorly-sorted conglomerate was first described in 1981 by Tietbohl (Evans and Green, 2003). The conglomeratic portions are localized, often not exceeding several tens of meters in lateral thickness and several meters in vertical thickness (Evans and Green, 2003). Total thickness of 600 to 1,500 m (Evans and Green, 2003).

**Yaf** Fine siltite member of the Apple Creek Formation (Mesoproterozoic) — Observed only in cross section A-A'. The fine siltite member of the Apple Creek Formation is typified by greenish gray planar laminated and locally ripple cross laminated siltite (Evans and Green, 2003). The fine siltite member is 1,000 m thick (Evans and Green, 2003).

**Yajl** Jahnke Lake member of the Apple Creek Formation (Mesoproterozoic)— The medium gray to black feldspathic fine- to very fine-grained vitreous quartzite is only exposed to the east of the Twin Peaks across the Salmon River. Feldspar content (specifically plagioclase) ranges from 2-20%. Minor amounts of mica can be present. While generally massive, bedding can be represented as dark hematite laminae. While the exposure is fault bounded in the mapping area, work by Burmester et al. (2013) estimates a thickness of 4,300 m.

**Ylc** Lawson Creek Formation (Mesoproterozoic) — Observed only in cross section A-A'. The Lawson Creek Formation is composed of siltite, and orthoquartzites. Thin to thick bedded gray to gray-blue-green beds can typically be seen crosslaminated (Evans and Green, 2003). The formation is 1,200 m thick (Evans and Green, 2003).

**Ys** Swauger Formation (Mesoproterozoic)— A light pink to gray and locally green, medium- to coarse-grained quartzite. The Swauger Formation contains distinct red chert clasts that range in size from medium sand grains to pebbles. The Swauger Formation also contains small amounts of feldspar (predominantly potassium feldspar) rarely exceeding 5%. Clasts are well-sorted and rounded and typically appear glassy, with hematite grains commonly creating a stippled appearance. In the northwestern portion of the map area, the Swauger Formation contains a small amount of pyrite, which adds a green hue to the vitreous and medium-grained rock. Planar and trough cross bedding can be locally present. The Swauger Formation is the most widespread of the Mesoproterozoic strata in the map area with an estimated thickness of 3,100 m (Evans and Green, 2003).

**Yg** Gunsight Formation (Mesoproterozoic) — Observed only in cross section A-A'. A 4,000 m thick light to dark gray feldspathic quartzite (Evans and Green, 2003).

### References

Blankenau, J.J., 1999, Cenozoic structural and stratigraphic evolution of the southeastern Salmon Basin, east-central Idaho (M.S. Thesis): Logan, Utah State University,143 p.

Burmester, R.F., Lonn, J.D., Lewis, R.S., and McFadden, M.D., 2013, Toward a grand unified theory for stratigraphy of the Lemhi subbasin of the Belt Supergroup: Northwest Geology, v. 42, p. 1-20.

Burmester, R.F. Lonn, J.D., Lewis, R.S., and McFadden, M.D., 2015, Stratigraphy of the Lemhi subbasin of the Belt Supergroup: Geological Society of America Special Publication (in press).

Evans, K. V., and Green, G.N., compilers, 2003, Geologic map of the Salmon National Forest and vicinity, eastern-central Idaho: Geologic Investigation Series I-2765, United States Geological Survey, 1:100,000.

Fisher, F.S., Mcintyre, D.H., and Johnson, K.M., 1983, Geologic map of the Challis 1° X 2° Quadrangle, Idaho: Miscellaneous Investigation Series Map I-1819, United States Geological Survey, 1:250,000.

Meyers, J., 2014, Eocene magmatic evolution and sychronous to subsequent extensional faulting, Little Wood River Reservoir Quadrangle, Blaine County Idaho (M.S. Thesis): Pocatello, Idaho State University, 1:24,000.

Ruppel, E.T., and Lopez, D. A., 1988, Regional geology and mineral deposits in and near the central part of the Lemhi Range, Lemhi County, Idaho: U.S. Geological Survey Professional Paper, v. 1480., 118 p.

Tietbohl, D.R., 1981, Structure and stratigraphy of the Hayden Creek area, Lemhi Range, east- central Idaho (M.S. Thesis): University Park, Pennsylvania State University, 121 p.

Tysdal, R.G., 2002, Structural geology of western part of Lemhi Range, east-central Idaho: U.S. Geological Survey Professional Paper, v. 1659, 31 p.

## ZIRCON (U-TH)/HE THERMOCHRONOMETRY RESULTS

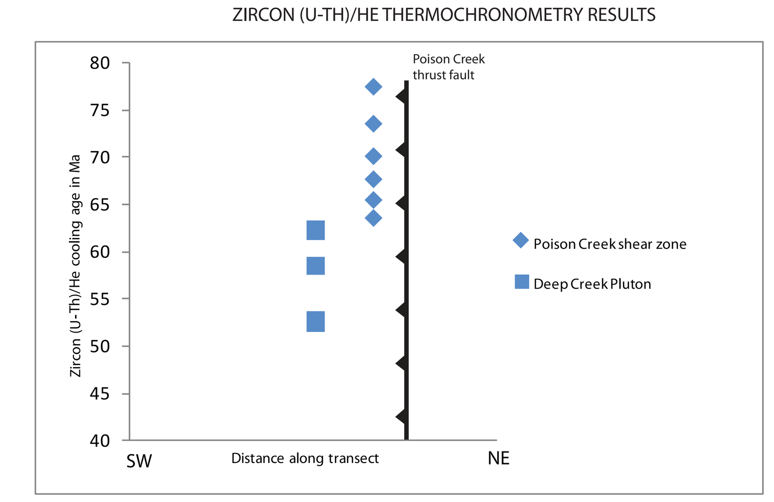


| | U (ppm) | Th (ppm) | Th/U (atomic) | 4He (nmol/g) | Mass (µg) | Half Width (µm) | HAC (FT) | Cooling Age (Ma) | 2σ (Ma) |
|---|---|---|---|---|---|---|---|---|---|
| CMH13-02 Poison Creek shear zone (44.877675°N; 113.893068°W) | | | | | | | | | |
| Grain | | | | | | | | | |
| 14B790_DP_AC_CMH_01_Z1 | 809 | 149 | 0.18 | 233 | 2.34 | 44.0 | 0.694 | 70.1 | 2.31 |
| 14B791_DP_AC_CMH_01_Z2 | 884 | 317 | 0.36 | 279 | 2.84 | 44.8 | 0.700 | 73.6 | 2.57 |
| 14B792_DP_AC_CMH_01_Z3 | 612 | 132 | 0.22 | 188 | 2.42 | 39.1 | 0.660 | 77.5 | 2.76 |
| 14B793_DP_AC_CMH_01_Z4 | 366 | 112 | 0.30 | 97.4 | 1.12 | 36.7 | 0.642 | 67.7 | 2.58 |
| 14B794_DP_AC_CMH_01_Z5 | 447 | 168 | 0.38 | 135 | 1.91 | 62.9 | 0.781 | 63.6 | 1.92 |
| 14B795_DP_AC_CMH_01_Z6 | 368 | 362 | 0.98 | 111 | 2.07 | 39.1 | 0.668 | 65.5 | 1.83 |
| Average | | | | | | | | 69.7 | 2.33 |
| Weighted Average | | | | | | | | 68.4 | 2.22 |
| 1LBK12 Deep Creek pluton (45.126159°N; 114.214251°W) | | | | | | | | | |
| Grain | | | | | | | | | |
| 14B801_DP_1LBK12_Z1 | na | na | na | na | na | 92.9 | na | 58.6 | 1.60 |
| 14B802_DP_1LBK12_Z2 | 13.8 | 3.87 | 0.28 | 1.38 | 183 | 83.8 | 0.109 | 52.8 | 1.53 |
| 14B803_DP_1LBK12_Z3 | 31.0 | 12.9 | 0.42 | 0.39 | 18.0 | 64.8 | 0.142 | 62.4 | 1.83 |
| 14B804_DP_1LBK12_Z4 | na | na | na | na | na | 87.9 | na | 62.2 | 1.82 |
| 14B805_DP_1LBK12_Z5 | 14.1 | 6.73 | 0.48 | 0.34 | 64.9 | 59.3 | 0.157 | 52.5 | 1.40 |
| Average | | | | | | | | 57.7 | 1.64 |
| Weighted Average | | | | | | | | 56.8 | 1.60 |

Table showing the zircon (U-Th)/He cooling ages from the hanging wall of the Poison Creek thrust fault. The Deep Creek pluton is located to the northwest of the map area roughly 20 km.

This Technical Report is a reproduction of a map originally submitted as part of a master's thesis. Its content and format may not conform to IGS standards.

Hansen, C.M., 2015, An investigation into the Poison Creek thrust: a Sevier fault with Proterozoic implications, Idaho State University, M.S. thesis, 78 p.

Thermochronometry and detrital zircon U-Pb analysis were conducted at the University of Arizona Radiogenic Helium Dating Laboratory and Laserchron Center, respectively.

## DETRITAL ZIRCON ANALYSIS OF THE ORDOVICIAN KINNIKINIC QUARTZITE

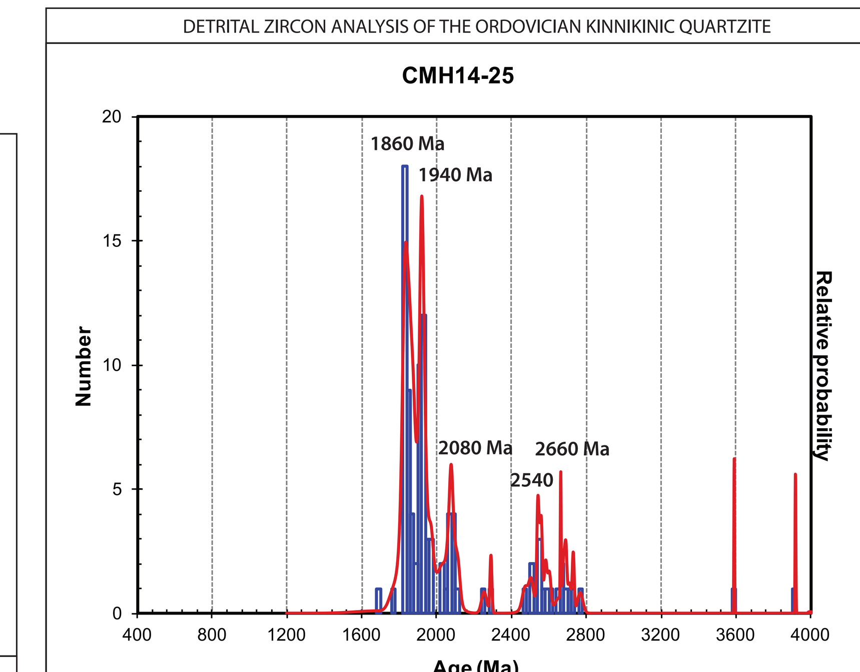


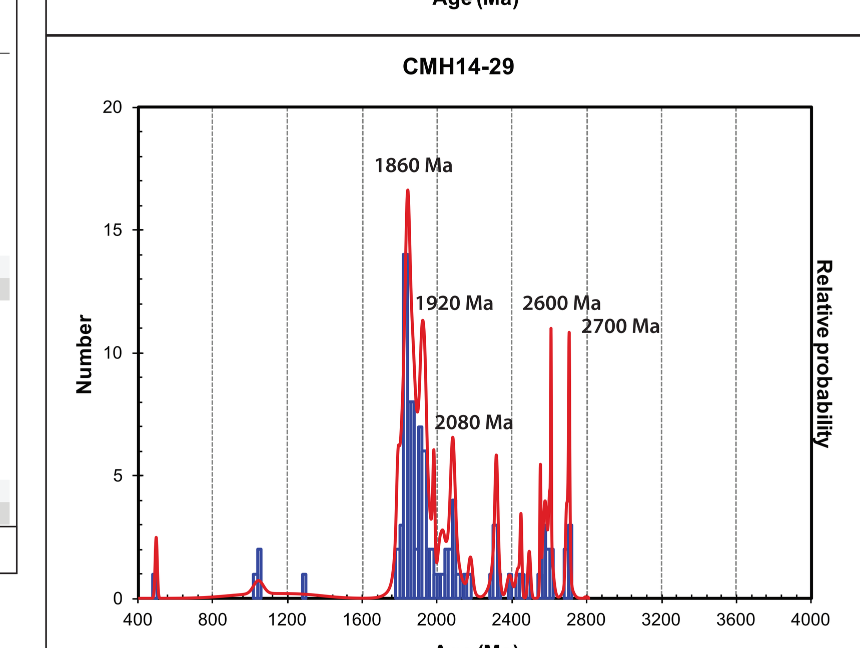


Two samples of Paleozoic quartzite were collected with the intent of the analyses to destinguish between two distinct quartzites vs. a single quartite unit duplicated by thrust faulting. The two samples are statistcally indistinguishable, suggesting they were imbricated by thrust faults